Equilibrium and Kinetics of Nitrous Oxide, Oxygen and Nitrogen Adsorption on Activated Carbon and Carbon Molecular Sieve

Citation for published version:
Park, D, Ju, Y, Kim, J-H, Ahn, H & Lee, C-H 2019, 'Equilibrium and Kinetics of Nitrous Oxide, Oxygen and Nitrogen Adsorption on Activated Carbon and Carbon Molecular Sieve', *Separation and Purification Technology*. https://doi.org/10.1016/j.seppur.2019.04.051

Digital Object Identifier (DOI):
10.1016/j.seppur.2019.04.051

Published In:
Separation and Purification Technology

Manuscript Details

Manuscript number	SEPPUR_2019_686_R1
Title	Equilibrium and kinetics of nitrous oxide, oxygen and nitrogen adsorption on activated carbon and carbon molecular sieve
Article type	Full Length Article

Abstract

To evaluate candidate adsorbents for the recovery of nitrous oxide (N2O) from adipic acid off-gases, the equilibrium and kinetics of N2O and O2 adsorption on activated carbon (AC) and of N2O, O2, and N2 adsorption on a carbon molecular sieve (CMS) were evaluated at 293, 308, and 323 K under pressures up to 1000 kPa using a high-pressure volumetric system. Adsorption amount of N2O on AC and CMS exceeded those of N2 and O2, and the adsorption isotherms for O2 and N2 were similar. The experimental N2O and O2 uptakes on AC and CMS were fitted to a non-isothermal adsorption model, whereas the model was ineffective for predicting N2 uptake on CMS. The isothermal dual-resistance model, considering surface barrier resistance and pore diffusion, adequately predicted N2 uptake on CMS. The rate of adsorption of N2O on AC was much lower than that of O2 and N2 whereas the rate of adsorption on CMS flowed the order: O2 > N2O >> N2, even though N2O has higher adsorption affinity and smaller kinetic diameter than O2. The Lewis structure of N2O was also found to influence the adsorption kinetics.

Keywords	Adsorption, activated carbon, carbon molecular sieve, nitrous oxide, non-carbon dioxide green-house gas
Manuscript category	Adsorption kinetics (experimental and theoretical aspects)

Corresponding Author	Chang-Ha Lee
Corresponding Author's Institution	Yonsei University
Order of Authors	Dooyong Park, Youngsan Ju, Jeong Hoon Kim, Hyungwoong Ahn, Chang-Ha Lee

Suggested reviewers	Shamsuzzaman Farooq, Zhong Li, Ki Bong Lee, Kazuyuki Nakai,, Carlos Grande

Submission Files Included in this PDF

File Name [File Type]

Cover letter.docx [Cover Letter]

Response_to_reviewer_final_web_ver.docx [Response to Reviewers]

Manuscript_revis_final_marked.docx [Revised Manuscript with Changes Marked]

Highlights.docx [Highlights]

Manuscript_revis_final.docx [Manuscript File]

Figure_revis_final.docx [Figure]

Table_revis_final.docx [Table]

Appendix table_fin.docx [Table]

To view all the submission files, including those not included in the PDF, click on the manuscript title on your EVISE Homepage, then click 'Download zip file'.

Department of Chemical and Biomolecular Engineering,
Yonsei University
50 Yonsei-ro, Seodaemun-gu
Seoul,03722, Republic of Korea

[February 25, 2019]

Prof. Bart Van der Bruggen
Editor-in-Chief
Separation and Purification Technology

Dear Editor,

I wish to submit an original article for publication in *Separation and Purification Technology*, titled "Equilibrium and kinetics of nitrous oxide, oxygen, and nitrogen adsorption on activated carbon and carbon molecular sieve" (co corresponding Author: Hyungwoong Ahn and Chang-Ha Lee)

Significance and originality of the manuscript:

This paper presents a theoretical and empirical evaluation of the isothermal adsorption of effluent gases from the production of adipic acid on two types of carbon-based adsorbents, i.e., activated carbon (AC), an equilibrium adsorbent, and carbon molecular sieves (CMSs) a kinetic adsorbent. The primary objective of this study is to determine the optimal adsorbent type for the recovery of N_2O from adipic acid effluent, in the presence of other gaseous components such as oxygen and nitrogen. Equilibrium and kinetic evaluations of the adsorption process were performed. The adsorption isotherms were fitted to both Dual-site Langmuir model and Sips model, and the isosteric heat of adsorption was calculated by applying the Clausius–Clapeyron equation. The kinetics were analyzed by applying two models, i.e., a non-isothermal adsorption model and an isothermal dual-resistance model. The data demonstrate that both adsorbents favorably capture N_2O compared to oxygen and nitrogen, with AC showing greater capacity for gas adsorption. The fundamental mechanistic findings of this study demonstrate that the adsorbate-adsorbate interactions contribute more to the adsorption of N_2O by AC than to the adsorption by CMS. Macropore diffusion could be neglected for both adsorbents, and the kinetics of N_2O and O_2 adsorption via micropore diffusion in both adsorbents could be predicted by the non-isothermal adsorption model. We further demonstrate that the rate of adsorption of the gases is not simply a function of the kinetic diameter, but may also be influenced by the electrical properties of the adsorbates, such as the dipole/quadrupole moment and/or polarizability. Furthermore, the Lewis

Department of Chemical and Biomolecular Engineering,
Yonsei University
50 Yonsei-ro, Seodaemun-gu
Seoul,03722, Republic of Korea

structure of N_2O, i.e., the linear or asymmetric molecular structure, might affect the rate of adsorption on the carbon surface.

We believe that our study makes a significant contribution to the literature because the fundamental evaluation provides a compendium of parameters and raw data for evaluating the feasibility of adsorbents and for the design of adsorptive cyclic processes for N_2O separation.

Further, we believe that this paper will be of interest to the readership of your journal given the i mportance of N_2O separation and recovery in the fields of medicine, rocket fuel, and the semicon ductor and optical industries, and for environmental remediation.

Please consider, as potential referees,

1. Prof. Zhong Li

School of Chemistry & Chemical Engineering, South China University of Technology

E-mail: celzhong@scut.edu.cn

Tel.: +86 20 87113735

2. Dr. Carlos A. Grande

Research Division of Materials and Chemistry, SINTEF

Email: carlos.grande@sintef.no

Tel.: +47 93207532

Fax: +47 22067350

3. Ph.D. Kazuyuki Nakai,

Microtrac BEL Corp., Japan

E-mail: kazu@nippon-bel.co.jp

Tel.: +81 668412161

Fax: +81 668412767

4. Prof. Ki Bong Lee

Department of Chemical and Biogolical Engineering, Korea University

E-mail: kibonglee@korea.ac.kr

Tel.: +82 2 3290 4851

Fax: +82 2 3290 3290

5. Prof. Farooq Shamsuzzaman

Department of Chemical and Biomolecular Engineering, National University of Singapore

E-mail: chesf@nus.edu.sg

Tel.: +65-65166545

Fax: +65-67791936

This manuscript has not been published or presented elsewhere in part or in entirety and is not under consideration by another journal. We have read and understood your journal's policies, and we believe that neither the manuscript nor the study violates any of these. There are no conflicts of interest to declare.

Thank you very much for your consideration.

Very Sincerely Yours,
Hyungwoong Ahn and Chang-Ha Lee
H.Ahn@ed.ac.uk (H. Ahn), leech@yonsei.ac.kr (C.-H. Lee)
Tel.: +82 2 2123 2762; Fax: +82 2 312 6401

Prof. Paul Webley, Editor
Separation and Purification Technology

Dear Editor,

I have enclosed the "Response to Reviewers' Comments" with the revised manuscript entitled **"Equilibrium and kinetics of nitrous oxide, oxygen, and nitrogen adsorption on activated carbon and carbon molecular sieve."(SEPPUR_2019_686)**

In the "Response to Reviewers' Comments," we have provided detailed explanations with a list of changes for each comment.

Thank you very much for your consideration.

Very Sincerely Yours,

Chang-Ha Lee (Corresponding Author)
Professor, Department of Chemical and Biomolecular Engineering, Yonsei University
50 Yonsei-ro Sudaemoon-ku, Seoul, 03722, Korea
General member, The National Academy of Engineering of Korea
Tel: +82 2 2123-2762/ Fax: +82 2 312-6401/ E-mail: leech@yonsei.ac.kr

Responses to reviewer's comments

Reviewer #1:

I sincerely appreciate the comments. Here are the responses to your comments.

Overall Comment: This manuscript reports adsorption and diffusion of O_2, N_2O and N_2 in AC and CMS. The data presented will be useful to study feasibility of an adsoprtion process to recover N_2O from adipic acid production off gas.

Comment 1) O_2 and N_2 diffusion in AC and CMS have been studied in the literature. So, this part is not new. It just adds to the database for another sample. So comparison to show the difference or agreement is desirable.

- **Response:** As listed in Table 8, many researches have studied the diffusion of O_2 and N_2 in CMS. And, in the study, the diffusion of O_2 and N_2 in CMS was appropriately compared with the published data.

  This study suggested the model parameters (α and β for the non-isothermal model, and L for the isothermal dual-resistance model) which can be derived from the physical properties and adsorption data. Therefore, the parameters were estimated from the theoretical physical properties and uptake curve. And their values and variation with experimental conditions were reasonable in the study. Let alone the diffusion values themselves, the results can help other researchers to analyze the effects of heat transfer, mass transfer, and the isosteric heat of adsorption.

  We do not want to discuss what the problems of previous studies are. However, to clearly describe what we did, the following corrections were made:

✓ **Marked manuscript page 4, line 17 (Added):**

The adsorption kinetics via micropore diffusion are analyzed from the experimental uptake curves by applying the non-isothermal adsorption model and isothermal dual-resistance model with reasonable physical meaning parameters. **The parameters showed a reasonable change with variations in the experimental conditions.** Finally, the obtained model parameters and experimental raw data are compiled as contributions to the database for evaluating the feasibility of adsorbents and for the design of adsorptive cyclic processes for N_2O separation.

✓ **Marked manuscript page 16, line 25 (Changed and added):**

The model parameters, α and β, were **reasonably** estimated from the properties of the **adsorbent and adsorbate** and the experimental adsorption data, **not just by fitting the experimental uptake curves**.

Comment 2) It has been shown in the literature with extensive experiments that diffusion of both O_2 and N_2 in CMS follow dual resistance model. The contribution of the two components change with temperature. It just so happens that in the temperature range used in this study the contribution of pore mouth (surface barrier) resistance is negligible compared to the diffusional resistance in the pore interior. By lowering temperature to -25C, it has been shown that (Langmuir, 2003, 19, 393-405) the barrier resistance rise to a measurable level for O_2. The same argument applies for N_2O. Hence, to suggest that different gases have different transport mechanism is misleading. This is an important fundamental issue and should be properly addressed.

Comment 3) It different gases have different transport mechanism, have the authors thought how to capture interaction in mixture diffusion?

- **Response:** Thank you for your valuable comment. As pointed out by the reviewer, the kinetics of the gas molecules on CMS are controlled by barrier resistance and interior diffusional resistance in pores (Langmuir, 2003, 19, 393-405). However, the heat transfer, macropore, adsorbate properties/structure, etc. can also contribute to the kinetics in pores.

  In the experimental range, the barrier resistance was negligible compared to the diffusional resistance in the pore interior for N_2O and O_2 adsorption on CMS. Therefore, as shown in Fig. R1 below, the non-isothermal diffusion model could predict the experimental uptakes better than the isothermal dual resistance model. However, both resistance should be considered for N_2 diffusion on CMS in the study.

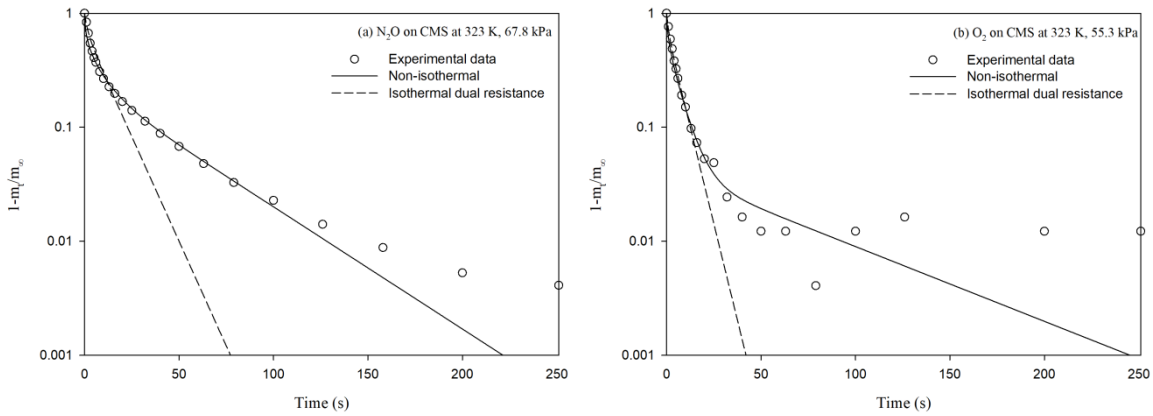

Figure R1. Non-isothermal adsorption model and isothermal dual resistance model for experimental

uptake curves of N_2O (a) and O_2 (b) on CMS: ○, experimental data; solid line, non-isothermal adsorption model; dashed line, isothermal dual resistance model

With respect to the mixture of N_2O, O_2 and N_2, the kinetic of N_2O on CMS will be dominant because the adsorption rate of N_2 is too slow and the adsorption affinity of O_2 is relatively much weaker than that of N_2O. Generally, the kinetics of the mixtures can be analyzed in various ways. Our group studied the Maxwell-Stefan model with the Dust Gas model for molecular diffusion of mixtures on porous materials. However, it is out of the scope of this study.

J.H. Moon, Y.J. Park, M.B. Kim, S.H. Hyun and C.-H Lee, "Permeation and separation of a carbon dioxide/nitrogen mixture in a methyltriethoxysilane templating silica/α-alumina composite membrane," J. Membr. Sci., 250 (2005) 195-205.

J.H. Moon, Y.S. Bae, S.H. H. and C.-H. Lee, "Equilibrium and Kinetic Characteristics of Five Single Gases in a Methyltriethoxysilane Templating silica/α-alumina Composite Membrane," J. Membr. Sci., 285 (2006) 343-352.

J.H. Moon and C.-H. Lee, "Hydrogen separation of methyltriethoxysilane templating silica membrane" AIChE J., 53 (2007) 3125-3136.

J.H. Moon, J.H. Bae, Y.S. Bae, J.T. Chung, C.-H. Lee, "Hydrogen Separation from Reforming Gas Using Organic Templating Silica/Alumina Composite Membrane", J. Membr. Sci., 318 (2008) 45-55.

J.H. Moon, J.H. Bae, Y.J. Han, and C.-H. Lee, "Adsorbent/membrane hybrid (AMH) system for hydrogen separation: Synergy effect between zeolite 5A and silica membrane," J. Membr. Sci., 356 (2010) 58-69.

To remove any misunderstandings of different mechanisms for different molecules, the following corrections were made.

- ✓ **Marked manuscript page 17, line 30 (added):**

This deviation indicates that the non-isothermal adsorption model was not adequate for describing the kinetics of **the** N_2 adsorption on CMS, and **the surface barrier resistance as well as the pore diffusion resistance should be considered for** the adsorptive uptake **of N_2 in the experimental range. It was also reported that the surface barrier resistance rises to a measurable level for O_2 on CMS at low temperature, 248 K (Table 8) [48]. It implies that the transport mechanism in small pores can be changed by experimental conditions.**

- ✓ **Marked manuscript page 20, line 11 (added):**

For all the adsorbates, macropore diffusion in both adsorbents could be neglected. The kinetics of

N_2O and O_2 adsorption via micropore diffusion in both adsorbents could be predicted by the non-isothermal adsorption model. **It also indicated that the surface barrier resistance on CMS was negligible in the experimental range.** On the other hand, due to the contribution of surface barrier resistance to N_2 adsorption on CMS, the non-isothermal adsorption model was unsuitable for this system.

- ✓ **Table 8 and references (Added):**

  'Langmuir, 2003, 19, 393-405' were added to Table 8 and References.

- ✓ **[48] H. Qinglin, S.M. Sundaram, S. Farooq, Revisiting Transport of Gases in the Micropores of Carbon Molecular Sieves, Langmuir, 19 (2003) 393-405**

- ✓ **Table 8**. Comparison of diffusion time constant and barrier mass transfer coefficient for N_2O, O_2 and N_2

Adsorbent	Manufacturer	T [K]	P [kPa]	D/r_c^2 $\times 10^4$ [s^{-1}]	k_b $\times 10^{4*}$ [s^{-1}]	Method**	Kinetic Model	Ref.
N_2O								
CMS A	Air products	303-323 303-343	0-9	0.14-0.24(1) -	2.25-22.0(1) 24.0-111	G	Combined barrier resistance Linear driving force	[8]
AC	Kuraray	293-323	10-80	28-74.9	-	V	Non-isothermal diffusion	This study
CMS	Kuraray	293-323	10-80	17-76.8	-	V	Non-isothermal diffusion	This study
O_2								
CMS	Air products	293	0-100	-	83.5-114	G	Linear driving force	[39]
CMS	Air products	273-313	0-100	-	18.3-196	G	Linear driving force	[35]
CMS A	-	275-333	400	-	205	G	Fickian and phenomenological	[42]
CMS 3A CMS 5A	Takeda	273-323	0-1300	20-84 14-117	-	G	Isothermal diffusion	[36]
CMS	Bergbau-Forschung	303		52	-			
CMS	Bergbau-Forschung	303	0-73 -	20 37	- -	G C	Dual-resistance	[43]
CMS	Bergbau-Forschung	300	1144	35	-	DAB	Isothermal diffusion	[18]
CMS	Takeda	293-313	0-1635	38.3-72.2(2)	-	V	Piezometric Method	[44]
CMS	**Bergbau-Forschung**	**253-302**	**Low coverage (3)**	**18.5-68.4**	**457-2400**	**V**	**Dual-resistance**	**[48]**
CMS 3A Ⅰ	**Takeda**	**253-267**		**28.0-47.8**	**445-810**			
CMS 3A Ⅱ	**Takeda**	**253-302**		**16.0-121.9**	**277-1248**			
AC	Kuraray	293-323	10-80	548-1179	-	V	Non-isothermal diffusion	This study

CMS	Kuraray	293-323	10-80	45.7-137.5	-	V	Non-isothermal diffusion	This study
N_2								
CMS	Air products	293	0-100	-	2.14-3.23	G	Linear driving force	[39]
CMS	Air products	303-343	0-9	-	3.07-23.65	G	Linear driving force	[35]
CMS A	Air products	303-343	0-100	-	2.85-23.45	G	Linear driving force	[8]
CMS A	-	275-333	400	-	5	G	Fickian and phenomenological	[42]
CMS 3A CMS 5A	Takeda	273-323	0-1300	1-8.3 4.2-29	- -	G	Isothermal diffusion	[36]
CMS	Bergbau-Forschung	303		2	-			
CMS	Bergbau-Forschung	303	0-88 -	1.0 1.2	- -	G C	Dual-resistance	[43]
CMS	Bergbau-Forschung	300	1144	0.095	-	DAB	Isothermal diffusion	[18]
CMS	Takeda	293-313	0-1665	1.0-35.1(2)	-	V	Piezometric Method	[44]
CMS	Shanli chemical materials	303-323	0-100	1.44-5.44	29-65	G	Dual-resistance	[34]
CMS 3K	TAKEDA	298-323	low P	2.77-8.31	60-72	G	Dual-resistance	[40]
AC	Kuraray	293-323	20-90	442-804 (2)	-	V	Non-isothermal diffusion	[45]
CMS	Kuraray	298-318	0-600	1.97-6.06	-	G	Isothermal diffusion	[30]
CMS	**Bergbau-Forschung**	**275-302**	**Low coverage (3)**	**1.3-4.3**	**44-106**			
CMS 3A Ⅰ	**Takeda**	**273-302**		**1.3-5.8**	**26-88**	**V**	**Dual-resistance**	**[48]**
CMS 3A Ⅱ	**Takeda**	**273-302**		**0.67-2.8**	**14-53**			
CMS	Kuraray	293-323	10-80	1.78-7.29	-	V	Isothermal dual resistance	This study

* Barrier mass transfer coefficient

** Experimental methods: Gravimetric (G), Volumetric (V), Chromatographic (C), Differential adsorption bed (DAB)

(1) Using a particle radius of 0.2 cm

(2) Apparent diffusion time constant

(3) **Surface coverage (θ) values varied in the range of 0.01-0.03**

Comment 4) (a) Eq (24) should be discussed in the proper context. This is valid only for Langmuir isotherm and (b) diffusion confined in micropores of crystalline materials with uniform micropore size (such as in zeolites). For CMS where there is pore size distribution, the concentration dependence is stronger than what Eq (24) suggests. (c) The other issue is even when Eq (24) is valid, it can be applied only for differential step measurements outside the linear range. When large step size is used, the D extracted cannot be corrected using this equation. Correction for D from large integral step measurement

is discussed in Ruthven's Principle of Adsorption ... (see Figure 6.4).

- **Response 4 (a):** Thank you for your valuable comment. The thermodynamic correction factor ($\frac{dlnp}{dlnq}$) can be derived from different isotherm models such as linear (1), Langmuir ($\frac{1}{1-\theta}$), and Volmer ($\frac{1}{(1-\theta)^2}$) (Adsorption Analysis: Equilibria and Kinetics, Duong D. Do, Vol. 2, table 10.2-1). The equation (24) can also be derived from the Sips isotherm model as mentioned in the manuscript.

$$q = q_m \frac{(bP)^{\frac{1}{n}}}{1+(bP)^{\frac{1}{n}}}$$

$$\frac{q}{q_m}(\theta) = \frac{(bP)^{\frac{1}{n}}}{1+(bP)^{\frac{1}{n}}}$$

$$dlnq = dlnq_m + \frac{1}{n}dln\,(bP) - dln(1+(bP)^{\frac{1}{n}})$$

$$\frac{dlnq}{dlnP} = \frac{1}{n}\frac{dln\,(bP)}{dlnP} - \frac{dln\left(1+(bP)^{\frac{1}{n}}\right)}{dlnP}$$

$$= \frac{1}{n} - \frac{1}{n}\left(\frac{(bP)^{\frac{1}{n}}}{1+(bP)^{\frac{1}{n}}}\right)$$

$$= \frac{1}{n}(1-\theta)$$

$$\frac{dlnp}{dlnq} = \frac{n}{1-\theta}$$

✓ **Marked manuscript page 10 (added and changed):**

$$\boldsymbol{\frac{dlnq}{dlnP} = \frac{1}{n}\frac{dln\,(bP)}{dlnP} - \frac{dln\left(1+(bP)^{\frac{1}{n}}\right)}{dlnP}}$$

$$\boldsymbol{= \frac{1}{n} - \frac{1}{n}\left(\frac{(bP)^{\frac{1}{n}}}{1+(bP)^{\frac{1}{n}}}\right)} \qquad \textbf{(24)}$$

$$\boldsymbol{= \frac{1}{n}(1-\theta)}$$

$$D = D_0\frac{d\ln P}{d\ln q} = D_0\frac{n}{1-\theta} \qquad (\cancel{24}\mathbf{25})$$

✓ **Marked manuscript page 13 (changed):**

The number of equation was changed (25) to (26) because Equation (25) was added.

$$P_{0,i+1}{}' = \frac{P_{e,\ \ i} \times V_{cell} + P_{0,i+1} \times V_{system}}{V_{cell} + V_{system}} \qquad (\cancel{25}\mathbf{26})$$

- **Response 4 (b):** As shown in Figure 5, we demonstrated that the contribution of the macropore diffusion to adsorption in AC and CMS was insignificant, and the micropore diffusion mechanism dominated the adsorption kinetics.

As shown in Fig. R2, the pore size distribution of CMS and AC was analyzed by using CO_2 and N_2. The pore size distribution peaks of CMS were observed around 0.3−0.4 nm and 0.4−0.7 nm while three micropore peaks of AC were measured around 0.35 nm and 0.52 nm in CO_2 adsorption analysis, and 1.17 nm and 1.33 nm in the N_2 adsorption analysis. The AC showed wider pore size distribution than the CMS. Considering the pore volume and adsorption isotherm, the pores with larger than 1.5 nm have less effect on adsorption in a low pressure region. It was also reported that zeolites shows broad pore size distribution even though the peak is narrow. (Figure R3, Applied Catalysis A: General 174 (1998) 137-146). As a result, equation 24 was expected to be applicable for the adsorption kinetics of CMS and AC at the low pressure region in the study even though the pore size distribution of CMS and AC was wider than that of zeolites.

To clearly present the pore characteristics of AC and CMS, the following correction was made by adding an additional figure:

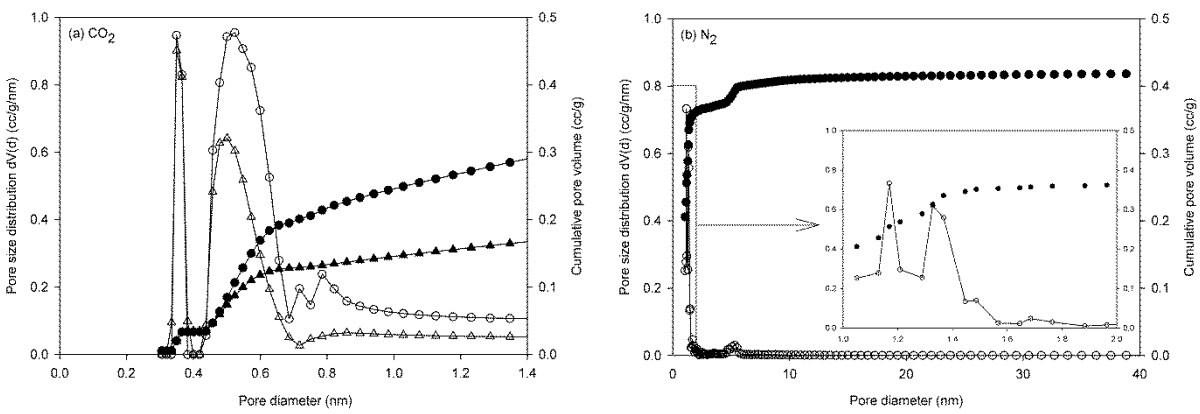

Figure R2. Cumulative pore volume and pore size distribution of AC and CMS from the density functional theory (○ and ●, activated carbon; △ and ▲, carbon molecular sieve [30]; closed symbol

for cumulative pore volume; open symbol for pore size distribution)

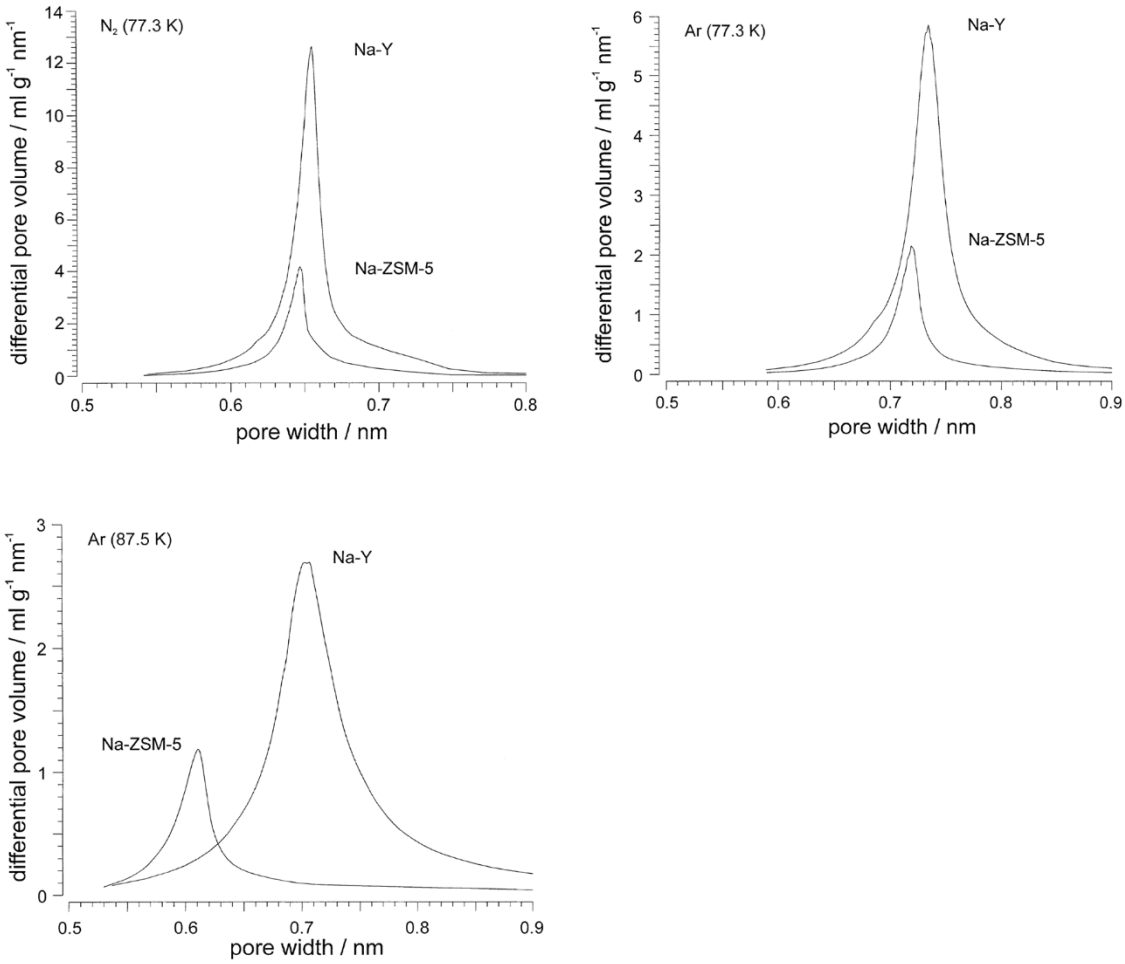

Figure R3. Pore-size distributions of Na-Y and Na-ZSM-5 according to the HK method with N_2 at 77.3 K, Ar at 77.3 K and Ar at 87.5 K (Applied Catalysis A: General 174 (1998) 137-146)

- ✓ **Figure 2 (added):**

  The figure numbers were corrected through the manuscript.

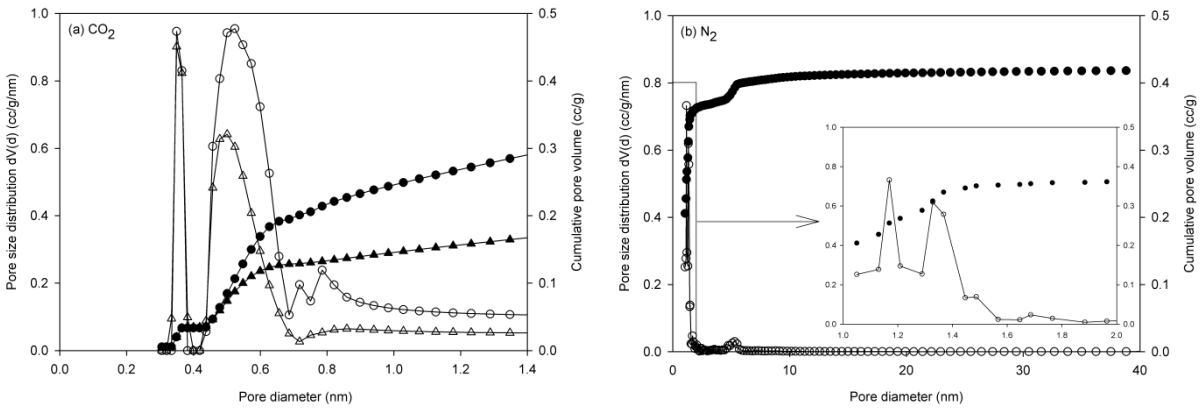

Figure 2. Cumulative pore volume and pore size distribution of AC and CMS from the density functional theory (○ and ●, activated carbon; △ and ▲, carbon molecular sieve [30]; closed symbol for cumulative pore volume; open symbol for pore size distribution)

✓ **Marked manuscript page 11, line 4 (added):**

The surface area of AC and CMS was 1306.4 and 640.9 $m^2 g^{-1}$, respectively. As shown in Figure 1, CMS contained macropores that were developed during pelletization. **Figure 2 showed the pore size distribution and cumulative pore volume of AC and CMS. The micropores of AC were distributed around 0.35 nm and 0.52 nm in the CO_2 adsorption analysis, and 1.17 nm and 1.33 nm in the N_2 adsorption analysis.** The pores of CMS were distributed within **two regions: 0.3−0.4 nm and 0.4−0.7 nm**. **Especially, the CMS showed relatively narrower pore size distribution than the AC.** The detailed physical properties of the adsorbents are listed in Table 1.

- **Response 4 (c):** As pointed out by the reviewer, it is well known that a differential step measurement within the linear range is required to obtain diffusivity from an uptake curve. As shown in Fig. 3, the isotherms in the low pressure range were measured at a small pressure step, but the pressure step change became larger after 100 kPa. In this study, the kinetics were analyzed under lower than 80 kPa.

As shown in the figures below, the experimental uptake data of adsorption and desorption coincided well with each other. The definition of a differential step change in pressure is strongly dependent on the adsorbent and adsorbate, not specified at a specific criterion.

To clearly describe the results, the following correction was made by adding an additional figure.

✓ **Figure 7 (Added):**

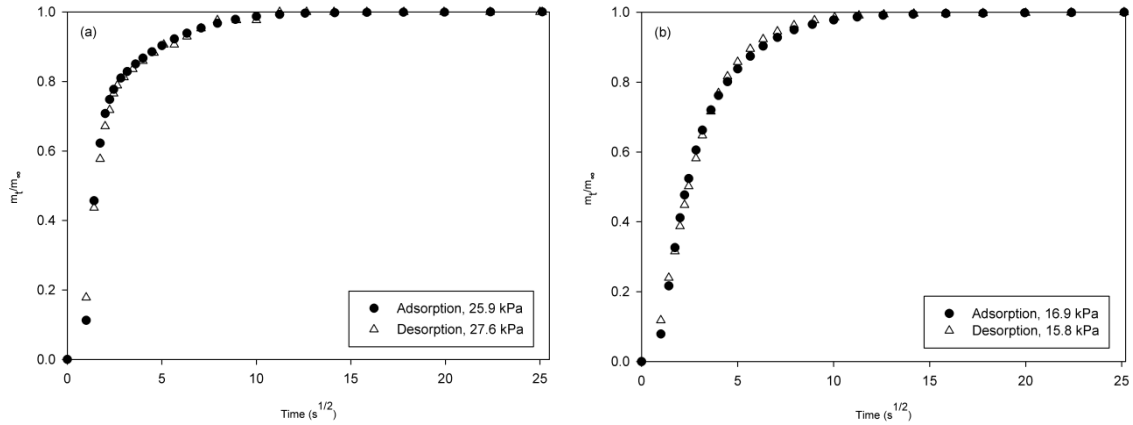

✓

Figure 7. Experimental uptake curves of adsorption and desorption for N_2O on (a) AC and (b) CMS at 308 K: ●, adsorption; △, desorption

✓ **Marked manuscript page 16, line 6 (added):**

The experimental uptake curves of adsorption and desorption for N_2O at 308 K were compared in Figure 7. Within the pressure range of lower than 80 kPa for the kinetic analysis, both uptake curves coincided well with each other, indicating the reliability of the pressure step change in the study. The experimental uptake curves were predicted using the non-isothermal adsorption model (Eq. 10) and the D_c/r^2 (micropore diffusion time constant) was obtained.

Reviewer #2:

I deeply appreciate your comments. Here are the responses to your comments.

Overall Comment: I have read with all attention the manuscript of Park et al. The manuscript is well organized, presents relevant data and is a nice reading. It is indeed another good work from the group of Prof. Lee. I would only suggest minor things that are optional, but I guess that can increase the impact of the manuscript

Comment 1) This is a new application to many people. I think it can be interesting to present in a couple of sentences, the current technologies for N_2O abatement and then introduce the idea of using adsorption for recovery. A composition of typical streams can help readers to get an idea of the feasibility.

- **Response:** Thank you for your comments. We changed the sentence and added two compositions of typical streams in the manuscript as follows.

✓ **Marked manuscript page 3, line 10 (changed):**

~~The effluent gas from adipic acid production mainly consists of N_2O, O_2, N_2, CO_2, and H_2O [5].~~

Typical compositions of effluent gas from adipic acid production processes are reported as $N_2O/NO_x/CO_2/CO/O_2/H_2O/N_2/VOC$; 30.5/0.7/6.0/0.03/3.9/2.0/57.0/0.03 mol.% [1] and $N_2O/NO_2/N_2/O_2/H_2O$; 23/17/47/7.5/3.0 mol.% [5]. After pretreating the effluent gas, the mixture of N_2O, O_2, N_2 and/or CO_2 is supplied to a N_2O recovery unit. The selection of proper adsorbents is crucial for the design of effective adsorptive cyclic processes for achieving efficient recovery of N_2O.

Comment 2) The number of parameters of the model seems to be related to the results. I guess that this discussion is old, but it may be proper here. I don't understand the theoretical validity of using a dual Langmuir in a carbonaceous material other than providing the numerical optimization with 6 parameters to choose.

- **Response:** Many studies reported that the adsorption isotherms on carbon-based adsorbents with adsorption sites of different energy levels can be presented well by the dual-site Langmuir model. In addition, the model can be appropriately applied for a mathematical model to design adsorptive processes.

As pointed out by the reviewer, 6 parameters should be re-optimized as they are applied for process modeling due to a lack of theoretical validity. Therefore, we have provided expected readers with raw experimental data (Appendix Tables) for further studies of isotherm models and process development.

To clearly describe the purpose and results, the following corrections was made.

- ✓ **Marked manuscript page 4, line 26 (Changed and added):**

~~The dual-site Langmuir model (DSL model) presents the discrete distribution of two bimodal sites based on the Langmuir isotherm [20]. The model has a flexible mathematical form for pure-gas adsorption because it considers two types of adsorption sites with different energy levels. Moreover, it provides a flexible way to describe the thermodynamic consistency and realistic energy distributions of an adsorbate-adsorbent system.~~

The dual-site Langmuir model (DSL model) assumes two types of adsorption sites with different energy levels based on the Langmuir isotherm model [20]. Since the surface of the carbon-based adsorbent is heterogeneous, the model can fit the experimental adsorption isotherm considering realistic energy distributions of an adsorbate-adsorbent system. In addition, it has a flexible mathematical form for pure-gas and multi-component adsorption.

- ✓ **Marked manuscript page 13, line 11 (Changed and added):**

The experimental isotherm data for N_2O, O_2, and N_2 adsorption are listed in the Appendix (Tables 1−3) **because the isotherm parameters given in the study should be re-optimized to model accurately adsorptive processes, considering the partial pressure of each component of the effluent gases. Therefore,** the raw data are useful for other types of isotherm model studies and the design of adsorptive processes.

Editors:

I deeply appreciate your comments.

Overall Comment: I have received comments from reviewers on your manuscript. Your paper should become acceptable for publication pending suitable minor revision and modification of the article in light of the appended reviewer comments.

- **Response:** Thank you for your comments. I have checked all the contents again. I am so sorry that I found a mistake in the figure caption (Figure 8).

✓ **Marked manuscript page 19, line 7 and figure captions (changed):**

Figure 10. Experimental uptake curves, non-isothermal adsorption model, and isothermal dual resistance model for adsorption of gases on AC (a) at 293 K and on CMS (b) at 308 K: solid line, non-isothermal ~~sorption~~ **adsorption** model; dashed line, isothermal dual resistance model (data for N2 adsorption on AC at 293 K are taken from the literature [45])

✓ **References (added):**

[48] H. Qinglin, S.M. Sundaram, S. Farooq, Revisiting Transport of Gases in the Micropores of Carbon Molecular Sieves, Langmuir, 19 (2003) 393-405.

Equilibrium and kinetics of nitrous oxide, oxygen and nitrogen adsorption on activated carbon and carbon molecular sieve

Dooyong Park[1], Youngsan Ju[1], Jeong-Hoon Kim[2], Hyungwoong Ahn[3,], Chang-Ha Lee[1,*]*

[1]Department of Chemical and Biomolecular Engineering, Yonsei University, Seoul, Republic of Korea

[2]Carbon Resources Institute, Korea Research Institute of Chemical Technology, Daejeon, Republic of Korea

[3]School of Engineering, Institute for Materials and Processes, The University of Edinburgh, Edinburgh, UK

ABSTRACT

To evaluate candidate adsorbents for the recovery of nitrous oxide (N_2O) from adipic acid off-gases, the equilibrium and kinetics of N_2O and O_2 adsorption on activated carbon (AC) and of N_2O, O_2, and N_2 adsorption on a carbon molecular sieve (CMS) were evaluated at 293, 308, and 323 K under pressures up to 1000 kPa using a high-pressure volumetric system. Adsorption amount of N_2O on AC and CMS exceeded those of N_2 and O_2, and the adsorption isotherms for O_2 and N_2 were similar. The experimental N_2O and O_2 uptakes on AC and CMS were fitted to a non-isothermal adsorption model, whereas the model was ineffective for predicting N_2 uptake on CMS. The isothermal dual-resistance model, considering surface barrier resistance and pore diffusion, adequately predicted N_2 uptake on CMS. The rate of adsorption of N_2O on AC was much lower than that of O_2 and N_2 whereas the rate of adsorption on CMS flowed the order: $O_2 > N_2O >> N_2$, even though N_2O has higher adsorption affinity and smaller kinetic diameter than O_2. The Lewis structure of N_2O was also found to influence the adsorption kinetics.

KEYWORDS: Adsorption, activated carbon, carbon molecular sieve, nitrous oxide, non-carbon dioxide green-house gas

1. Introduction

N_2O is emitted as a by-product in the second-stage of adipic acid production and is one of the essential materials for the production of synthetic fibers such as nylon-6/6 [1]. N_2O is widely used in medical applications, especially in surgery and dentistry where it is considered the most effective and safe anesthetic and analgesic [2]. It also is used as a multi-purpose propellant in rocket engines [3]. In recent years, high-purity nitrous oxide (99.999%) has been used in the semiconductor and optical industries [4]. However, because N_2O is considered a non-CO_2 greenhouse gas and a dominant ozone-depleting substance, it must be recovered from effluent gas for the mitigation of global climate change.

Typical compositions of effluent gas from adipic acid production processes are reported as N_2O/ NO_x /CO_2/ CO/O_2/H_2O/N_2/VOC; 30.5/0.7/6.0/0.03/3.9/2.0/57.0/0.03 mol.% [1] and N_2O/NO_2/N_2/O_2/H_2O; 23/17/47/7.5/3.0 mol.% [5]. After pretreating the effluent gas, the mixture of N_2O, O_2, N_2, and/or CO_2 is supplied to a N_2O recovery unit. The selection of proper adsorbents is crucial for the design of effective adsorptive cyclic processes for achieving efficient recovery of N_2O. The characteristics of N_2O adsorption on various adsorbents have been investigated by employing adsorption isotherms, models (Langmuir, Freundlich, and Toth models), and by investigating the experimental N_2O uptake on zeolites such as 4A and 13X [6]. The adsorption isotherms of N_2O on three different activated carbons have also been studied at various temperatures up to 100 kPa [7], and the adsorption isotherms and rate were evaluated using the linear driving force model for N_2O adsorption on carbon molecular sieves (CMSs) in the pressure range of 0−9 kPa [8]. The adsorption isotherms and isosteric heats of adsorption [9] and experimental uptake [10] of N_2O on natural zeolites such as erionite, mordenite, and clinoptilolite have also been reported. Comparative evaluation of the adsorption equilibrium and kinetics of N_2O on MOF-5, MOF-177, and zeolite 5A [11], and on ordered mesoporous carbon [12] were conducted

Multiple adsorbents have been simultaneously utilized in attempts to enhance the adsorptive cyclic processes [13-15]. The separation mechanism is dependent on the adsorbates and adsorbents, where equilibrium separation and/or kinetic separation contribute to various extents [15, 16]. To achieve equilibrium separation, adsorption isotherm data for candidate adsorbents up to the partial pressure of each gas in an effluent mixture are valuable for the

design of adsorptive cyclic processes, but accurate adsorption isotherm data in the low pressure region are also critical for evaluating the separation performance.

The Fickian diffusion-type model, i.e., non-isothermal diffusion model, is one of the most rigorous chemical potential driving force models for evaluating separation kinetics, and is often used for analyzing the adsorption rate based on the adsorption uptake curves [17]. If the adsorption rate significantly depends on the characteristics of adsorbent/adsorbate system, the application of model considering various adsorption resistances becomes more important to interpret the adsorption rate of the system. In CMS pellets with a bidisperse structure of macropore and micropore, the adsorption rate is typically known as the micropore diffusion control. However, the diffusion mechanism in CMS, especially in micropore diffusion, is still not fully understood [18, 19].

In this study, we evaluate the adsorption equilibrium and kinetics of N_2O, O_2, and N_2 on activated carbon (AC) and a carbon molecular sieve (CMS), as representative carbon-based adsorbents for equilibrium and kinetic separation, respectively. The adsorption isotherms measured at 293, 308 and 323 K up to 1000 kPa are fitted to both the dual-site Langmuir model and Sips model, and the isosteric heat of adsorption is calculated by applying the Clausius–Clapeyron equation. The adsorption kinetics via micropore diffusion are analyzed from the experimental uptake curves by applying the non-isothermal adsorption model and isothermal dual-resistance model. **The parameters showed a reasonable change with variations in the experimental conditions.** Finally, the obtained model parameters and experimental raw data are compiled as contributions to the database for evaluating the feasibility of adsorbents and for the design of adsorptive cyclic processes for N_2O separation.

2. Adsorption model

2.1 Adsorption isotherm models

The dual-site Langmuir model (DSL model) assumes two types of adsorption sites with different energy levels based on the Langmuir isotherm model [20]. Since the surface of the carbon-based adsorbent is heterogeneous, the model can fit the experimental adsorption isotherm considering realistic energy distributions of an adsorbate-adsorbent

system. In addition, it has a flexible mathematical form for pure-gas and multi-component adsorption.

$$q = \frac{q_{m,d1} b_{d1} P}{1 + b_{d1} P} + \frac{q_{m,d2} b_{d2} P}{1 + b_{d2} P} \tag{1}$$

$$b_{d1} = k_{d1} * exp(k_{d2}/T) \tag{2}$$

$$b_{d2} = k_{d3} * exp(k_{d4}/T) \tag{3}$$

In Equations (1)−(3), $q_{m,d1}$, $q_{m,d2}$, and b_{d1}, b_{d2} are parameters for the DSL model, where the former two represent the amount of adsorbate at equilibrium adsorption for each site, and b_{d1} and b_{d2} indicate the affinity of each site for the adsorbate (hereafter, the adsorption affinity).

In this study, the Sips model was also applied to the experimental isotherms. Although the model lacks thermodynamic consistency [21], it is widely used in the design of adsorptive processes due to its simplicity and accuracy.

$$q = q_{m,s} \frac{(b_s P)^{\frac{1}{n}}}{1 + (b_s P)^{\frac{1}{n}}} \tag{4}$$

$$b_s = k_{s1} * exp(k_{s2}/T) \tag{5}$$

$$1/n = k_{s3} + k_{s4}/T \tag{6}$$

Here, $q_{m,s}$, b_s, and n are parameters for the Sips equation; $q_{m,s}$ represents the amount of adsorbate at equilibrium and b_s indicates the adsorption affinity. The heterogeneity of the adsorption sites is represented by the parameter n.

The temperature-dependent adsorption affinity parameters were determined from the correlation of the experimental data with the DSL (Eqs. (1)−(3)) and Sips (Eqs. (4)−(6)) models. The deviation of the experimental data from the model was determined as the mean absolute percentage error (MAPE):

$$MAPE\ (\%) = \frac{100}{k} \sum_{i=1}^{k} \left| \frac{q_{i,exp} - q_{i,model}}{q_{i,exp}} \right| \tag{7}$$

where, k is the number of the experimental data points, q_{exp} is the experimental data, and q_{model} is the value from the isotherm model.

The isosteric heats of adsorption of the components of a gas mixture are critical variables for the design of adsorption beds for gas separation [22] because this parameter affects the amount of adsorbate captured by the adsorbent (adsorption amount) and the adsorption kinetics. Therefore, the effect of the isosteric heat on the adsorption process is considered in determining the optimal conditions for the adsorptive separation process.

The isosteric heat of adsorption, Q_{st}, was calculated from the experimental data or isotherm models at different temperatures by using the Clausius-Clapeyron equation.

$$\frac{\Delta Q_{st}}{RT^2} = \left[\frac{\partial lnP}{\partial T}\right]_q \tag{8}$$

$$\frac{\Delta Q_{st}}{\mathbb{R}T^2} dT = dlnP \tag{9}$$

where, $\mathbb{R}$ is the gas constant.

It was reported that the adsorption forces for carbon-type adsorbents consist of $\Phi_{adsorbate\text{-}adsorbate}$ and $\Phi_{adsorbate\text{-}adsorbent}$ [23]. Since Q_{st} is affected by the surface coverage, the contribution of the interaction forces, $\Phi_{adsorbate\text{-}adsorbate}$ and $\Phi_{adsorbate\text{-}adsorbent}$, to adsorption can be analyzed from the changes in Q_{st} [24].

2.2 Kinetic models

Pelletized adsorbents characterized by micropores and macropores are widely used in adsorptive processes. Intra-crystalline (micropore) diffusion in adsorbent pellets generally plays a significant role in adsorptive separation processes [25]. However, when the adsorption heat is high, inter-crystalline (macropore) diffusion can contribute to the adsorption kinetics due to thermal resistance. Therefore, the kinetic mechanism must be investigated in detail, especially for kinetic separation agents (such as CMS).

A simple analytical solution for a constant volume system was developed by assuming isothermal conditions and a linear equilibrium relationship [26]. However, the adsorption process is accompanied by the generation of isosteric heat. Since the adsorption heat dissipated

to the surroundings affects the uptake curve, the adsorption kinetics can be strongly controlled by heat transfer through the surface [27]. Therefore, a non-isothermal adsorption model based on the following assumptions is suggested [25, 27]:

1. The adsorbent consists of uniform spherical particles.
2. Micropore diffusion is the only significant resistance to mass transfer. Therefore, the concentration of the adsorbate at the surface of each particle is always in equilibrium.
3. Heat conduction through the particle is sufficiently fast, and the only significant heat transfer resistance is heat dissipation at the external surface
4. The equilibrium relationships are linear, and the micropore diffusivity is constant (temperature-independence).

Subject to the above approximation, the uptake curve for non-isothermal adsorption can be described as:

$$\frac{m_t - m_0}{m_\infty - m_0} = 1 - \sum_{n=1}^{\infty} \frac{9\left(1 + K\frac{V_s}{V_g}\right)\left[\frac{Y_n}{-\beta_n^2}\right]^2 exp\left(-\beta_n^2 \frac{D}{R^2} t\right)}{\frac{1}{\varphi_n} + \frac{3\beta'}{2\varphi_n}\left[\beta_n cot\,\beta_n\left(\frac{Y_n}{\beta_n^2}\right) + 1\right] + \frac{3}{2}K\frac{V_s\ 1\ A_n}{V_g \beta_n^4 \varphi_n}} \tag{10}$$

where β_n is given by the roots of:

$$(-\beta_n + \alpha) + 3\beta Y_n - 3K\frac{V_s\ 1}{V_g \beta_n^2}(-\beta_n + \alpha)Y_n = 0 \tag{11}$$

and

$$A_n = Y_n\left[(\beta_n^2 - \alpha)\beta_n cot\beta_n - 2\alpha\right] + \beta_n^2(\beta_n^2 - \alpha) \tag{12}$$

$$Y_n = \beta_n cot\beta_n - 1 \tag{13}$$

$$\frac{1}{\varphi_n} = \frac{1}{\beta}\left(1 - 3K\frac{V_s Y_n}{V_g \beta_n^2}\right) \tag{14}$$

In Equation (10), m_t, m_0, and m_∞ represent the adsorption amount at time t, at the initial time 0, and at equilibrium, respectively. K, defined as $(\Delta q \cdot \rho_p)/(\Delta P/\ \mathbb{R}\ T)$, is the equilibrium constant. V_s and V_g are the adsorbent volume and gas phase volume, respectively.

When micropore diffusion dominates, the diffusion time constant (D/R^2) consists of micropore diffusivity and the micropore particle radius (D_c/r^2). On the other hand, when macropore diffusion dominates, the diffusion time constant can be presented by macropore diffusivity and the adsorbent pellet radius (D_p/R^2). In this study, since micropore diffusion dominates the adsorption rate for both adsorbents, the diffusion time constant is described as (D_c/r^2). The details are presented below in the discussion of the experimental data.

The non-isothermal adsorption model involves two dimensionless parameters, α and β. When α tends to infinity or β approaches 0, the effect of mass transfer dominates and the thermal effect becomes negligible [25, 27].

$$\alpha = \left(\frac{ha}{\rho_p C_p}\right) \Big/ \left(\frac{D_c}{r^2}\right) \tag{15}$$

$$\beta = \frac{\Delta Q_{st}}{\rho_p C_p}\left(\frac{\partial q^*}{\partial T}\right)_{c_0, T_0} \tag{16}$$

Here, h is the overall heat transfer coefficient; a is the external surface area per unit volume; D_c is the micropore diffusivity; r is the micropore particle radius, ρ_p and C_p represent the density and heat capacity of the adsorbent respectively, ΔQ_{st} is the change in the isosteric heat of adsorption, and $\partial q^*/\partial T$ is the temperature dependence of the adsorption capacity at equilibrium. Using these equations, two parameters (α and β, described below) can be derived from the physical properties and adsorption data. However, the heat transfer, mass transfer, and generated heat also have a complex influence on the adsorption rate.

The parameter α is the ratio of the heat transfer ($ha/\rho_p C_p$) to diffusion time constant (D_c/r^2). As a descriptor of the heat transfer, a large α value indicates that the heat dissipates to the surroundings rapidly and the molecules diffuse slowly. On the other hand, a small α value indicates that the heat dissipates to the surroundings slowly and the molecules diffuse rapidly.

The parameter β is the product of the isosteric heat of adsorption ($\Delta Q_{st}/\rho_p C_p$) and the temperature dependence of the adsorption capacity at equilibrium ($\partial q^*/\partial T$). Until the generated heat is fully dissipated out of the system, the retained heat changes the equilibrium and the behavior of the uptake curve. Under the above limiting conditions, the uptake curve assumes an asymptotic form [27]:

$$\frac{m_t - m_0}{m_\infty - m_0} = 1 - \frac{\beta}{1+\beta}\ exp\left[\frac{-hat}{\rho_p C_p(1+\beta)}\right] \tag{17}$$

Values of α and β in the non-isothermal adsorption model have been suggested in many cases by fitting the experimental uptake curves. However, as shown in Eqs. (15) and (16), the parameters can be theoretically calculated. In this study, the theoretical values of α and β were calculated from the physical properties of the gas molecules and adsorbents as a first step. By using these theoretical values as initial values, the parameters α and β in the non-isothermal adsorption model were re-estimated via non-linear regression of the experimental uptake curves within a range similar to that of the calculated values. Thus, the parameters (α and β) were analyzed by considering the effects of heat transfer, mass transfer, and the isosteric heat of adsorption.

When the contribution of the surface barrier resistance to the overall kinetics cannot be neglected, there is a large deviation between the micropore diffusion model results and the experimental data. An isothermal dual-resistance model combining micropore diffusion resistance and surface barrier resistance was suggested as follows [28]:

$$\frac{m_t - m_0}{m_\infty - m_0} = 1 - \sum_{n=1}^{\infty} \frac{6L^2 exp\left(-\delta_n^2 \frac{D_c}{r^2} t\right)}{\delta_n{}^2(\delta_n{}^2 + L(L-1))} \tag{18}$$

$$\delta_n cot\delta_n + L - 1 = 0 \tag{19}$$

$$L = \frac{k_f r}{D_c K} = \frac{k_f r}{D_m} \times \frac{D_m}{D_c K} = \frac{Sh}{2} \times \frac{D_m}{D_c K} \tag{20}$$

where, δ_n represents the roots of the equation, k_f is the film mass transfer coefficient and Sh is the Sherwood number. D_c and D_m are the micropore diffusivity and molecular diffusivity, respectively. The molecular diffusivity was calculated from both the Knudsen diffusivity (D_K) and viscous diffusivity (D_v) [29].

$$D_K = \frac{2}{3} R \sqrt{\frac{8\mathbb{R}T1}{\pi M\ \zeta}} \tag{21}$$

$$D_v = \frac{PR^2}{8\eta} \tag{22}$$

$$D_m = \frac{\varepsilon_P(D_K + D_v)}{\tau(\varepsilon_P + (1 - \varepsilon_P)K)} \tag{23}$$

where, ζ is the diffuse reflection coefficient, η is the viscosity, τ is the tortuosity, and ε_P is the porosity. The tortuosity was assumed to be 1/porosity.

The diffusivity when the adsorption amount is low is called the corrected diffusivity [28]. The thermodynamic correction factor ($d\ln P/d\ln q$) calculated from the Sips isotherm model becomes:

$$\begin{aligned}\frac{\boldsymbol{dlnq}}{\boldsymbol{dlnP}} &= \frac{\mathbf{1}\boldsymbol{d}\mathbf{ln}\,(\boldsymbol{bP})}{\boldsymbol{n}\ \ \boldsymbol{dlnP}} - \frac{\boldsymbol{dln}\left(\mathbf{1} + (\boldsymbol{bP})^{\frac{\mathbf{1}}{\boldsymbol{n}}}\right)}{\boldsymbol{dlnP}} \\ &= \frac{\mathbf{1}}{\boldsymbol{n}} - \frac{\mathbf{1}}{\boldsymbol{n}}\left(\frac{(\boldsymbol{bP})^{\frac{\mathbf{1}}{\boldsymbol{n}}}}{\mathbf{1} + (\boldsymbol{bP})^{\frac{\mathbf{1}}{\boldsymbol{n}}}}\right) \\ &= \frac{\mathbf{1}}{\boldsymbol{n}}(\mathbf{1} - \boldsymbol{\theta})\end{aligned} \tag{24}$$

$$D = D_0\frac{d\ln P}{d\ln q} = D_0\frac{n}{1 - \theta} \tag{25}$$

where, D_0 is the corrected diffusivity and θ is defined as ($q/q_{m,s}$). In this study, D corresponds to D_c.

The parameters of both kinetic models were obtained from the experimental uptake curves. Using MATLAB (Mathworks, Inc.), the incremental search method (ISM) and the secant method were used to find the roots of Equations (11) and (19). The least-squares method was then used for non-linear regression of Equations (10) and (18).

3. Experimental section

3.1. Materials

Activated carbon (AC, 2GA-H2J) and carbon molecular sieves (CMS, GN-UC-H) were supplied by KURARAY CHEMICAL Co., Japan. The physical properties of AC and CMS were evaluated from the N_2 adsorption isotherm at 77 K for AC and the CO_2 adsorption isotherm at 293 K for CMS using a volumetric sorption analyzer (Autosorb IQ, Quantachrome

Corporation). The macropore characteristics of CMS were investigated via mercury porosimetry (PM33GT, Quantachrome Corporation). The Brunauer–Emmett–Teller (BET) theory and Dubinin-Radushkevitch (DR) equation were applied to the adsorption isotherms.

The surface area of AC and CMS was 1306.4 and 640.9 $m^2 g^{-1}$, respectively. As shown in Figure 1, CMS contained macropores that were developed during pelletization. **Figure 2 showed the pore size distribution and cumulative pore volume of AC and CMS. The micropores of AC were distributed around 0.35 nm and 0.52 nm, ultra micropore region, and 1.17 nm and 1.33 nm in the N_2 adsorption analysis.** The pores of CMS were distributed within **two ranges: 0.3−0.4 nm and 0.4−0.7 nm. Especially, the CMS showed relatively narrower pore size distribution than AC.** The detailed physical properties of the adsorbents are listed in Table 1.

The properties of the adsorbate gases are listed in Table 2. N_2O (kinetic diameter: 330 pm), O_2 (kinetic diameter: 346 pm), and N_2 (kinetic diameter: 364 pm) were all of 99.999% purity, and were supplied by CHEMGAS KOREA, Daedeok Gas Co. and DAESUNG Industrial Gases Co., Korea. The adsorbate gases were used in the experiments without further purification.

Figure 1. (a) Macropore size distribution and (b) cumulative volume of CMS, determined via mercury porosimetry

Figure 2. Cumulative pore volume and pore size distribution of AC and CMS from the density functional theory (○ and ●, activated carbon; △ and ▲, carbon molecular sieve [30]; closed symbol for cumulative pore volume; open symbol for pore size distribution)

Table 1. Physical properties of adsorbents

Table 2. Properties of adsorbate gases

3.2. Volumetric experiments

The adsorption isotherms and uptake curves were constructed from the data acquired by using a high-pressure adsorption system (BELSORP-HP, Japan); a schematic diagram of the volumetric system is presented in Figure 3. Two high accuracy absolute pressure

transducers were installed in the adsorption system. One pressure transducer (PT1: PMP 4015, DRUCK Inc., USA; full scale: 0.133 MPa (abs)) was used in the low-pressure range (up to 90 kPa) and the other (PT2: PMP 4015, DRUCK Inc., USA; full scale: 12.1 MPa (abs)) was used in the high-pressure range (up to 1000 kPa). The degree of uncertainty for both pressure transducers was within ±0.08% of each full-scale range. The temperature of the internal high-pressure system was kept constant with a system temperature controller. The temperature of the adsorption cell located outside the system was kept constant using a water-bath circulator (F25-ME, Julabo, Germany). The measured temperature and pressure of the system were recorded automatically during the uptake experiments. The adsorption amount was determined from the virial equation using the temperature, pressure, and compressibility factor from NIST [31].

Figure 3. Schematic diagram of high-pressure adsorption system

Prior to the adsorption experiments, the adsorbents were activated by heating in an oven (OV-11, JEIO TECH, Korea) for 8 h at 423 K under vacuum (GLD-136C vacuum pump, ULVAC KIKO Inc., Japan). Once the adsorbents were activated, the mass was measured with a microbalance (AND, HR-200, Japan) having an accuracy of ±10 μg. The adsorbent was placed into the adsorption cell with a VCR gasket (SS-8-VCR-2-GR-5M, Swagelok, USA). After installing the adsorption cell in the system, the adsorbent was again evacuated under the same conditions described above to remove any possible contaminants transferred during the assembly. After the in-situ activation, the system was purged with helium gas and evacuated with a vacuum pump. The adsorbate was then supplied to the adsorption cell through a controlled needle valve. The uptake experiment was allowed to proceed until the system pressure change was within 0.1% of the full-scale range for 500 s. However, the uptake of N_2 on CMS was evaluated over 5400 s under each condition due to the slow adsorption rate.

The amount adsorbed at each pressure step was calculated from the measured temperature, pressure, and system volume. When the adsorption cell reached the equilibrium state ($P_{e,\,i}$), the adsorption cell was isolated by closing a pneumatic valve connected to the system. Subsequently, the adsorbate gas was injected into the system (dosing cell) for another uptake run. The gas phase pressure of the system was changed from $P_{e,\,i}$ to $P_{0,\,i+1}$. At $t = 0$ (the initial point of the i+1th step), when the pneumatic valve linked to the adsorption cell was opened, the pressure of the adsorption cell was determined as:

$$P_{0,i+1}{}' = \frac{P_{e,\ \ i} \times V_{cell} + P_{0,i+1} \times V_{system}}{V_{cell} + V_{system}} \quad \textbf{(26)}$$

The adsorption cell gradually reached the i+1th equilibrium state ($P_{e,\ i+1}$). The experimental reproducibility within 2% was confirmed from duplicate equilibrium experiments.

4. Results and discussion

4.1. Adsorption equilibria

The adsorption of N_2O and O_2 on AC and that of N_2O, O_2, and N_2 on CMS were evaluated in the temperature and pressure range of 293−323 K and 0−1000 kPa, respectively, by a volumetric method. Figure 4 presents the isotherms for N_2 adsorption on AC from a previous study [30] for comparison with the present isotherms. In the experimental pressure range, the isotherms of N_2O, O_2, and N_2 were of Type 1 based on the IUPAC classification. The experimental isotherm data for N_2O, O_2, and N_2 adsorption are listed in the Appendix (Tables 1−3) **because the isotherm parameters given in the study should be re-optimized to model accurately adsorptive processes, considering the partial pressure of each component of the effluent gases. Therefore,** the raw data are useful for other types of isotherm model studies and the design of adsorptive processes.

The amount of gases adsorbed on AC and CMS and the heats of adsorption for N_2O, O_2, and N_2 are compared with the results from previous studies in Figure 4 and Table 3. Although the manufacturers and physical properties differed for the carbon materials, the results were reasonably similar to those of previous studies. The isotherm data in Figure 4 are comparable with the isotherms of the (a) N_2O/AC [7], (a) CO_2/AC [32], (b) CO_2/CMS [30], (c) O_2/AC [33] and (f) N_2/CMS [34] systems from previous studies. Since the adsorption isotherm data of N_2O on AC were limited in the low pressure range, a comparison is presented in the inset of Figure 4 (a).

N_2O was strongly adsorbed on both adsorbents, and to a greater extent than O_2 and N_2. At 1000 kPa, the difference in the amount of N_2O versus the other gases adsorbed was much higher with AC than with CMS. The amount of O_2 adsorbed on AC was slightly higher than the amount of N_2, whereas the amount of O_2 and N_2 adsorbed on CMS was comparable.

Figure 4. Experimental adsorption isotherms and DSL model for AC and CMS: ●, 293 K; ▲, 308 K; ■, 323 K; (e) N_2/AC [32]; solid line, DSL model (○, N_2O/AC at 323 K [7]; △, CO_2/AC at 323 K [32]; □, CO_2/CMS at 318 K [30]; +, O_2/AC at 303 K [33]; x, N_2/CMS at 323 K [34])

Table 3. Comparison of adsorption equilibrium parameters for N_2O, O_2, and N_2

The adsorption of N_2O, O_2, and N_2 on AC (170, 125, and 135%) was greater than that on CMS at 1000 kPa. This difference mainly resulted from the higher surface area and pore volume of AC, as indicated in Table 1. Furthermore, even though the molar mass of N_2O and CO_2 is the same, more N_2O than CO_2 was adsorbed on both adsorbents, as shown in Figures 4 (a) and (b), where the difference was more pronounced when using AC. The difference in the adsorption amount of N_2O between AC and CMS was prominent even in the low pressure region (<100 kPa). However, the difference in the O_2 and N_2 adsorption on both adsorbents was minute, with almost linear isotherms in the low pressure region (inset of Figure 4).

The experimental data were fitted to the DSL and Sips models, and the model parameters are listed in Table 4. As shown in Figure 4, the DSL model was adequate for predicting the experimental isotherms for both adsorbents. The mean absolute percentage errors (MAPEs) for N_2O, O_2, and N_2 adsorption on AC were 2.68, 0.50, and 1.24%, respectively, for the DSL model and 2.40, 1.68, and 1.82%, respectively, for the Sips model. The MAPEs for N_2O, O_2, and N_2 adsorption on CMS were 1.50, 0.29, and 0.40%, respectively, for the DSL model and 1.57, 2.12, and 2.20%, respectively, for the Sips model. For both adsorbents, the experimental values fit slightly better to the DSL model than the Sips model.

Table 4. Parameters for dual-site Langmuir and Sips models

The parameters from the DSL model can be used to interpret the $\Phi_{adsorbate\text{-}adsorbate}$ and $\Phi_{adsorbate\text{-}adsorbent}$ contributions to the adsorption process [23]. In the experimental range, the parameter $q_{m,\,d1}$ was greater than $q_{m,\,d2}$, and b_{d1} was smaller than b_{d2} (Table 4). It indicates that more molecules are adsorbed at adsorption site 1 than at adsorption site 2, whereas they are more strongly adsorbed at adsorption site 2 than at adsorption site 1. The initial adsorption was mainly affected by the strong adsorption site (site 2), with a large $\Phi_{adsorbate\text{-}adsorbent}$ value, and thereafter, more molecules were adsorbed on the weak adsorption sites (site 1) with increasing $\Phi_{adsorbate\text{-}adsorbate}$. The difference between the $q_{m,\,d1}$ value for AC and CMS was large (over 180%

in the experimental range, Table 4). This is consistent with the micropore volume of AC being over 150% higher than that of CMS. On the other hand, considering the difference in the surface area (200% difference, Table 1), the difference in the $q_{m,\ d2}$ value for both adsorbents was relatively small.

The isosteric heats of adsorption (Q_{st}) calculated from the Clausius-Clapeyron equation are presented with the surface coverage in Figure 5. If different surface energy levels exist and the interactions between the adsorbed molecules cannot be neglected, Q_{st} varies with the surface coverage [38]. For both adsorbents, the Q_{st} of N_2O was much higher than that of O_2 and N_2. The decrease in Q_{st} with increasing surface coverage was relatively smaller for CMS than for AC. In addition, with both adsorbents, a very small linear decrease in Q_{st} was observed for O_2 and N_2 adsorption with increasing surface coverage. The Q_{st} values for the adsorption of both gases on AC were almost the same, whereas that for O_2 on CMS was higher than that of N_2 because the paramagnetic properties of O_2 might induce strong spin-spin interaction between the molecules in the pores of CMS [38, 41].

$\Phi_{adsorbate\text{-}adsorbent}$ was initially dominant for both adsorbents. However, with increasing surface coverage, $\Phi_{adsorbate\text{-}adsorbate}$ contributed more to the adsorption for AC than for CMS. This difference might be derived from the difference in the micropore volume of the two adsorbents because more molecular layers can be formed in the pores of AC.

Figure 5. Isosteric heats of adsorption for AC (a) and CMS (b): solid line, N_2O; dotted line, O_2; dashed line, N_2

4.2. Adsorption Kinetics

The kinetics of N_2O, O_2, and N_2 adsorption on AC and CMS were analyzed by using the volumetric experimental uptake data. First, to clarify the dominant diffusion mechanism during adsorption on AC and CMS, N_2O adsorption experiments were performed with AC and CMS samples of different sizes, i.e., particles (200−500 μm) and pellets. The average radius of the pelletized AC and CMS samples were 2.0 and 1.4 mm, respectively. As shown in Figure 6, the difference in the experimental uptake curves for the particle and corresponding pellet samples of AC and CMS was minute within a similar pressure range. The difference in the

diffusional time constant from the uptake curves of the particle and corresponding pellet sample was also very small. This suggests that the contribution of macropore diffusion to adsorption was insignificant, and the micropore diffusion mechanism dominated the adsorption kinetics.

Figure 6. Experimental uptake curves for N_2O on AC (a) and CMS (b) at 308 K (closed symbol, particle (200−500 μm); open symbol, pellet)

The experimental uptake curves of adsorption and desorption for N_2O at 308 K were compared in Figure 7. Within the pressure range of lower than 80 kPa for the kinetic analysis, both uptake curves were well coincided with each other, indicating the reliability of pressure step change in the study. The experimental uptake curves were predicted using the non-isothermal adsorption model (Eq. 10) and the D_c/r^2 (micropore diffusion time constant) was obtained. The uptake curves, predicted by the non-isothermal adsorption model for N_2O and O_2, are shown in Figure 8, and the micropore diffusion time constant and parameters are listed in Tables 5 (AC) and 6 (CMS). In the early stage of adsorption, the slope of the experimental uptake curve was steeper at higher pressure, but under higher pressures over longer periods, the curvature was greater. These characteristics were more prominent for AC than CMS.

Figure 7. Experimental uptake curves of adsorption and desorption for N_2O on (a) AC and (b) CMS at 308 K: ●, adsorption; △, desorption

Figure 8. Experimental uptake curves and non-isothermal adsorption model for AC ((a) and (c)) and CMS ((b) and (d)) at 308 K: solid line, non-isothermal adsorption model

Table 5. Micropore diffusion time constant and parameters for AC from non-isothermal adsorption model

Table 6. Micropore diffusion time constant and parameters for CMS from non-isothermal adsorption model

The model parameters, α and β, were **reasonably** estimated from the properties of the **adsorbent and adsorbate** and the experimental adsorption data**, not just by fitting the**

experimental uptake curves. The parameter α, $((h\alpha/\rho_s C_s)/(D_c/r^2))$, is the ratio of the heat transfer term to the mass transfer term. Since the mass transfer term, D_c/r^2, increased with increasing pressure in the experimental region, the parameter α generally decreased with increasing pressure. Further, for both adsorbents, α was greater for N_2O than for O_2 because of the substantial difference in the mass transfer rate of the two molecules. Moreover, the variation of α with pressure was relatively small for O_2 on both adsorbents. In addition, the α values for O_2 adsorption on CMS were higher than those for adsorption on AC, and the variation in α values for N_2O with pressure was more significant for adsorption on AC. On the other hand, the heat transfer term, $h\alpha/\rho_s C_s$, was relatively constant for each adsorbent.

The parameter β, $((Q_{st}/\rho_s C_s)\cdot(\partial q^*/\partial T))$, representing the thermal effects, increased with increasing pressure in the experimental range. For both adsorbents, the absolute value of $\partial q^*/\partial T$ (the temperature-dependence of the adsorption capacity at equilibrium) increased with increasing pressure. In the early stage of adsorption, the adsorption capacity decreased due to the exothermic nature of the adsorption (Q_{st}) process. Therefore, time was required to reach the adsorption equilibrium, governed by the equilibrium temperature. Since the curvature of the uptake curve corresponds to the Q_{st} and $\partial q^*/\partial T$ data, it also depends on the amount of substrate adsorbed, where the generated heat of adsorption causes the uptake curve to bend earlier at high pressure than at low pressure. The parameter β for N_2O was greater than that for O_2 as more of the former gas was adsorbed with higher heat of adsorption, which implies stronger interaction for N_2O adsorption. However, the difference in the β values for each adsorbate on AC and CMS was insignificant. Furthermore, the absolute values and variation of β for O_2 was minute, as shown in Tables 5 and 6.

For N_2 adsorption on CMS, the experimental uptake curves were almost linear (Figure 9). The slope of the uptake curves was slightly steeper at higher pressure, but the difference was small under the various pressure conditions. The values of D_c/r^2 for N_2 adsorption on CMS could be obtained from the non-isothermal adsorption model when the physical property parameters (α and β) were used as fitting parameters. However, the values of α and β were far from the calculated theoretical values at the experimental pressures and temperatures. Furthermore, when a reasonable range of α and β values was applied to the N_2 uptake curves of CMS, large deviations were observed (Figure 9). This deviation indicates that the non-isothermal adsorption model was not adequate for describing the kinetics of **the** N_2 adsorption

on CMS, and **the surface barrier resistance as well as the pore diffusion resistance should be considered for** the adsorptive uptake **of N_2 in the experimental range. It was also reported that the surface barrier resistance rise to a measurable level for O_2 on CMS at low temperature, 248 K (Table 8) [48]. It implies that the transport mechanism in small pores can be changed by experimental conditions.**

Figure 9. Experimental uptake curves, non-isothermal adsorption model, and isothermal dual resistance model for N_2 on CMS: solid line, non-isothermal adsorption model; dashed line, isothermal dual resistance model

The data shown in Figure 9 suggest that N_2 adsorption on CMS was firstly controlled by the pore mouth when N_2 diffused through the micropore. Herein, the dual-resistance model (Eq. 18) was applied to the experimental uptake curves. This model utilizes the parameter L (D_m/D_cK), representing the ratio of micropore resistances to the surface barrier resistance [28], which can be estimated from the Sherwood number (Sh), equilibrium constant (K), and molecular diffusivity (D_m). The Sherwood number was considered as 2 because the molecules were adsorbed in the stagnant fluid. The equilibrium constant, K, was calculated from the experimental data, and the molecular diffusivity was estimated from Equations (21)–(23). Figure 9 shows that the isothermal dual-resistance model could accurately predict the uptake curves for N_2 in CMS. The diffusion time constant and parameter L are presented in Table 7. The micropore diffusion time constant, D_c/r^2, increased reasonably with pressure and temperature.

Table 7. Micropore diffusion time constant and parameters for N_2 adsorption on CMS using isothermal dual resistance model

Table 8. Comparison of diffusion time constant and barrier mass transfer coefficient for N_2O, O_2, and N_2

The rate of adsorption of the gases on AC followed the order: $O_2 \geq N_2 >> N_2O$, where the corresponding order for CMS was $O_2 > N_2O >> N_2$. These orders are the same as those reported in previous studies (Table 8) in the experimental range. Interestingly, the rates of adsorption of O_2 and N_2 on AC were much faster than the corresponding values for CMS,

whereas the rate of adsorption of N_2O was similar for both adsorbents. Furthermore, although the kinetic diameter of N_2O is smaller than those of O_2 and N_2 (see Table 2) and the adsorption affinity of the adsorbents for N_2O was much higher than for the other gases. N_2O adsorbed more slowly on AC than the other gases and more slowly on CMS than O_2, as shown in Figure 10. The heat resistance in the macropores is not sufficient for explaining these trends, as mentioned in relation to Figure 6.

Figure 10. Experimental uptake curves, non-isothermal adsorption model, and isothermal dual resistance model for adsorption of gases on AC (a) at 293 K and on CMS (b) at 308 K: solid line, non-isothermal **adsorption** model; dashed line, isothermal dual resistance model (data for N_2 adsorption on AC at 293 K are taken from the literature [45])

The kinetic diameter is related to the mean free path of a molecule in a gas, which is an indication of the size of the molecule as a target [46]. Therefore, the kinetic diameter is not the same as the atomic diameter, defined in terms of the size of the atom's electron shell, which is usually much smaller. Rather, it is the size of the sphere of influence that can lead to a scattering event. However, the adsorption rate is influenced by various factors such as the molecular size, structure, and electronic properties [8, 38]. Therefore, the kinetic diameter does not adequately account for the observed the adsorption rates.

Elemental nitrogen (N≡N) has an extremely strong triple bond, and the second strongest bond in any diatomic molecule after carbon monoxide. Therefore, N_2 adsorption on CMS, where N_2 has the largest kinetic diameter, was restricted in the pore mouth because of the adsorbent geometry and kinetic diameter. On the other hand, N_2O has a magnetic susceptibility of 18.9×10^{-6} cm^3 mol^{-1}. Furthermore, the Lewis structure of N_2O reportedly has mobile electrons, usually in pairs that can be moved to generate valid structures [47]. The linear and asymmetric molecule, which has a permanent dipole moment, presents three fundamental vibrational modes (symmetric stretch, asymmetric stretch, and bend) (Table 2). Based on these results, the Lewis structure of N_2O and the heat of adsorption might affect the adsorption rate in both adsorbents, whereas adsorption on AC (with relatively large micropore diameters) was not affected by the kinetic diameter of N_2, unlike adsorption on CMS.

4. Conclusion

To evaluate candidate adsorbents for the adsorptive separation and recovery of N_2O from adipic acid off-gases, the equilibrium and kinetics of N_2O, O_2, and N_2 adsorption on AC and CMS were studied. The adsorption was experimentally evaluated by a volumetric method at 293−323 K under pressures up to 1000 kPa. The experimental isotherms were well fitted by the DSL model and Sips model. The amount of N_2O adsorbed and heat of adsorption were much greater than those for O_2 and N_2 with both adsorbents. For all the component gases, the Q_{st} values were slightly higher with CMS than with AC, although the amount of gas adsorbed was larger for AC than for CMS. Based on the adsorption model parameters and Q_{st}, the contribution of $\Phi_{adsorbate\text{-}adsorbate}$ to the adsorption of N_2O was higher with AC than with CMS.

For all the adsorbates, macropore diffusion in both adsorbents could be neglected. The kinetics of N_2O and O_2 adsorption via micropore diffusion in both adsorbents could be predicted by the non-isothermal adsorption model. **It also indicated that the surface barrier resistance on CMS was negligible in the experimental range.** On the other hand, due to the contribution of surface barrier resistance to N_2 adsorption on CMS, the non-isothermal adsorption model was unsuitable for this system. The dual-resistance model could provide a reasonable prediction of the uptake curves of N_2 in CMS. The parameters for both models were estimated within a theoretically reasonable range and the variation of these parameters with pressure and temperature was consistent. The D_c/r^2 values increased with increasing pressure and temperature for both adsorbents, regardless the type of model used.

The rate of adsorption followed the order: $O_2 \geq N_2 >> N_2O$ for AC and $O_2 > N_2O >> N_2$ for CMS. Since the adsorption affinity of both adsorbents for N_2O was the highest and the kinetic diameter of this gas was the smallest, it is hard to interpret trends in the rate of adsorption simply in terms of the kinetic diameter. The rate of adsorption could also be affected by the electrical properties of the adsorbates, such as the dipole/quadrupole moment and/or polarizability. Furthermore, it was expected that the Lewis structure of N_2O, i.e., the linear and asymmetric molecular structure, might affect the rate of adsorption on the carbon surface.

Nomenclature

		Unit
a	external surface area per unit volume of adsorbent	m^{-1}
A_n	solution of the Eq. (14) - (16)	-
b_{d1}	dual-site Langmuir isotherm model parameter	kPa^{-1}
b_{d2}	dual-site Langmuir isotherm model parameter	kPa^{-1}
b_L	Langmuir isotherm model parameter	kPa^{-1}
b_s	Sips isotherm model parameter	kPa^{-1}
C_s	heat capacity of the adsorbent	$J\ g^{-1}\ K^{-1}$
D_0	corrected diffusivity	$m^2\ s^{-1}$
D_c	micropore diffusivity	$m^2\ s^{-1}$
D_K	Knudsen diffusivity	$m^2\ s^{-1}$
D_m	molecular diffusivity	$m^2\ s^{-1}$
D_v	viscous diffusivity	$m^2\ s^{-1}$
D_c/r^2	micropore diffusion time constant	s^{-1}
$D_{c,0}/r^2$	corrected micropore diffusion time constant	s^{-1}
D_p/R^2	macropore diffusion time constant	s^{-1}
h	overall heat transfer coefficient	$J\ m^{-1}\ s^{-1}\ K^{-1}$
k	number of experimental data	-
k_f	mass transfer coefficient	$m\ s^{-1}$
K	equilibrium constant	-
k_{d1}	Dual-site Langmuir isotherm model parameter	kPa^{-1}
k_{d2}	Dual-site Langmuir isotherm model parameter	K
k_{d3}	Dual-site Langmuir isotherm model parameter	kPa^{-1}
k_{d4}	Dual-site Langmuir isotherm model parameter	K
k_{s1}	Sips isotherm model parameter	kPa^{-1}
k_{s2}	Sips isotherm model parameter	K
k_{s3}	Sips isotherm model parameter	-
k_{s4}	Sips isotherm model parameter	K
L	isothermal dual-resistance model parameter	-
m_0	adsorption amount at initial time 0	$mol\ kg^{-1}$
m_∞	adsorption amount at equilibrium	$mol\ kg^{-1}$
m_t	adsorption amount at ambient time t	$mol\ kg^{-1}$
n	Sips isotherm model parameter	-
P	pressure	kPa
q	adsorption amount	$mol\ kg^{-1}$
q_{cal}	adsorption amount calculated by isotherm model	$mol\ kg^{-1}$
q_{exp}	adsorption amount measured by experiment	$mol\ kg^{-1}$
$q_{m,d1}$	Dual-site Langmuir isotherm model parameter	$mol\ kg^{-1}$
$q_{m,d2}$	Dual-site Langmuir isotherm model parameter	$mol\ kg^{-1}$
$q_{m,s}$	Sips isotherm model parameter	$mol\ kg^{-1}$
Q_{st}	isosteric heat of adsorption	$kJ\ mol^{-1}$

r	micropore particle radius	m
R	adsorbent particle radius	m
$\mathbb{R}$	ideal gas constant	J mol^{-1} K^{-1}
Sh	Sherwood number	-
t	time	s
T	temperature	K
V_g	volume occupied by adsorbate	m^3
V_s	volume occupied by adsorbent	m^3
Y_n	solution of the Eq. (14) - (16)	-

Greek letters

α	non-isothermal kinetic model parameter defined by the Eq. (15)	-
β	non-isothermal kinetic model parameter defined by the Eq. (16) - (17)	-
β_n	solution of the Eq. (11)	-
δ_n	solution of the Eq. (18) - (19)	-
ε_P	porosity	-
ζ	diffuse reflection coefficient	-
η	viscosity	cP
τ	tortuosity	-
φ_n	solution of the Eq. (12) - (14)	-

Acknowledgement

This research is supported by the "R&D Center for reduction of Non-CO_2 Greenhouse Gases (2016001690005)" funded by Korea Ministry of Environment (MOE) as "Global Top Environment R&D Program"

AUTHOR INFORMATION

Corresponding Author

*Co-corresponding authors: leech@yonsei.ac.kr (C.-H. Lee), H.Ahn@ed.ac.uk (H. Ahn)

Tel.: +82 2 2123 2762; Fax: +82 2 312 6401

Funding

This research is supported by the "R&D Center for reduction of Non-CO_2 Greenhouse Gases (2016001690005)" funded by the Korea Ministry of Environment (MOE) as the "Global Top Environment R&D Program"

Declarations of interest: none

References

[1] R.A. Reimer, C.S. Slaten, M. Seapan, M.W. Lower, P.E. Tomlinson, Abatement of N2O emissions produced in the adipic acid industry, Environmental Progress, 13 (1994) 134-137.
[2] D.E. Becker, M. Rosenberg, Nitrous oxide and the inhalation anesthetics, Anesthesia progress, 55 (2008) 124-132.
[3] V. Zakirov, M. Sweeting, T. Lawrence, J. Sellers, Nitrous oxide as a rocket propellant, Acta Astronautica, 48 (2001) 353-362.
[4] L. Martinu, D. Poitras, Plasma deposition of optical films and coatings: A review, Journal of Vacuum Science & Technology A: Vacuum, Surfaces, and Films, 18 (2000) 2619-2645.
[5] A. Shimizu, K. Tanaka, M. Fujimori, Abatement technologies for N2O emissions in the adipic acid industry, Chemosphere - Global Change Science, 2 (2000) 425-434.
[6] D. Saha, S.G. Deng, Adsorption Equilibrium, Kinetics, and Enthalpy of N2O on Zeolite 4A and 13X, Journal of Chemical and Engineering Data, 55 (2010) 3312-3317.
[7] Y. Peng, F. Zhang, C. Xu, Q. Xiao, Y. Zhong, W. Zhu, Adsorption of Nitrous Oxide on Activated Carbons, Journal of Chemical & Engineering Data, 54 (2009) 3079-3081.
[8] C.R. Reid, K.M. Thomas, Adsorption of Gases on a Carbon Molecular Sieve Used for Air Separation: Linear Adsorptives as Probes for Kinetic Selectivity, Langmuir, 15 (1999) 3206-3218.
[9] G. Domínguez, R. Hernández-Huesca, G. Aguilar-Armenta, Isosteric Heats of Adsorption of N2O and NO on Natural Zeolites, Journal of the Mexican Chemical Society, 54 (2010) 111-116.
[10] R. Hernández Huesca, J. Pérez Arcos, D. Vargas Hernández, M.A. Pérez Cruz, Adsorption kinetics of N2O on natural zeolites, Revista Internacional de Contaminación Ambiental, 32 (2016) 237-242.
[11] D. Saha, Z. Bao, F. Jia, S. Deng, Adsorption of CO2, CH4, N2O, and N2 on MOF-5, MOF-177, and Zeolite 5A, Environmental Science & Technology, 44 (2010) 1820-1826.
[12] D. Saha, S. Deng, Adsorption equilibrium and kinetics of CO2, CH4, N2O, and NH3 on ordered mesoporous carbon, Journal of Colloid and Interface Science, 345 (2010) 402-409.
[13] Y.-H. Kim, J.-J. Kim, C.-H. Lee, Adsorptive cyclic purification process for CO2 mixtures captured from coal power plants, AIChE Journal, 63 (2017) 1051-1063.
[14] S.-C. Jang, S.-I. Yang, S.-G. Oh, D.-K. Choi, Adsorption dynamics and effects of carbon to zeolite ratio of layered beds for multicomponent gas adsorption, Korean Journal of Chemical Engineering, 28 (2011) 583-590.
[15] D.-K. Moon, D.-G. Lee, C.-H. Lee, H2 pressure swing adsorption for high pressure syngas from an integrated gasification combined cycle with a carbon capture process, Applied Energy,

183 (2016) 760-774.
[16] M.-B. Kim, Y.-S. Bae, D.-K. Choi, C.-H. Lee, Kinetic Separation of Landfill Gas by a Two-Bed Pressure Swing Adsorption Process Packed with Carbon Molecular Sieve: Nonisothermal Operation, Industrial & Engineering Chemistry Research, 45 (2006) 5050-5058.
[17] S. Sircar, J.R. Hufton, Why Does the Linear Driving Force Model for Adsorption Kinetics Work?, Adsorption, 6 (2000) 137-147.
[18] Y.D. Chen, R.T. Yang, P. Uawithya, Diffusion of oxygen, nitrogen and their mixtures in carbon molecular sieve, AIChE Journal, 40 (1994) 577-585.
[19] S. Farooq, H. Qinglin, I.A. Karimi, Identification of Transport Mechanism in Adsorbent Micropores from Column Dynamics, Industrial & Engineering Chemistry Research, 41 (2002) 1098-1106.
[20] A.L. Myers, Activity coefficients of mixtures adsorbed on heterogeneous surfaces, AIChE Journal, 29 (1983) 691-693.
[21] D. D Do, Adsorption Analysis: Equilibria and Kinetics, Imperial College Press, London, 1998.
[22] S. Sircar, R. Mohr, C. Ristic, M.B. Rao, Isosteric Heat of Adsorption: Theory and Experiment, The Journal of Physical Chemistry B, 103 (1999) 6539-6546.
[23] R.T. Yang, Fundamental Factors for Designing Adsorbent, in: Adsorbents: Fundamentals and Applications, John Wiley & Sons, Inc., 2003.
[24] S. Chowdhury, R. Mishra, P. Saha, P. Kushwaha, Adsorption thermodynamics, kinetics and isosteric heat of adsorption of malachite green onto chemically modified rice husk, Desalination, 265 (2011) 159-168.
[25] M. Kocirik, P. Struve, M. Bulow, Analytical solution of simultaneous mass and heat transfer in zeolite crystals under constant-volume/variable-pressure conditions, Journal of the Chemical Society, Faraday Transactions 1: Physical Chemistry in Condensed Phases, 80 (1984) 2167-2174.
[26] J. CRANK, The Mathematics of Diffusion, 2nd Edn, Oxford University Press, Oxford, 1975.
[27] D.M. Ruthven, L.-K. Lee, H. Yucel, Kinetics of non-isothermal sorption in molecular sieve crystals, AIChE Journal, 26 (1980) 16-23.
[28] J. Kärger, D.M. Ruthven, Diffusion in zeolites and other microporous solids, Wiley, 1992.
[29] J.-J. Kim, S.-J. Lim, H. Ahn, C.-H. Lee, Adsorption equilibria and kinetics of propane and propylene on zeolite 13X pellets, Microporous and Mesoporous Materials, 274 (2019) 286-298.
[30] Y. Park, D.-K. Moon, D. Park, M. Mofarahi, C.-H. Lee, Adsorption equilibria and kinetics of CO2, CO, and N2 on carbon molecular sieve, Separation and Purification Technology, 212 (2019) 952-964.
[31] NIST Chemistry WebBook, Thermophysical Properties of Fluid Systems, http://webbook.nist.gov/chemistry/fluid/, in, 2017.
[32] Y. Park, D.-K. Moon, Y.-H. Kim, H. Ahn, C.-H. Lee, Adsorption isotherms of CO2, CO, N2, CH4, Ar and H2 on activated carbon and zeolite LiX up to 1.0 MPa, Adsorption, 20 (2014) 631-647.
[33] R.E. Bazan, M. Bastos-Neto, A. Moeller, F. Dreisbach, R. Staudt, Adsorption equilibria of O2, Ar, Kr and Xe on activated carbon and zeolites: single component and mixture data, Adsorption, 17 (2011) 371-383.
[34] Y. Yang, A.M. Ribeiro, P. Li, J.-G. Yu, A.E. Rodrigues, Adsorption Equilibrium and Kinetics of Methane and Nitrogen on Carbon Molecular Sieve, Industrial & Engineering Chemistry Research, 53 (2014) 16840-16850.
[35] C.R. Reid, I.P. O'Koy, K.M. Thomas, Adsorption of Gases on Carbon Molecular Sieves Used for Air Separation. Spherical Adsorptives as Probes for Kinetic Selectivity, Langmuir,

14 (1998) 2415-2425.
[36] H.M. Yi, S. Weiruo, B. Maruti, W. Jinqu, G.W. Miller, Adsorption and diffusion of nitrogen, oxygen, argon, and methane in molecular sieve carbon at elevated pressures, Separations Technology, 1 (1991) 90-98.
[37] Y.-J. Park, S.-J. Lee, J.-H. Moon, D.-K. Choi, C.-H. Lee, Adsorption Equilibria of O2, N2, and Ar on Carbon Molecular Sieve and Zeolites 10X, 13X, and LiX, Journal of Chemical & Engineering Data, 51 (2006) 1001-1008.
[38] Y.S. Bae, C.H. Lee, Sorption kinetics of eight gases on a carbon molecular sieve at elevated pressure, Carbon, 43 (2005) 95-107.
[39] I.P. O'Koye, M. Benham, K.M. Thomas, Adsorption of Gases and Vapors on Carbon Molecular Sieves, Langmuir, 13 (1997) 4054-4059.
[40] S. Cavenati, C.A. Grande, A.E. Rodrigues, Separation of Methane and Nitrogen by Adsorption on Carbon Molecular Sieve, Separation Science and Technology, 40 (2005) 2721-2743.
[41] K. Kaneko, Molecular assembly formation in a solid nanospace, Colloids and Surfaces A: Physicochemical and Engineering Aspects, 109 (1996) 319-333.
[42] H.K. Chagger, F.E. Ndaji, M.L. Sykes, K.M. Thomas, Kinetics of adsorption and diffusional characteristics of carbon molecular sieves, Carbon, 33 (1995) 1405-1411.
[43] D.M. Ruthven, N.S. Raghavan, M.M. Hassan, Adsorption and diffusion of nitrogen and oxygen in a carbon molecular sieve, Chemical Engineering Science, 41 (1986) 1325-1332.
[44] Y.-S. Bae, J.-H. Moon, H. Ahn, C.-H. Lee, Effects of adsorbate properties on adsorption mechanism in a carbon molecular sieve, Korean Journal of Chemical Engineering, 21 (2004) 712-720.
[45] Y. Ju, Y. Park, D. Park, J.-J. Kim, C.-H. Lee, Adsorption kinetics of CO2, CO, N2 and CH4 on zeolite LiX pellet and activated carbon granule, Adsorption, 21 (2015) 419-432.
[46] M. Jahandar Lashaki, M. Fayaz, S. Niknaddaf, Z. Hashisho, Effect of the adsorbate kinetic diameter on the accuracy of the Dubinin–Radushkevich equation for modeling adsorption of organic vapors on activated carbon, Journal of Hazardous Materials, 241-242 (2012) 154-163.
[47] S.-Y. Wu, C.-H. Su, J.-G. Chang, H.-T. Chen, C.-H. Hou, H.-L. Chen, Adsorption and dissociation of N2O molecule on Fe(111) surface: A DFT study, Computational Materials Science, 50 (2011) 3311-3314.
[48] H. Qinglin, S.M. Sundaram, S. Farooq, Revisiting Transport of Gases in the Micropores of Carbon Molecular Sieves, Langmuir, 19 (2003) 393-405.

HIGHLIGHTS

- Adsorption of N_2O on activated carbon and carbon molecular sieve was studied.
- The adsorbed amount of N_2O on AC and CMS was much greater than those for O_2 and N_2.
- The adsorption rate of N_2O was slower than N_2 on AC, but much faster than N_2 on CMS.
- The adsorption rate of N_2O was affected by the kinetic diameter and Lewis structure.

Equilibrium and kinetics of nitrous oxide, oxygen and nitrogen adsorption on activated carbon and carbon molecular sieve

Dooyong Park[1], Youngsan Ju[1], Jeong-Hoon Kim[2], Hyungwoong Ahn[3,], Chang-Ha Lee[1,*]*

[1]Department of Chemical and Biomolecular Engineering, Yonsei University, Seoul, Republic of Korea

[2]Carbon Resources Institute, Korea Research Institute of Chemical Technology, Daejeon, Republic of Korea

[3]School of Engineering, Institute for Materials and Processes, The University of Edinburgh, Edinburgh, UK

ABSTRACT

To evaluate candidate adsorbents for the recovery of nitrous oxide (N_2O) from adipic acid off-gases, the equilibrium and kinetics of N_2O and O_2 adsorption on activated carbon (AC) and of N_2O, O_2, and N_2 adsorption on a carbon molecular sieve (CMS) were evaluated at 293, 308, and 323 K under pressures up to 1000 kPa using a high-pressure volumetric system. Adsorption amount of N_2O on AC and CMS exceeded those of N_2 and O_2, and the adsorption isotherms for O_2 and N_2 were similar. The experimental N_2O and O_2 uptakes on AC and CMS were fitted to a non-isothermal adsorption model, whereas the model was ineffective for predicting N_2 uptake on CMS. The isothermal dual-resistance model, considering surface barrier resistance and pore diffusion, adequately predicted N_2 uptake on CMS. The rate of adsorption of N_2O on AC was much lower than that of O_2 and N_2 whereas the rate of adsorption on CMS flowed the order: $O_2 > N_2O >> N_2$, even though N_2O has higher adsorption affinity and smaller kinetic diameter than O_2. The Lewis structure of N_2O was also found to influence the adsorption kinetics.

KEYWORDS: Adsorption, activated carbon, carbon molecular sieve, nitrous oxide, non-carbon dioxide green-house gas

1. Introduction

N_2O is emitted as a by-product in the second-stage of adipic acid production and is one of the essential materials for the production of synthetic fibers such as nylon-6/6 [1]. N_2O is widely used in medical applications, especially in surgery and dentistry where it is considered the most effective and safe anesthetic and analgesic [2]. It also is used as a multi-purpose propellant in rocket engines [3]. In recent years, high-purity nitrous oxide (99.999%) has been used in the semiconductor and optical industries [4]. However, because N_2O is considered a non-CO_2 greenhouse gas and a dominant ozone-depleting substance, it must be recovered from effluent gas for the mitigation of global climate change.

Typical compositions of effluent gas from adipic acid production processes are reported as N_2O/ NO_x /CO_2/ CO/O_2/H_2O/N_2/VOC; 30.5/0.7/6.0/0.03/3.9/2.0/57.0/0.03 mol.% [1] and N_2O/NO_2/N_2/O_2/H_2O; 23/17/47/7.5/3.0 mol.% [5]. After pretreating the effluent gas, the mixture of N_2O, O_2, N_2, and/or CO_2 is supplied to a N_2O recovery unit. The selection of proper adsorbents is crucial for the design of effective adsorptive cyclic processes for achieving efficient recovery of N_2O. The characteristics of N_2O adsorption on various adsorbents have been investigated by employing adsorption isotherms, models (Langmuir, Freundlich, and Toth models), and by investigating the experimental N_2O uptake on zeolites such as 4A and 13X [6]. The adsorption isotherms of N_2O on three different activated carbons have also been studied at various temperatures up to 100 kPa [7], and the adsorption isotherms and rate were evaluated using the linear driving force model for N_2O adsorption on carbon molecular sieves (CMSs) in the pressure range of 0−9 kPa [8]. The adsorption isotherms and isosteric heats of adsorption [9] and experimental uptake [10] of N_2O on natural zeolites such as erionite, mordenite, and clinoptilolite have also been reported. Comparative evaluation of the adsorption equilibrium and kinetics of N_2O on MOF-5, MOF-177, and zeolite 5A [11], and on ordered mesoporous carbon [12] were conducted

Multiple adsorbents have been simultaneously utilized in attempts to enhance the adsorptive cyclic processes [13-15]. The separation mechanism is dependent on the adsorbates and adsorbents, where equilibrium separation and/or kinetic separation contribute to various extents [15, 16]. To achieve equilibrium separation, adsorption isotherm data for candidate adsorbents up to the partial pressure of each gas in an effluent mixture are valuable for the

design of adsorptive cyclic processes, but accurate adsorption isotherm data in the low pressure region are also critical for evaluating the separation performance.

The Fickian diffusion-type model, i.e., non-isothermal diffusion model, is one of the most rigorous chemical potential driving force models for evaluating separation kinetics, and is often used for analyzing the adsorption rate based on the adsorption uptake curves [17]. If the adsorption rate significantly depends on the characteristics of adsorbent/adsorbate system, the application of model considering various adsorption resistances becomes more important to interpret the adsorption rate of the system. In CMS pellets with a bidisperse structure of macropore and micropore, the adsorption rate is typically known as the micropore diffusion control. However, the diffusion mechanism in CMS, especially in micropore diffusion, is still not fully understood [18, 19].

In this study, we evaluate the adsorption equilibrium and kinetics of N_2O, O_2, and N_2 on activated carbon (AC) and a carbon molecular sieve (CMS), as representative carbon-based adsorbents for equilibrium and kinetic separation, respectively. The adsorption isotherms measured at 293, 308 and 323 K up to 1000 kPa are fitted to both the dual-site Langmuir model and Sips model, and the isosteric heat of adsorption is calculated by applying the Clausius–Clapeyron equation. The adsorption kinetics via micropore diffusion are analyzed from the experimental uptake curves by applying the non-isothermal adsorption model and isothermal dual-resistance model. The parameters showed a reasonable change with variations in the experimental conditions. Finally, the obtained model parameters and experimental raw data are compiled as contributions to the database for evaluating the feasibility of adsorbents and for the design of adsorptive cyclic processes for N_2O separation.

2. Adsorption model

2.1 Adsorption isotherm models

The dual-site Langmuir model (DSL model) assumes two types of adsorption sites with different energy levels based on the Langmuir isotherm model [20]. Since the surface of the carbon-based adsorbent is heterogeneous, the model can fit the experimental adsorption isotherm considering realistic energy distributions of an adsorbate-adsorbent system. In addition, it has a flexible mathematical form for pure-gas and multi-component adsorption.

$$q = \frac{q_{m,d1} b_{d1} P}{1 + b_{d1} P} + \frac{q_{m,d2} b_{d2} P}{1 + b_{d2} P} \quad (1)$$

$$b_{d1} = k_{d1} * exp(k_{d2}/T) \quad (2)$$

$$b_{d2} = k_{d3} * exp(k_{d4}/T) \quad (3)$$

In Equations (1)−(3), $q_{m,d1}$, $q_{m,d2}$, and b_{d1}, b_{d2} are parameters for the DSL model, where the former two represent the amount of adsorbate at equilibrium adsorption for each site, and b_{d1} and b_{d2} indicate the affinity of each site for the adsorbate (hereafter, the adsorption affinity).

In this study, the Sips model was also applied to the experimental isotherms. Although the model lacks thermodynamic consistency [21], it is widely used in the design of adsorptive processes due to its simplicity and accuracy.

$$q = q_{m,s} \frac{(b_s P)^{\frac{1}{n}}}{1 + (b_s P)^{\frac{1}{n}}} \quad (4)$$

$$b_s = k_{s1} * exp(k_{s2}/T) \quad (5)$$

$$1/n = k_{s3} + k_{s4}/T \quad (6)$$

Here, $q_{m,s}$, b_s, and n are parameters for the Sips equation; $q_{m,s}$ represents the amount of adsorbate at equilibrium and b_s indicates the adsorption affinity. The heterogeneity of the adsorption sites is represented by the parameter n.

The temperature-dependent adsorption affinity parameters were determined from the correlation of the experimental data with the DSL (Eqs. (1)−(3)) and Sips (Eqs. (4)−(6)) models. The deviation of the experimental data from the model was determined as the mean absolute percentage error (MAPE):

$$MAPE\ (\%) = \frac{100}{k} \sum_{i=1}^{k} \left| \frac{q_{i,exp} - q_{i,model}}{q_{i,exp}} \right| \quad (7)$$

where, k is the number of the experimental data points, q_{exp} is the experimental data, and q_{model} is the value from the isotherm model.

The isosteric heats of adsorption of the components of a gas mixture are critical variables for the design of adsorption beds for gas separation [22] because this parameter affects the amount of adsorbate captured by the adsorbent (adsorption amount) and the adsorption kinetics. Therefore, the effect of the isosteric heat on the adsorption process is considered in determining the optimal conditions for the adsorptive separation process.

The isosteric heat of adsorption, Q_{st}, was calculated from the experimental data or isotherm models at different temperatures by using the Clausius-Clapeyron equation.

$$\frac{\Delta Q_{st}}{RT^2} = \left[\frac{\partial lnP}{\partial T}\right]_q \tag{8}$$

$$\frac{\Delta Q_{st}}{\mathbb{R}T^2} dT = dlnP \tag{9}$$

where, $\mathbb{R}$ is the gas constant.

It was reported that the adsorption forces for carbon-type adsorbents consist of $\Phi_{adsorbate\text{-}adsorbate}$ and $\Phi_{adsorbate\text{-}adsorbent}$ [23]. Since Q_{st} is affected by the surface coverage, the contribution of the interaction forces, $\Phi_{adsorbate\text{-}adsorbate}$ and $\Phi_{adsorbate\text{-}adsorbent}$, to adsorption can be analyzed from the changes in Q_{st} [24].

2.2 Kinetic models

Pelletized adsorbents characterized by micropores and macropores are widely used in adsorptive processes. Intra-crystalline (micropore) diffusion in adsorbent pellets generally plays a significant role in adsorptive separation processes [25]. However, when the adsorption heat is high, inter-crystalline (macropore) diffusion can contribute to the adsorption kinetics due to thermal resistance. Therefore, the kinetic mechanism must be investigated in detail, especially for kinetic separation agents (such as CMS).

A simple analytical solution for a constant volume system was developed by assuming isothermal conditions and a linear equilibrium relationship [26]. However, the adsorption process is accompanied by the generation of isosteric heat. Since the adsorption heat dissipated to the surroundings affects the uptake curve, the adsorption kinetics can be strongly controlled

by heat transfer through the surface [27]. Therefore, a non-isothermal adsorption model based on the following assumptions is suggested [25, 27]:

1. The adsorbent consists of uniform spherical particles.
2. Micropore diffusion is the only significant resistance to mass transfer. Therefore, the concentration of the adsorbate at the surface of each particle is always in equilibrium.
3. Heat conduction through the particle is sufficiently fast, and the only significant heat transfer resistance is heat dissipation at the external surface
4. The equilibrium relationships are linear, and the micropore diffusivity is constant (temperature-independence).

Subject to the above approximation, the uptake curve for non-isothermal adsorption can be described as:

$$\frac{m_t - m_0}{m_\infty - m_0} = 1 - \sum_{n=1}^{\infty} \frac{9\left(1 + K\frac{V_s}{V_g}\right)\left[\frac{Y_n}{-\beta_n^2}\right]^2 exp\left(-\beta_n^2\frac{D}{R^2}t\right)}{\frac{1}{\varphi_n} + \frac{3\beta'}{2\varphi_n}\left[\beta_n cot\,\beta_n\left(\frac{Y_n}{\beta_n^2}\right) + 1\right] + \frac{3}{2}K\frac{V_s\,1\,A_n}{V_g\beta_n^4\varphi_n}} \tag{10}$$

where β_n is given by the roots of:

$$(-\beta_n + \alpha) + 3\beta Y_n - 3K\frac{V_s\,1}{V_g\beta_n^2}(-\beta_n + \alpha)Y_n = 0 \tag{11}$$

and

$$A_n = Y_n\left[(\beta_n^2 - \alpha)\beta_n cot\beta_n - 2\alpha\right] + \beta_n^2(\beta_n^2 - \alpha) \tag{12}$$

$$Y_n = \beta_n cot\beta_n - 1 \tag{13}$$

$$\frac{1}{\varphi_n} = \frac{1}{\beta}\left(1 - 3K\frac{V_s Y_n}{V_g\beta_n^2}\right) \tag{14}$$

In Equation (10), m_t, m_0, and m_∞ represent the adsorption amount at time t, at the initial time 0, and at equilibrium, respectively. K, defined as $(\Delta q \cdot \rho_p)/(\Delta P/\ \mathbb{R}\ T)$, is the equilibrium constant. V_s and V_g are the adsorbent volume and gas phase volume, respectively.

When micropore diffusion dominates, the diffusion time constant (D/R^2) consists of micropore diffusivity and the micropore particle radius (D_c/r^2). On the other hand, when

macropore diffusion dominates, the diffusion time constant can be presented by macropore diffusivity and the adsorbent pellet radius (D_p/R^2). In this study, since micropore diffusion dominates the adsorption rate for both adsorbents, the diffusion time constant is described as (D_c/r^2). The details are presented below in the discussion of the experimental data.

The non-isothermal adsorption model involves two dimensionless parameters, α and β. When α tends to infinity or β approaches 0, the effect of mass transfer dominates and the thermal effect becomes negligible [25, 27].

$$\alpha = \left(\frac{ha}{\rho_p C_p}\right) \Big/ \left(\frac{D_c}{r^2}\right) \tag{15}$$

$$\beta = \frac{\Delta Q_{st}}{\rho_p C_p}\left(\frac{\partial q^*}{\partial T}\right)_{c_0, T_0} \tag{16}$$

Here, h is the overall heat transfer coefficient; a is the external surface area per unit volume; D_c is the micropore diffusivity; r is the micropore particle radius, ρ_p and C_p represent the density and heat capacity of the adsorbent respectively, ΔQ_{st} is the change in the isosteric heat of adsorption, and $\partial q^*/\partial T$ is the temperature dependence of the adsorption capacity at equilibrium. Using these equations, two parameters (α and β, described below) can be derived from the physical properties and adsorption data. However, the heat transfer, mass transfer, and generated heat also have a complex influence on the adsorption rate.

The parameter α is the ratio of the heat transfer ($ha/\rho_p C_p$) to diffusion time constant (D_c/r^2). As a descriptor of the heat transfer, a large α value indicates that the heat dissipates to the surroundings rapidly and the molecules diffuse slowly. On the other hand, a small α value indicates that the heat dissipates to the surroundings slowly and the molecules diffuse rapidly.

The parameter β is the product of the isosteric heat of adsorption ($\Delta Q_{st}/\rho_p C_p$) and the temperature dependence of the adsorption capacity at equilibrium ($\partial q^*/\partial T$). Until the generated heat is fully dissipated out of the system, the retained heat changes the equilibrium and the behavior of the uptake curve. Under the above limiting conditions, the uptake curve assumes an asymptotic form [27]:

$$\frac{m_t - m_0}{m_\infty - m_0} = 1 - \frac{\beta}{1+\beta}\ exp\left[\frac{-hat}{\rho_p C_p (1+\beta)}\right] \tag{17}$$

Values of α and β in the non-isothermal adsorption model have been suggested in many cases by fitting the experimental uptake curves. However, as shown in Eqs. (15) and (16), the parameters can be theoretically calculated. In this study, the theoretical values of α and β were calculated from the physical properties of the gas molecules and adsorbents as a first step. By using these theoretical values as initial values, the parameters α and β in the non-isothermal adsorption model were re-estimated via non-linear regression of the experimental uptake curves within a range similar to that of the calculated values. Thus, the parameters (α and β) were analyzed by considering the effects of heat transfer, mass transfer, and the isosteric heat of adsorption.

When the contribution of the surface barrier resistance to the overall kinetics cannot be neglected, there is a large deviation between the micropore diffusion model results and the experimental data. An isothermal dual-resistance model combining micropore diffusion resistance and surface barrier resistance was suggested as follows [28]:

$$\frac{m_t - m_0}{m_\infty - m_0} = 1 - \sum_{n=1}^{\infty} \frac{6L^2 exp\left(-\delta_n^2 \frac{D_c}{r^2} t\right)}{\delta_n{}^2(\delta_n{}^2 + L(L-1))} \tag{18}$$

$$\delta_n cot\delta_n + L - 1 = 0 \tag{19}$$

$$L = \frac{k_f r}{D_c K} = \frac{k_f r}{D_m} \times \frac{D_m}{D_c K} = \frac{Sh}{2} \times \frac{D_m}{D_c K} \tag{20}$$

where, δ_n represents the roots of the equation, k_f is the film mass transfer coefficient and Sh is the Sherwood number. D_c and D_m are the micropore diffusivity and molecular diffusivity, respectively. The molecular diffusivity was calculated from both the Knudsen diffusivity (D_K) and viscous diffusivity (D_v) [29].

$$D_K = \frac{2}{3} R \sqrt{\frac{8\mathbb{R}T}{\pi M}} \frac{1}{\zeta} \tag{21}$$

$$D_v = \frac{PR^2}{8\eta} \tag{22}$$

$$D_m = \frac{\varepsilon_P (D_K + D_v)}{\tau(\varepsilon_P + (1 - \varepsilon_P)K)} \tag{23}$$

where, ζ is the diffuse reflection coefficient, η is the viscosity, τ is the tortuosity, and ε_P is the porosity. The tortuosity was assumed to be 1/porosity.

The diffusivity when the adsorption amount is low is called the corrected diffusivity [28]. The thermodynamic correction factor ($d\ln P/d\ln q$) calculated from the Sips isotherm model becomes:

$$\frac{dlnq}{dlnP} = \frac{1}{n}\frac{dln\,(bP)}{dlnP} - \frac{dln\left(1+(bP)^{\frac{1}{n}}\right)}{dlnP}$$

$$= \frac{1}{n} - \frac{1}{n}\left(\frac{(bP)^{\frac{1}{n}}}{1+(bP)^{\frac{1}{n}}}\right) \tag{24}$$

$$= \frac{1}{n}(1-\theta)$$

$$D = D_0\frac{d\ln P}{d\ln q} = D_0\frac{n}{1-\theta} \tag{25}$$

where, D_0 is the corrected diffusivity and θ is defined as ($q/q_{m,s}$). In this study, D corresponds to D_c.

The parameters of both kinetic models were obtained from the experimental uptake curves. Using MATLAB (Mathworks, Inc.), the incremental search method (ISM) and the secant method were used to find the roots of Equations (11) and (19). The least-squares method was then used for non-linear regression of Equations (10) and (18).

3. Experimental section

3.1. Materials

Activated carbon (AC, 2GA-H2J) and carbon molecular sieves (CMS, GN-UC-H) were supplied by KURARAY CHEMICAL Co., Japan. The physical properties of AC and CMS were evaluated from the N_2 adsorption isotherm at 77 K for AC and the CO_2 adsorption isotherm at 293 K for CMS using a volumetric sorption analyzer (Autosorb IQ, Quantachrome Corporation). The macropore characteristics of CMS were investigated via mercury

porosimetry (PM33GT, Quantachrome Corporation). The Brunauer–Emmett–Teller (BET) theory and Dubinin-Radushkevitch (DR) equation were applied to the adsorption isotherms.

The surface area of AC and CMS was 1306.4 and 640.9 $m^2 g^{-1}$, respectively. As shown in Figure 1, CMS contained macropores that were developed during pelletization. Figure 2 showed the pore size distribution and cumulative pore volume of AC and CMS. The micropores of AC were distributed around 0.35 nm and 0.52 nm, ultra micropore region, and 1.17 nm and 1.33 nm in the N_2 adsorption analysis. The pores of CMS were distributed within two ranges: 0.3−0.4 nm and 0.4−0.7 nm. Especially, the CMS showed relatively narrower pore size distribution than AC. The detailed physical properties of the adsorbents are listed in Table 1.

The properties of the adsorbate gases are listed in Table 2. N_2O (kinetic diameter: 330 pm), O_2 (kinetic diameter: 346 pm), and N_2 (kinetic diameter: 364 pm) were all of 99.999% purity, and were supplied by CHEMGAS KOREA, Daedeok Gas Co. and DAESUNG Industrial Gases Co., Korea. The adsorbate gases were used in the experiments without further purification.

Figure 1. (a) Macropore size distribution and (b) cumulative volume of CMS, determined via mercury porosimetry

Figure 2. Cumulative pore volume and pore size distribution of AC and CMS from the density functional theory (○ and ●, activated carbon; △ and ▲, carbon molecular sieve [30]; closed symbol for cumulative pore volume; open symbol for pore size distribution)

Table 1. Physical properties of adsorbents

Table 2. Properties of adsorbate gases

3.2. Volumetric experiments

The adsorption isotherms and uptake curves were constructed from the data acquired by using a high-pressure adsorption system (BELSORP-HP, Japan); a schematic diagram of the volumetric system is presented in Figure 3. Two high accuracy absolute pressure transducers were installed in the adsorption system. One pressure transducer (PT1: PMP 4015, DRUCK Inc., USA; full scale: 0.133 MPa (abs)) was used in the low-pressure range (up to 90

kPa) and the other (PT2: PMP 4015, DRUCK Inc., USA; full scale: 12.1 MPa (abs)) was used in the high-pressure range (up to 1000 kPa). The degree of uncertainty for both pressure transducers was within ±0.08% of each full-scale range. The temperature of the internal high-pressure system was kept constant with a system temperature controller. The temperature of the adsorption cell located outside the system was kept constant using a water-bath circulator (F25-ME, Julabo, Germany). The measured temperature and pressure of the system were recorded automatically during the uptake experiments. The adsorption amount was determined from the virial equation using the temperature, pressure, and compressibility factor from NIST [31].

Figure 3. Schematic diagram of high-pressure adsorption system

Prior to the adsorption experiments, the adsorbents were activated by heating in an oven (OV-11, JEIO TECH, Korea) for 8 h at 423 K under vacuum (GLD-136C vacuum pump, ULVAC KIKO Inc., Japan). Once the adsorbents were activated, the mass was measured with a microbalance (AND, HR-200, Japan) having an accuracy of ±10 μg. The adsorbent was placed into the adsorption cell with a VCR gasket (SS-8-VCR-2-GR-5M, Swagelok, USA). After installing the adsorption cell in the system, the adsorbent was again evacuated under the same conditions described above to remove any possible contaminants transferred during the assembly. After the in-situ activation, the system was purged with helium gas and evacuated with a vacuum pump. The adsorbate was then supplied to the adsorption cell through a controlled needle valve. The uptake experiment was allowed to proceed until the system pressure change was within 0.1% of the full-scale range for 500 s. However, the uptake of N_2 on CMS was evaluated over 5400 s under each condition due to the slow adsorption rate.

The amount adsorbed at each pressure step was calculated from the measured temperature, pressure, and system volume. When the adsorption cell reached the equilibrium state ($P_{e,\,i}$), the adsorption cell was isolated by closing a pneumatic valve connected to the system. Subsequently, the adsorbate gas was injected into the system (dosing cell) for another uptake run. The gas phase pressure of the system was changed from $P_{e,\,i}$ to $P_{0,\,i+1}$. At $t = 0$ (the initial point of the i+1th step), when the pneumatic valve linked to the adsorption cell was opened, the pressure of the adsorption cell was determined as:

$$P_{0,i+1}{}' = \frac{P_{e,\ \ i} \times V_{cell} + P_{0,i+1} \times V_{system}}{V_{cell} + V_{system}} \tag{26}$$

The adsorption cell gradually reached the i+1th equilibrium state ($P_{e,\ i+1}$). The experimental reproducibility within 2% was confirmed from duplicate equilibrium experiments.

4. Results and discussion

4.1. Adsorption equilibria

The adsorption of N_2O and O_2 on AC and that of N_2O, O_2, and N_2 on CMS were evaluated in the temperature and pressure range of 293−323 K and 0−1000 kPa, respectively, by a volumetric method. Figure 4 presents the isotherms for N_2 adsorption on AC from a previous study [30] for comparison with the present isotherms. In the experimental pressure range, the isotherms of N_2O, O_2, and N_2 were of Type 1 based on the IUPAC classification. The experimental isotherm data for N_2O, O_2, and N_2 adsorption are listed in the Appendix (Tables 1−3) because the isotherm parameters given in the study should be re-optimized to model accurately adsorptive processes, considering the partial pressure of each component of the effluent gases. Therefore, the raw data are useful for other types of isotherm model studies and the design of adsorptive processes.

The amount of gases adsorbed on AC and CMS and the heats of adsorption for N_2O, O_2, and N_2 are compared with the results from previous studies in Figure 4 and Table 3. Although the manufacturers and physical properties differed for the carbon materials, the results were reasonably similar to those of previous studies. The isotherm data in Figure 4 are comparable with the isotherms of the (a) N_2O/AC [7], (a) CO_2/AC [32], (b) CO_2/CMS [30], (c) O_2/AC [33] and (f) N_2/CMS [34] systems from previous studies. Since the adsorption isotherm data of N_2O on AC were limited in the low pressure range, a comparison is presented in the inset of Figure 4 (a).

N_2O was strongly adsorbed on both adsorbents, and to a greater extent than O_2 and N_2. At 1000 kPa, the difference in the amount of N_2O versus the other gases adsorbed was much higher with AC than with CMS. The amount of O_2 adsorbed on AC was slightly higher than the amount of N_2, whereas the amount of O_2 and N_2 adsorbed on CMS was comparable.

Figure 4. Experimental adsorption isotherms and DSL model for AC and CMS: ●, 293 K; ▲, 308 K; ■, 323 K; (e) N_2/AC [32]; solid line, DSL model (○, N_2O/AC at 323 K [7]; △, CO_2/AC at 323 K [32]; □, CO_2/CMS at 318 K [30]; +, O_2/AC at 303 K [33]; x, N_2/CMS at 323 K [34])

Table 3. Comparison of adsorption equilibrium parameters for N_2O, O_2, and N_2

The adsorption of N_2O, O_2, and N_2 on AC (170, 125, and 135%) was greater than that on CMS at 1000 kPa. This difference mainly resulted from the higher surface area and pore volume of AC, as indicated in Table 1. Furthermore, even though the molar mass of N_2O and CO_2 is the same, more N_2O than CO_2 was adsorbed on both adsorbents, as shown in Figures 4 (a) and (b), where the difference was more pronounced when using AC. The difference in the adsorption amount of N_2O between AC and CMS was prominent even in the low pressure region (<100 kPa). However, the difference in the O_2 and N_2 adsorption on both adsorbents was minute, with almost linear isotherms in the low pressure region (inset of Figure 4).

The experimental data were fitted to the DSL and Sips models, and the model parameters are listed in Table 4. As shown in Figure 4, the DSL model was adequate for predicting the experimental isotherms for both adsorbents. The mean absolute percentage errors (MAPEs) for N_2O, O_2, and N_2 adsorption on AC were 2.68, 0.50, and 1.24%, respectively, for the DSL model and 2.40, 1.68, and 1.82%, respectively, for the Sips model. The MAPEs for N_2O, O_2, and N_2 adsorption on CMS were 1.50, 0.29, and 0.40%, respectively, for the DSL model and 1.57, 2.12, and 2.20%, respectively, for the Sips model. For both adsorbents, the experimental values fit slightly better to the DSL model than the Sips model.

Table 4. Parameters for dual-site Langmuir and Sips models

The parameters from the DSL model can be used to interpret the $\Phi_{adsorbate\text{-}adsorbate}$ and $\Phi_{adsorbate\text{-}adsorbent}$ contributions to the adsorption process [23]. In the experimental range, the parameter $q_{m,\,d1}$ was greater than $q_{m,\,d2}$, and b_{d1} was smaller than b_{d2} (Table 4). It indicates that more molecules are adsorbed at adsorption site 1 than at adsorption site 2, whereas they are more strongly adsorbed at adsorption site 2 than at adsorption site 1. The initial adsorption was mainly affected by the strong adsorption site (site 2), with a large $\Phi_{adsorbate\text{-}adsorbent}$ value, and thereafter, more molecules were adsorbed on the weak adsorption sites (site 1) with increasing $\Phi_{adsorbate\text{-}adsorbate}$. The difference between the $q_{m,\,d1}$ value for AC and CMS was large (over 180%

in the experimental range, Table 4). This is consistent with the micropore volume of AC being over 150% higher than that of CMS. On the other hand, considering the difference in the surface area (200% difference, Table 1), the difference in the $q_{m,\ d2}$ value for both adsorbents was relatively small.

The isosteric heats of adsorption (Q_{st}) calculated from the Clausius-Clapeyron equation are presented with the surface coverage in Figure 5. If different surface energy levels exist and the interactions between the adsorbed molecules cannot be neglected, Q_{st} varies with the surface coverage [38]. For both adsorbents, the Q_{st} of N_2O was much higher than that of O_2 and N_2. The decrease in Q_{st} with increasing surface coverage was relatively smaller for CMS than for AC. In addition, with both adsorbents, a very small linear decrease in Q_{st} was observed for O_2 and N_2 adsorption with increasing surface coverage. The Q_{st} values for the adsorption of both gases on AC were almost the same, whereas that for O_2 on CMS was higher than that of N_2 because the paramagnetic properties of O_2 might induce strong spin-spin interaction between the molecules in the pores of CMS [38, 41].

$\Phi_{adsorbate\text{-}adsorbent}$ was initially dominant for both adsorbents. However, with increasing surface coverage, $\Phi_{adsorbate\text{-}adsorbate}$ contributed more to the adsorption for AC than for CMS. This difference might be derived from the difference in the micropore volume of the two adsorbents because more molecular layers can be formed in the pores of AC.

Figure 5. Isosteric heats of adsorption for AC (a) and CMS (b): solid line, N_2O; dotted line, O_2; dashed line, N_2

4.2. Adsorption Kinetics

The kinetics of N_2O, O_2, and N_2 adsorption on AC and CMS were analyzed by using the volumetric experimental uptake data. First, to clarify the dominant diffusion mechanism during adsorption on AC and CMS, N_2O adsorption experiments were performed with AC and CMS samples of different sizes, i.e., particles (200−500 μm) and pellets. The average radius of the pelletized AC and CMS samples were 2.0 and 1.4 mm, respectively. As shown in Figure 6, the difference in the experimental uptake curves for the particle and corresponding pellet samples of AC and CMS was minute within a similar pressure range. The difference in the

diffusional time constant from the uptake curves of the particle and corresponding pellet sample was also very small. This suggests that the contribution of macropore diffusion to adsorption was insignificant, and the micropore diffusion mechanism dominated the adsorption kinetics.

Figure 6. Experimental uptake curves for N_2O on AC (a) and CMS (b) at 308 K (closed symbol, particle (200−500 μm); open symbol, pellet)

The experimental uptake curves of adsorption and desorption for N_2O at 308 K were compared in Figure 7. Within the pressure range of lower than 80 kPa for the kinetic analysis, both uptake curves were well coincided with each other, indicating the reliability of pressure step change in the study. The experimental uptake curves were predicted using the non-isothermal adsorption model (Eq. 10) and the D_c/r^2 (micropore diffusion time constant) was obtained. The uptake curves, predicted by the non-isothermal adsorption model for N_2O and O_2, are shown in Figure 8, and the micropore diffusion time constant and parameters are listed in Tables 5 (AC) and 6 (CMS). In the early stage of adsorption, the slope of the experimental uptake curve was steeper at higher pressure, but under higher pressures over longer periods, the curvature was greater. These characteristics were more prominent for AC than CMS.

Figure 7. Experimental uptake curves of adsorption and desorption for N_2O on (a) AC and (b) CMS at 308 K: ●, adsorption; △, desorption

Figure 8. Experimental uptake curves and non-isothermal adsorption model for AC ((a) and (c)) and CMS ((b) and (d)) at 308 K: solid line, non-isothermal adsorption model

Table 5. Micropore diffusion time constant and parameters for AC from non-isothermal adsorption model

Table 6. Micropore diffusion time constant and parameters for CMS from non-isothermal adsorption model

The model parameters, α and β, were reasonably estimated from the properties of the adsorbent and adsorbate and the experimental adsorption data, not just by fitting the experimental uptake curves. The parameter α, $((h\sigma/\rho_s C_s)/(D_c/r^2))$, is the ratio of the heat

transfer term to the mass transfer term. Since the mass transfer term, D_c/r^2, increased with increasing pressure in the experimental region, the parameter α generally decreased with increasing pressure. Further, for both adsorbents, α was greater for N_2O than for O_2 because of the substantial difference in the mass transfer rate of the two molecules. Moreover, the variation of α with pressure was relatively small for O_2 on both adsorbents. In addition, the α values for O_2 adsorption on CMS were higher than those for adsorption on AC, and the variation in α values for N_2O with pressure was more significant for adsorption on AC. On the other hand, the heat transfer term, $h\alpha/\rho_s C_s$, was relatively constant for each adsorbent.

The parameter β, $((Q_{st}/\rho_s C_s)\cdot(\partial q^*/\partial T))$, representing the thermal effects, increased with increasing pressure in the experimental range. For both adsorbents, the absolute value of $\partial q^*/\partial T$ (the temperature-dependence of the adsorption capacity at equilibrium) increased with increasing pressure. In the early stage of adsorption, the adsorption capacity decreased due to the exothermic nature of the adsorption (Q_{st}) process. Therefore, time was required to reach the adsorption equilibrium, governed by the equilibrium temperature. Since the curvature of the uptake curve corresponds to the Q_{st} and $\partial q^*/\partial T$ data, it also depends on the amount of substrate adsorbed, where the generated heat of adsorption causes the uptake curve to bend earlier at high pressure than at low pressure. The parameter β for N_2O was greater than that for O_2 as more of the former gas was adsorbed with higher heat of adsorption, which implies stronger interaction for N_2O adsorption. However, the difference in the β values for each adsorbate on AC and CMS was insignificant. Furthermore, the absolute values and variation of β for O_2 was minute, as shown in Tables 5 and 6.

For N_2 adsorption on CMS, the experimental uptake curves were almost linear (Figure 9). The slope of the uptake curves was slightly steeper at higher pressure, but the difference was small under the various pressure conditions. The values of D_c/r^2 for N_2 adsorption on CMS could be obtained from the non-isothermal adsorption model when the physical property parameters (α and β) were used as fitting parameters. However, the values of α and β were far from the calculated theoretical values at the experimental pressures and temperatures. Furthermore, when a reasonable range of α and β values was applied to the N_2 uptake curves of CMS, large deviations were observed (Figure 9). This deviation indicates that the non-isothermal adsorption model was not adequate for describing the kinetics of the N_2 adsorption on CMS, and the surface barrier resistance as well as the pore diffusion resistance should be considered for the adsorptive uptake of N_2 in the experimental range. It was also reported that

the surface barrier resistance rise to a measurable level for O_2 on CMS at low temperature, 248 K (Table 8) [48]. It implies that the transport mechanism in small pores can be changed by experimental conditions.

Figure 9. Experimental uptake curves, non-isothermal adsorption model, and isothermal dual resistance model for N_2 on CMS: solid line, non-isothermal adsorption model; dashed line, isothermal dual resistance model

The data shown in Figure 9 suggest that N_2 adsorption on CMS was firstly controlled by the pore mouth when N_2 diffused through the micropore. Herein, the dual-resistance model (Eq. 18) was applied to the experimental uptake curves. This model utilizes the parameter L (D_m/D_cK), representing the ratio of micropore resistances to the surface barrier resistance [28], which can be estimated from the Sherwood number (Sh), equilibrium constant (K), and molecular diffusivity (D_m). The Sherwood number was considered as 2 because the molecules were adsorbed in the stagnant fluid. The equilibrium constant, K, was calculated from the experimental data, and the molecular diffusivity was estimated from Equations (21)–(23). Figure 9 shows that the isothermal dual-resistance model could accurately predict the uptake curves for N_2 in CMS. The diffusion time constant and parameter L are presented in Table 7. The micropore diffusion time constant, D_c/r^2, increased reasonably with pressure and temperature.

Table 7. Micropore diffusion time constant and parameters for N_2 adsorption on CMS using isothermal dual resistance model

Table 8. Comparison of diffusion time constant and barrier mass transfer coefficient for N_2O, O_2, and N_2

The rate of adsorption of the gases on AC followed the order: $O_2 \geq N_2 >> N_2O$, where the corresponding order for CMS was $O_2 > N_2O >> N_2$. These orders are the same as those reported in previous studies (Table 8) in the experimental range. Interestingly, the rates of adsorption of O_2 and N_2 on AC were much faster than the corresponding values for CMS, whereas the rate of adsorption of N_2O was similar for both adsorbents. Furthermore, although the kinetic diameter of N_2O is smaller than those of O_2 and N_2 (see Table 2) and the adsorption

affinity of the adsorbents for N_2O was much higher than for the other gases. N_2O adsorbed more slowly on AC than the other gases and more slowly on CMS than O_2, as shown in Figure 10. The heat resistance in the macropores is not sufficient for explaining these trends, as mentioned in relation to Figure 6.

Figure 10. Experimental uptake curves, non-isothermal adsorption model, and isothermal dual resistance model for adsorption of gases on AC (a) at 293 K and on CMS (b) at 308 K: solid line, non-isothermal adsorption model; dashed line, isothermal dual resistance model (data for N_2 adsorption on AC at 293 K are taken from the literature [45])

The kinetic diameter is related to the mean free path of a molecule in a gas, which is an indication of the size of the molecule as a target [46]. Therefore, the kinetic diameter is not the same as the atomic diameter, defined in terms of the size of the atom's electron shell, which is usually much smaller. Rather, it is the size of the sphere of influence that can lead to a scattering event. However, the adsorption rate is influenced by various factors such as the molecular size, structure, and electronic properties [8, 38]. Therefore, the kinetic diameter does not adequately account for the observed the adsorption rates.

Elemental nitrogen (N≡N) has an extremely strong triple bond, and the second strongest bond in any diatomic molecule after carbon monoxide. Therefore, N_2 adsorption on CMS, where N_2 has the largest kinetic diameter, was restricted in the pore mouth because of the adsorbent geometry and kinetic diameter. On the other hand, N_2O has a magnetic susceptibility of 18.9×10^{-6} cm^3 mol^{-1}. Furthermore, the Lewis structure of N_2O reportedly has mobile electrons, usually in pairs that can be moved to generate valid structures [47]. The linear and asymmetric molecule, which has a permanent dipole moment, presents three fundamental vibrational modes (symmetric stretch, asymmetric stretch, and bend) (Table 2). Based on these results, the Lewis structure of N_2O and the heat of adsorption might affect the adsorption rate in both adsorbents, whereas adsorption on AC (with relatively large micropore diameters) was not affected by the kinetic diameter of N_2, unlike adsorption on CMS.

4. Conclusion

To evaluate candidate adsorbents for the adsorptive separation and recovery of N_2O from adipic acid off-gases, the equilibrium and kinetics of N_2O, O_2, and N_2 adsorption on AC and CMS were studied. The adsorption was experimentally evaluated by a volumetric method at 293−323 K under pressures up to 1000 kPa. The experimental isotherms were well fitted by the DSL model and Sips model. The amount of N_2O adsorbed and heat of adsorption were much greater than those for O_2 and N_2 with both adsorbents. For all the component gases, the Q_{st} values were slightly higher with CMS than with AC, although the amount of gas adsorbed was larger for AC than for CMS. Based on the adsorption model parameters and Q_{st}, the contribution of $\Phi_{adsorbate\text{-}adsorbate}$ to the adsorption of N_2O was higher with AC than with CMS.

For all the adsorbates, macropore diffusion in both adsorbents could be neglected. The kinetics of N_2O and O_2 adsorption via micropore diffusion in both adsorbents could be predicted by the non-isothermal adsorption model. It also indicated that the surface barrier resistance on CMS was negligible in the experimental range. On the other hand, due to the contribution of surface barrier resistance to N_2 adsorption on CMS, the non-isothermal adsorption model was unsuitable for this system. The dual-resistance model could provide a reasonable prediction of the uptake curves of N_2 in CMS. The parameters for both models were estimated within a theoretically reasonable range and the variation of these parameters with pressure and temperature was consistent. The D_c/r^2 values increased with increasing pressure and temperature for both adsorbents, regardless the type of model used.

The rate of adsorption followed the order: $O_2 \geq N_2 >> N_2O$ for AC and $O_2 > N_2O >> N_2$ for CMS. Since the adsorption affinity of both adsorbents for N_2O was the highest and the kinetic diameter of this gas was the smallest, it is hard to interpret trends in the rate of adsorption simply in terms of the kinetic diameter. The rate of adsorption could also be affected by the electrical properties of the adsorbates, such as the dipole/quadrupole moment and/or polarizability. Furthermore, it was expected that the Lewis structure of N_2O, i.e., the linear and asymmetric molecular structure, might affect the rate of adsorption on the carbon surface.

Nomenclature

	Unit

a	external surface area per unit volume of adsorbent	m^{-1}
A_n	solution of the Eq. (14) - (16)	-
b_{d1}	dual-site Langmuir isotherm model parameter	kPa^{-1}
b_{d2}	dual-site Langmuir isotherm model parameter	kPa^{-1}
b_L	Langmuir isotherm model parameter	kPa^{-1}
b_s	Sips isotherm model parameter	kPa^{-1}
C_s	heat capacity of the adsorbent	$J\ g^{-1}\ K^{-1}$
D_0	corrected diffusivity	$m^2\ s^{-1}$
D_c	micropore diffusivity	$m^2\ s^{-1}$
D_K	Knudsen diffusivity	$m^2\ s^{-1}$
D_m	molecular diffusivity	$m^2\ s^{-1}$
D_v	viscous diffusivity	$m^2\ s^{-1}$
D_c/r^2	micropore diffusion time constant	s^{-1}
$D_{c,0}/r^2$	corrected micropore diffusion time constant	s^{-1}
D_p/R^2	macropore diffusion time constant	s^{-1}
h	overall heat transfer coefficient	$J\ m^{-1}\ s^{-1}\ K^{-1}$
k	number of experimental data	-
k_f	mass transfer coefficient	$m\ s^{-1}$
K	equilibrium constant	-
k_{d1}	Dual-site Langmuir isotherm model parameter	kPa^{-1}
k_{d2}	Dual-site Langmuir isotherm model parameter	K
k_{d3}	Dual-site Langmuir isotherm model parameter	kPa^{-1}
k_{d4}	Dual-site Langmuir isotherm model parameter	K
k_{s1}	Sips isotherm model parameter	kPa^{-1}
k_{s2}	Sips isotherm model parameter	K
k_{s3}	Sips isotherm model parameter	-
k_{s4}	Sips isotherm model parameter	K
L	isothermal dual-resistance model parameter	-
m_0	adsorption amount at initial time 0	$mol\ kg^{-1}$
m_∞	adsorption amount at equilibrium	$mol\ kg^{-1}$
m_t	adsorption amount at ambient time t	$mol\ kg^{-1}$
n	Sips isotherm model parameter	-
P	pressure	kPa
q	adsorption amount	$mol\ kg^{-1}$
q_{cal}	adsorption amount calculated by isotherm model	$mol\ kg^{-1}$
q_{exp}	adsorption amount measured by experiment	$mol\ kg^{-1}$
$q_{m,d1}$	Dual-site Langmuir isotherm model parameter	$mol\ kg^{-1}$
$q_{m,d2}$	Dual-site Langmuir isotherm model parameter	$mol\ kg^{-1}$
$q_{m,s}$	Sips isotherm model parameter	$mol\ kg^{-1}$
Q_{st}	isosteric heat of adsorption	$kJ\ mol^{-1}$
r	micropore particle radius	m

R	adsorbent particle radius	m
$\mathbb{R}$	ideal gas constant	J mol^{-1} K^{-1}
Sh	Sherwood number	-
t	time	s
T	temperature	K
V_g	volume occupied by adsorbate	m^3
V_s	volume occupied by adsorbent	m^3
Y_n	solution of the Eq. (14) - (16)	-

Greek letters

α	non-isothermal kinetic model parameter defined by the Eq. (15)	-
β	non-isothermal kinetic model parameter defined by the Eq. (16) - (17)	-
β_n	solution of the Eq. (11)	-
δ_n	solution of the Eq. (18) - (19)	-
ε_P	porosity	-
ζ	diffuse reflection coefficient	-
η	viscosity	cP
τ	tortuosity	-
φ_n	solution of the Eq. (12) - (14)	-

Acknowledgement

This research is supported by the "R&D Center for reduction of Non-CO_2 Greenhouse Gases (2016001690005)" funded by Korea Ministry of Environment (MOE) as "Global Top Environment R&D Program"

AUTHOR INFORMATION

Corresponding Author

*Co-corresponding authors: leech@yonsei.ac.kr (C.-H. Lee), H.Ahn@ed.ac.uk (H. Ahn)

Tel.: +82 2 2123 2762; Fax: +82 2 312 6401

Funding

This research is supported by the "R&D Center for reduction of Non-CO_2 Greenhouse Gases (2016001690005)" funded by the Korea Ministry of Environment (MOE) as the "Global Top Environment R&D Program"

Declarations of interest: none

References

[1] R.A. Reimer, C.S. Slaten, M. Seapan, M.W. Lower, P.E. Tomlinson, Abatement of N2O emissions produced in the adipic acid industry, Environmental Progress, 13 (1994) 134-137.
[2] D.E. Becker, M. Rosenberg, Nitrous oxide and the inhalation anesthetics, Anesthesia progress, 55 (2008) 124-132.
[3] V. Zakirov, M. Sweeting, T. Lawrence, J. Sellers, Nitrous oxide as a rocket propellant, Acta Astronautica, 48 (2001) 353-362.
[4] L. Martinu, D. Poitras, Plasma deposition of optical films and coatings: A review, Journal of Vacuum Science & Technology A: Vacuum, Surfaces, and Films, 18 (2000) 2619-2645.
[5] A. Shimizu, K. Tanaka, M. Fujimori, Abatement technologies for N2O emissions in the adipic acid industry, Chemosphere - Global Change Science, 2 (2000) 425-434.
[6] D. Saha, S.G. Deng, Adsorption Equilibrium, Kinetics, and Enthalpy of N2O on Zeolite 4A and 13X, Journal of Chemical and Engineering Data, 55 (2010) 3312-3317.
[7] Y. Peng, F. Zhang, C. Xu, Q. Xiao, Y. Zhong, W. Zhu, Adsorption of Nitrous Oxide on Activated Carbons, Journal of Chemical & Engineering Data, 54 (2009) 3079-3081.
[8] C.R. Reid, K.M. Thomas, Adsorption of Gases on a Carbon Molecular Sieve Used for Air Separation: Linear Adsorptives as Probes for Kinetic Selectivity, Langmuir, 15 (1999) 3206-3218.
[9] G. Domínguez, R. Hernández-Huesca, G. Aguilar-Armenta, Isosteric Heats of Adsorption of N2O and NO on Natural Zeolites, Journal of the Mexican Chemical Society, 54 (2010) 111-116.
[10] R. Hernández Huesca, J. Pérez Arcos, D. Vargas Hernández, M.A. Pérez Cruz, Adsorption kinetics of N2O on natural zeolites, Revista Internacional de Contaminación Ambiental, 32 (2016) 237-242.
[11] D. Saha, Z. Bao, F. Jia, S. Deng, Adsorption of CO2, CH4, N2O, and N2 on MOF-5, MOF-177, and Zeolite 5A, Environmental Science & Technology, 44 (2010) 1820-1826.
[12] D. Saha, S. Deng, Adsorption equilibrium and kinetics of CO2, CH4, N2O, and NH3 on ordered mesoporous carbon, Journal of Colloid and Interface Science, 345 (2010) 402-409.
[13] Y.-H. Kim, J.-J. Kim, C.-H. Lee, Adsorptive cyclic purification process for CO2 mixtures captured from coal power plants, AIChE Journal, 63 (2017) 1051-1063.
[14] S.-C. Jang, S.-I. Yang, S.-G. Oh, D.-K. Choi, Adsorption dynamics and effects of carbon to zeolite ratio of layered beds for multicomponent gas adsorption, Korean Journal of Chemical Engineering, 28 (2011) 583-590.
[15] D.-K. Moon, D.-G. Lee, C.-H. Lee, H2 pressure swing adsorption for high pressure syngas from an integrated gasification combined cycle with a carbon capture process, Applied Energy,

183 (2016) 760-774.
[16] M.-B. Kim, Y.-S. Bae, D.-K. Choi, C.-H. Lee, Kinetic Separation of Landfill Gas by a Two-Bed Pressure Swing Adsorption Process Packed with Carbon Molecular Sieve: Nonisothermal Operation, Industrial & Engineering Chemistry Research, 45 (2006) 5050-5058.
[17] S. Sircar, J.R. Hufton, Why Does the Linear Driving Force Model for Adsorption Kinetics Work?, Adsorption, 6 (2000) 137-147.
[18] Y.D. Chen, R.T. Yang, P. Uawithya, Diffusion of oxygen, nitrogen and their mixtures in carbon molecular sieve, AIChE Journal, 40 (1994) 577-585.
[19] S. Farooq, H. Qinglin, I.A. Karimi, Identification of Transport Mechanism in Adsorbent Micropores from Column Dynamics, Industrial & Engineering Chemistry Research, 41 (2002) 1098-1106.
[20] A.L. Myers, Activity coefficients of mixtures adsorbed on heterogeneous surfaces, AIChE Journal, 29 (1983) 691-693.
[21] D. D Do, Adsorption Analysis: Equilibria and Kinetics, Imperial College Press, London, 1998.
[22] S. Sircar, R. Mohr, C. Ristic, M.B. Rao, Isosteric Heat of Adsorption: Theory and Experiment, The Journal of Physical Chemistry B, 103 (1999) 6539-6546.
[23] R.T. Yang, Fundamental Factors for Designing Adsorbent, in: Adsorbents: Fundamentals and Applications, John Wiley & Sons, Inc., 2003.
[24] S. Chowdhury, R. Mishra, P. Saha, P. Kushwaha, Adsorption thermodynamics, kinetics and isosteric heat of adsorption of malachite green onto chemically modified rice husk, Desalination, 265 (2011) 159-168.
[25] M. Kocirik, P. Struve, M. Bulow, Analytical solution of simultaneous mass and heat transfer in zeolite crystals under constant-volume/variable-pressure conditions, Journal of the Chemical Society, Faraday Transactions 1: Physical Chemistry in Condensed Phases, 80 (1984) 2167-2174.
[26] J. CRANK, The Mathematics of Diffusion, 2nd Edn, Oxford University Press, Oxford, 1975.
[27] D.M. Ruthven, L.-K. Lee, H. Yucel, Kinetics of non-isothermal sorption in molecular sieve crystals, AIChE Journal, 26 (1980) 16-23.
[28] J. Kärger, D.M. Ruthven, Diffusion in zeolites and other microporous solids, Wiley, 1992.
[29] J.-J. Kim, S.-J. Lim, H. Ahn, C.-H. Lee, Adsorption equilibria and kinetics of propane and propylene on zeolite 13X pellets, Microporous and Mesoporous Materials, 274 (2019) 286-298.
[30] Y. Park, D.-K. Moon, D. Park, M. Mofarahi, C.-H. Lee, Adsorption equilibria and kinetics of CO2, CO, and N2 on carbon molecular sieve, Separation and Purification Technology, 212 (2019) 952-964.
[31] NIST Chemistry WebBook, Thermophysical Properties of Fluid Systems, http://webbook.nist.gov/chemistry/fluid/, in, 2017.
[32] Y. Park, D.-K. Moon, Y.-H. Kim, H. Ahn, C.-H. Lee, Adsorption isotherms of CO2, CO, N2, CH4, Ar and H2 on activated carbon and zeolite LiX up to 1.0 MPa, Adsorption, 20 (2014) 631-647.
[33] R.E. Bazan, M. Bastos-Neto, A. Moeller, F. Dreisbach, R. Staudt, Adsorption equilibria of O2, Ar, Kr and Xe on activated carbon and zeolites: single component and mixture data, Adsorption, 17 (2011) 371-383.
[34] Y. Yang, A.M. Ribeiro, P. Li, J.-G. Yu, A.E. Rodrigues, Adsorption Equilibrium and Kinetics of Methane and Nitrogen on Carbon Molecular Sieve, Industrial & Engineering Chemistry Research, 53 (2014) 16840-16850.
[35] C.R. Reid, I.P. O'Koy, K.M. Thomas, Adsorption of Gases on Carbon Molecular Sieves Used for Air Separation. Spherical Adsorptives as Probes for Kinetic Selectivity, Langmuir,

14 (1998) 2415-2425.
[36] H.M. Yi, S. Weiruo, B. Maruti, W. Jinqu, G.W. Miller, Adsorption and diffusion of nitrogen, oxygen, argon, and methane in molecular sieve carbon at elevated pressures, Separations Technology, 1 (1991) 90-98.
[37] Y.-J. Park, S.-J. Lee, J.-H. Moon, D.-K. Choi, C.-H. Lee, Adsorption Equilibria of O2, N2, and Ar on Carbon Molecular Sieve and Zeolites 10X, 13X, and LiX, Journal of Chemical & Engineering Data, 51 (2006) 1001-1008.
[38] Y.S. Bae, C.H. Lee, Sorption kinetics of eight gases on a carbon molecular sieve at elevated pressure, Carbon, 43 (2005) 95-107.
[39] I.P. O'Koye, M. Benham, K.M. Thomas, Adsorption of Gases and Vapors on Carbon Molecular Sieves, Langmuir, 13 (1997) 4054-4059.
[40] S. Cavenati, C.A. Grande, A.E. Rodrigues, Separation of Methane and Nitrogen by Adsorption on Carbon Molecular Sieve, Separation Science and Technology, 40 (2005) 2721-2743.
[41] K. Kaneko, Molecular assembly formation in a solid nanospace, Colloids and Surfaces A: Physicochemical and Engineering Aspects, 109 (1996) 319-333.
[42] H.K. Chagger, F.E. Ndaji, M.L. Sykes, K.M. Thomas, Kinetics of adsorption and diffusional characteristics of carbon molecular sieves, Carbon, 33 (1995) 1405-1411.
[43] D.M. Ruthven, N.S. Raghavan, M.M. Hassan, Adsorption and diffusion of nitrogen and oxygen in a carbon molecular sieve, Chemical Engineering Science, 41 (1986) 1325-1332.
[44] Y.-S. Bae, J.-H. Moon, H. Ahn, C.-H. Lee, Effects of adsorbate properties on adsorption mechanism in a carbon molecular sieve, Korean Journal of Chemical Engineering, 21 (2004) 712-720.
[45] Y. Ju, Y. Park, D. Park, J.-J. Kim, C.-H. Lee, Adsorption kinetics of CO2, CO, N2 and CH4 on zeolite LiX pellet and activated carbon granule, Adsorption, 21 (2015) 419-432.
[46] M. Jahandar Lashaki, M. Fayaz, S. Niknaddaf, Z. Hashisho, Effect of the adsorbate kinetic diameter on the accuracy of the Dubinin–Radushkevich equation for modeling adsorption of organic vapors on activated carbon, Journal of Hazardous Materials, 241-242 (2012) 154-163.
[47] S.-Y. Wu, C.-H. Su, J.-G. Chang, H.-T. Chen, C.-H. Hou, H.-L. Chen, Adsorption and dissociation of N2O molecule on Fe(111) surface: A DFT study, Computational Materials Science, 50 (2011) 3311-3314.
[48] H. Qinglin, S.M. Sundaram, S. Farooq, Revisiting Transport of Gases in the Micropores of Carbon Molecular Sieves, Langmuir, 19 (2003) 393-405.

Figure captions

Figure 1. (a) Macropore size distribution and (b) cumulative volume of CMS, determined via mercury porosimetry

Figure 2. Cumulative pore volume and pore size distribution of AC and CMS from the density functional theory (○ and ●, activated carbon; △ and ▲, carbon molecular sieve [30]; closed symbol for cumulative pore volume; open symbol for pore size distribution)

Figure 3. Schematic diagram of high-pressure adsorption system

Figure 4. Experimental adsorption isotherms and DSL model for AC and CMS: ●, 293 K; ▲, 308 K; ■, 323 K; (e) N_2/AC [32]; solid line, DSL model (○, N_2O/AC at 323 K [7]; △, CO_2/AC at 323 K [32]; □, CO_2/CMS at 318 K [30]; +, O_2/AC at 303 K [33]; x, N_2/CMS at 323 K [34])

Figure 5. Isosteric heats of adsorption for AC (a) and CMS (b): solid line, N_2O; dotted line, O_2; dashed line, N_2

Figure 6. Experimental uptake curves for N_2O on AC (a) and CMS (b) at 308K (closed symbol, particle (200-500 μm); open symbol, pellet)

Figure 7. Experimental uptake curves of adsorption and desorption for N_2O on (a) AC and (b) CMS at 308 K: ●, adsorption; △, desorption

Figure 8. Experimental uptake curves and non-isothermal adsorption model for AC ((a) and (c)) and CMS ((b) and (d)) at 308K: solid line, non-isothermal adsorption model

Figure 9. Experimental uptake curves, non-isothermal adsorption model, and isothermal dual resistance model for N_2 on CMS: solid line, non-isothermal adsorption model; dashed line, isothermal dual resistance model

Figure 10. Experimental uptake curves, non-isothermal adsorption model, and isothermal dual resistance model for adsorption of gases on AC (a) at 293 K and on CMS (b) at 308 K: solid line, non-isothermal adsorption model; dashed line, isothermal dual resistance model (data for N_2 adsorption on AC at 293 K are taken from the literature [45])

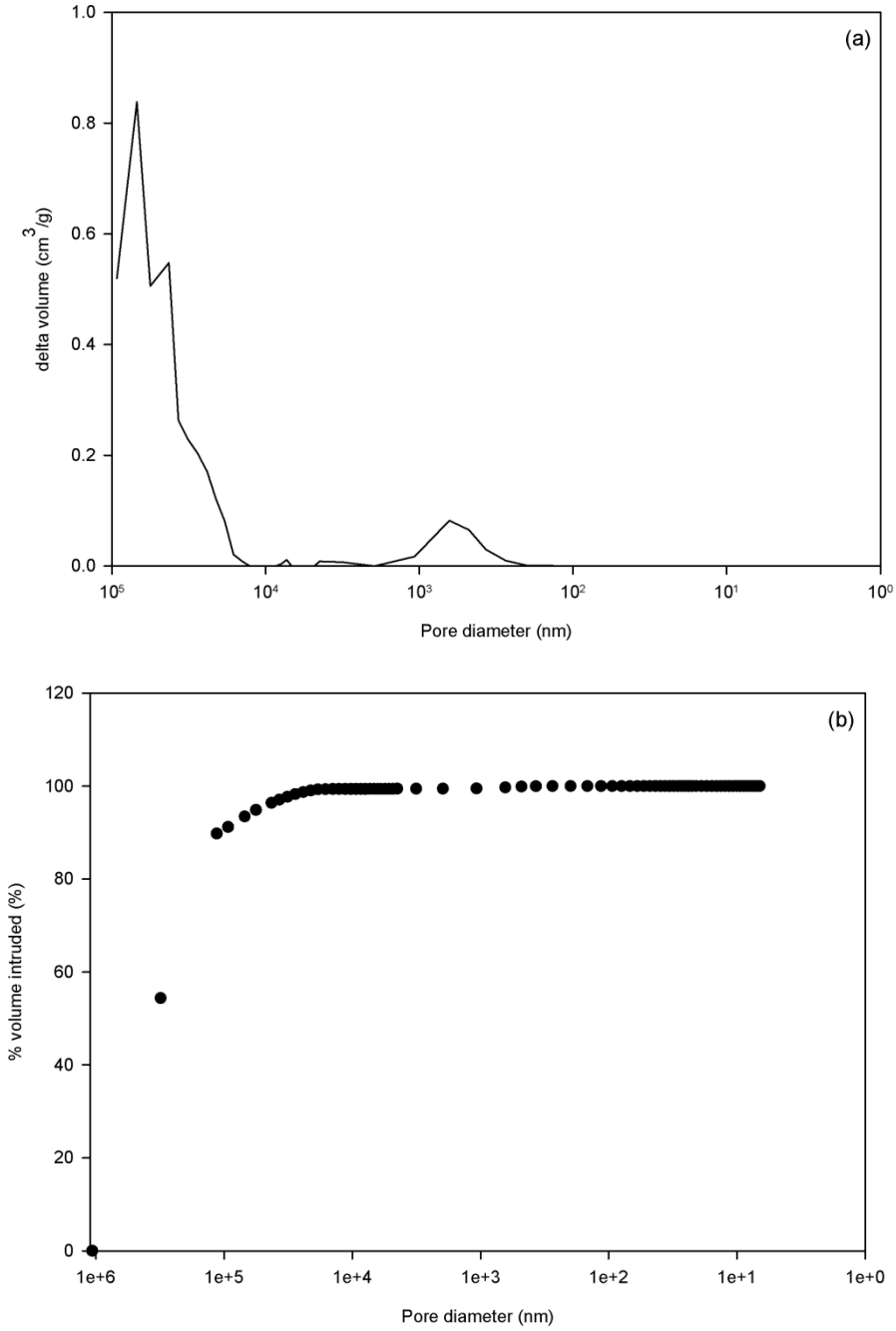

Figure 1. (a) Macropore size distribution and (b) cumulative volume of CMS, determined via mercury porosimetry.

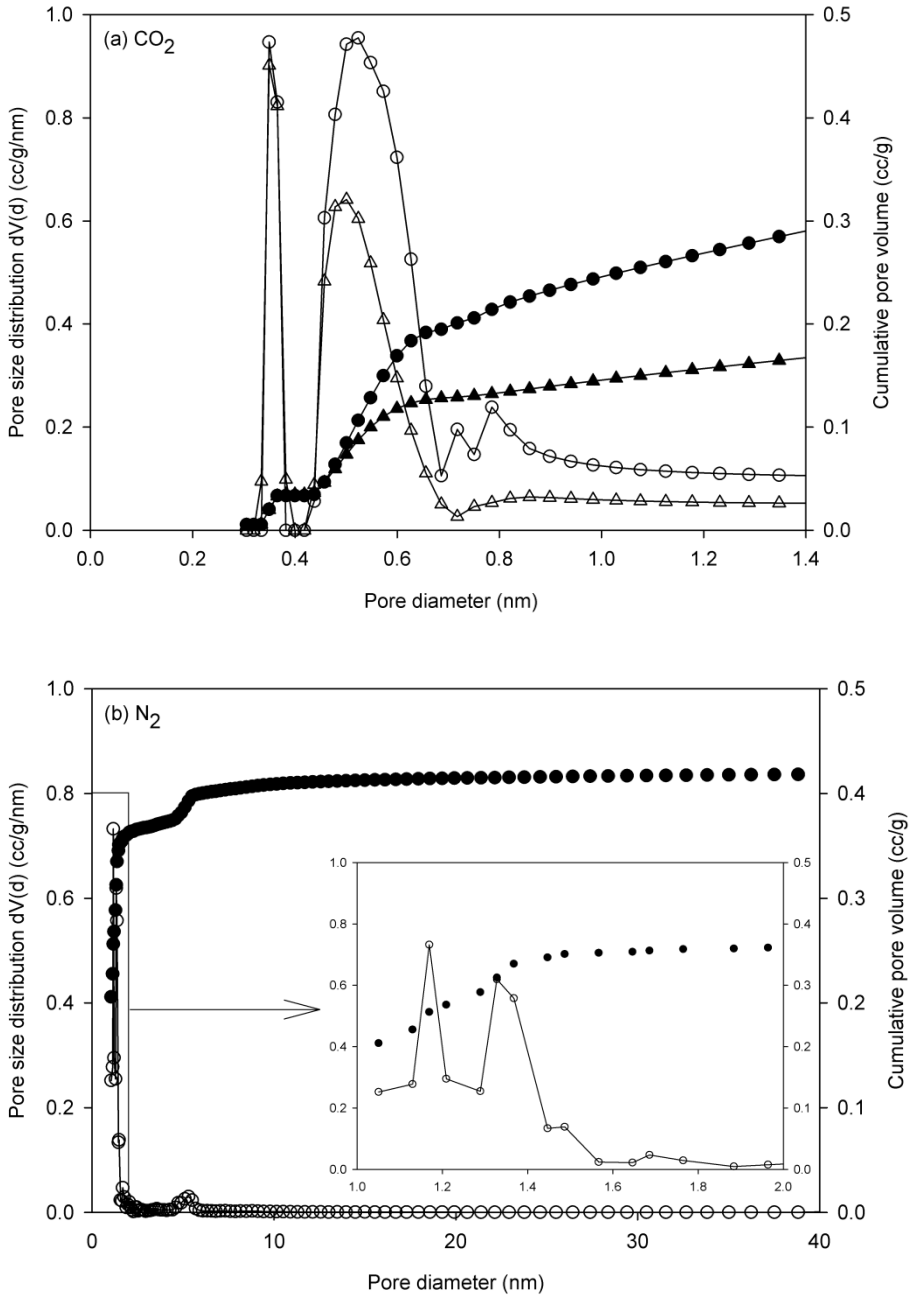

Figure 2. Cumulative pore volume and pore size distribution of AC and CMS from the density functional theory (○ and ●, activated carbon; △ and ▲, carbon molecular sieve [30]; closed symbol for cumulative pore volume; open symbol for pore size distribution)

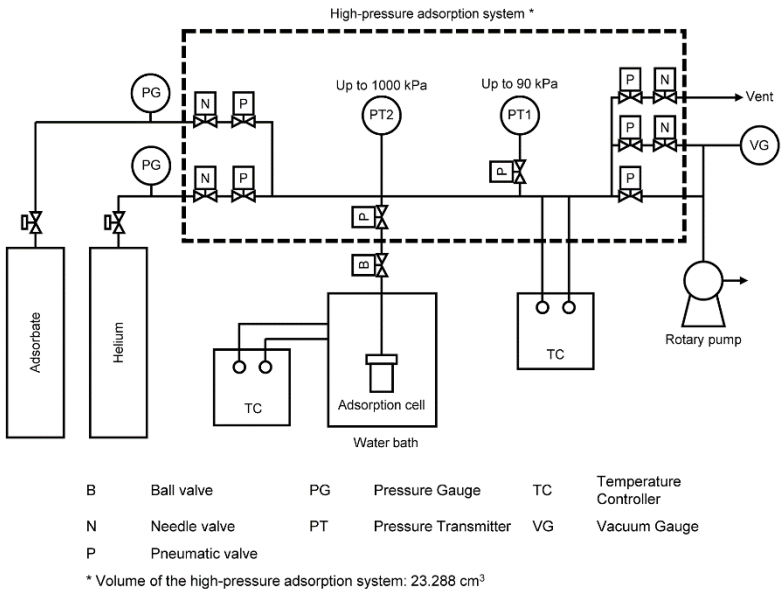

B	Ball valve	PG	Pressure Gauge	TC	Temperature Controller
N	Needle valve	PT	Pressure Transmitter	VG	Vacuum Gauge
P	Pneumatic valve				

* Volume of the high-pressure adsorption system: 23.288 cm^3

Figure 3. Schematic diagram of high-pressure adsorption system.

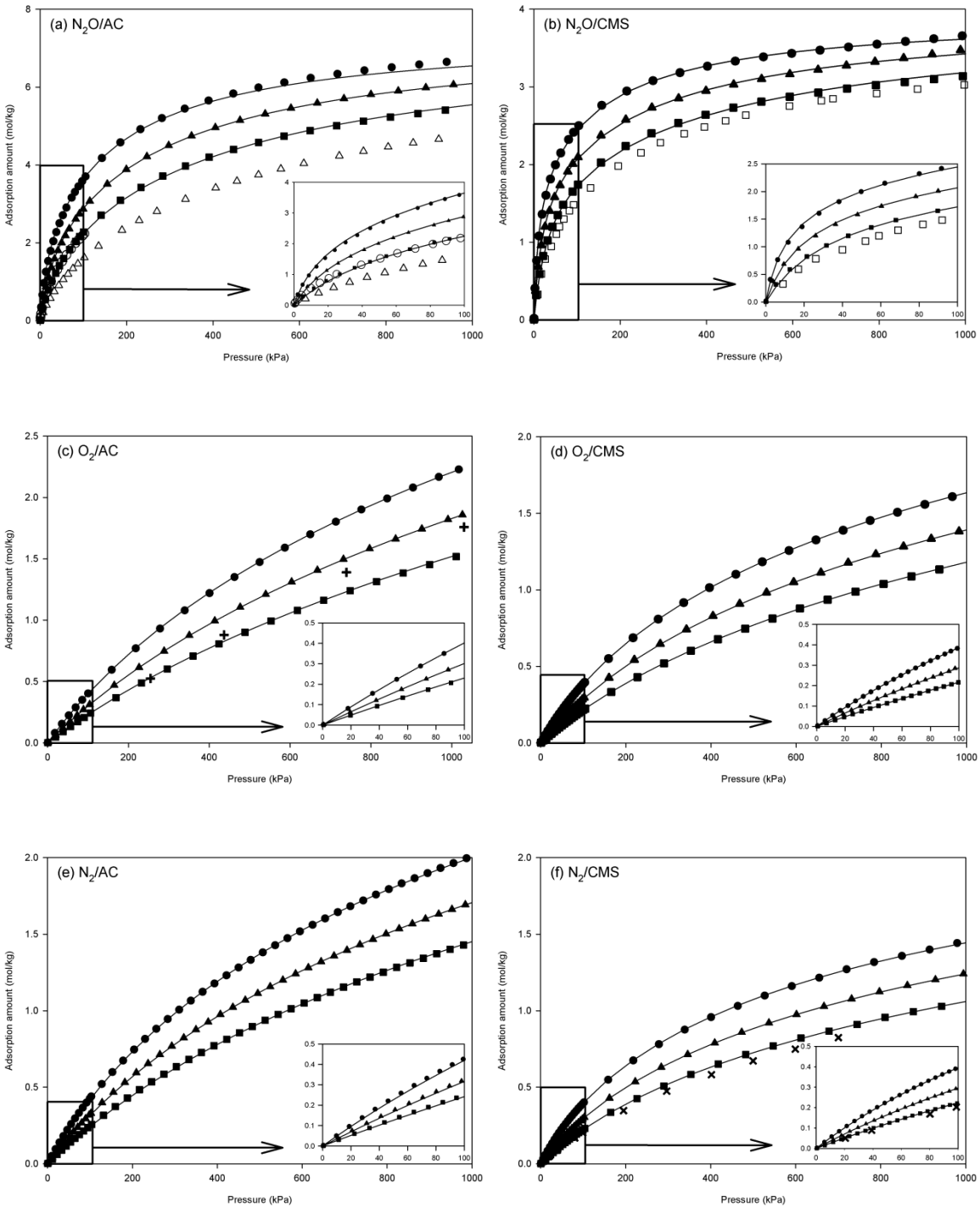

Figure 4. Experimental adsorption isotherms and DSL model for AC and CMS: ●, 293 K; ▲, 308 K; ■, 323 K; (e) N_2/AC [32]; solid line, DSL model (○, N_2O/AC at 323 K [7]; △, CO_2/AC at 323 K [32]; □, CO_2/CMS at 318 K [30]; +, O_2/AC at 303 K [33]; x, N_2/CMS at 323 K [34]).

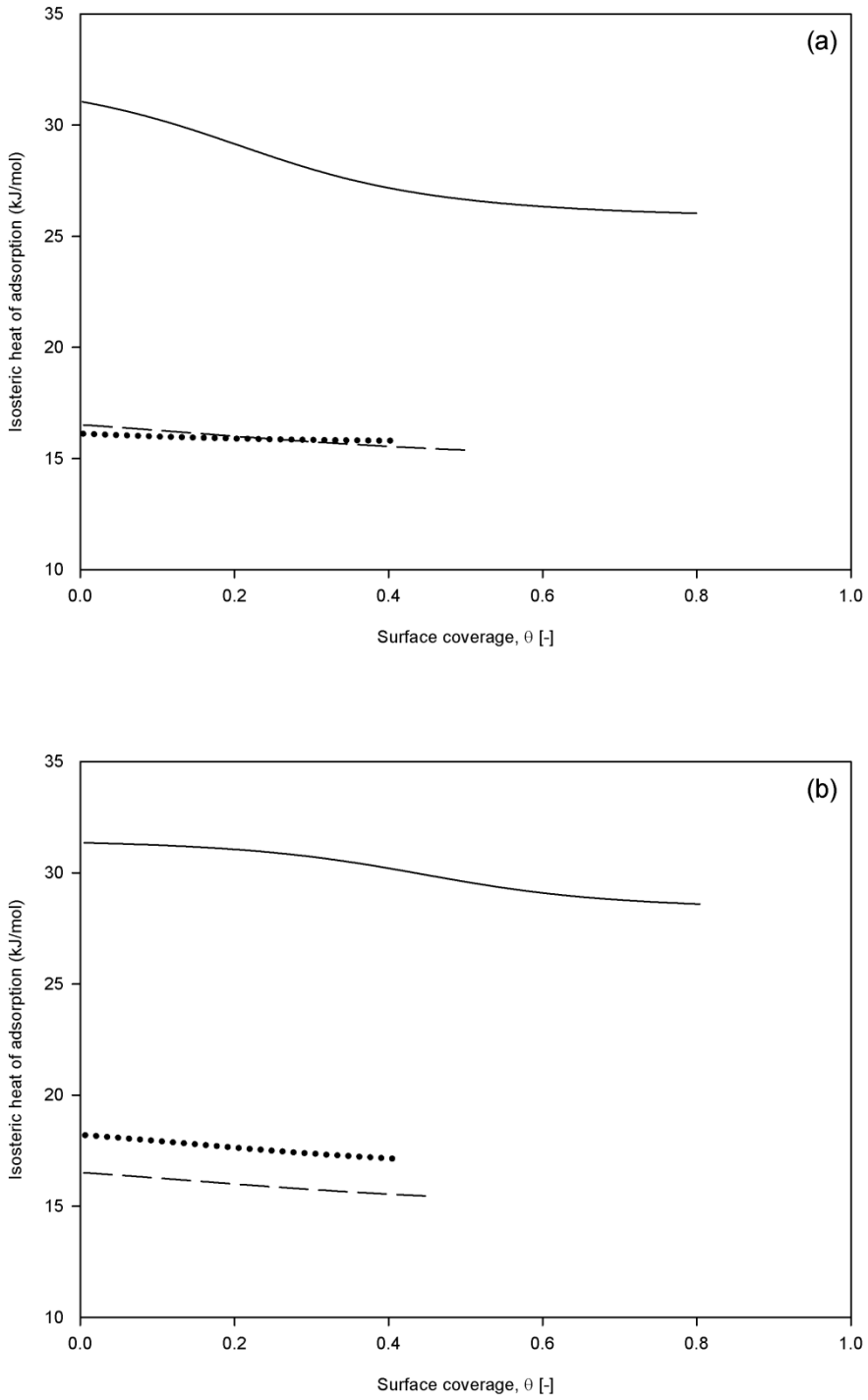

Figure 5. Isosteric heats of adsorption for AC (a) and CMS (b): solid line, N_2O; dotted line, O_2; dashed line, N_2.

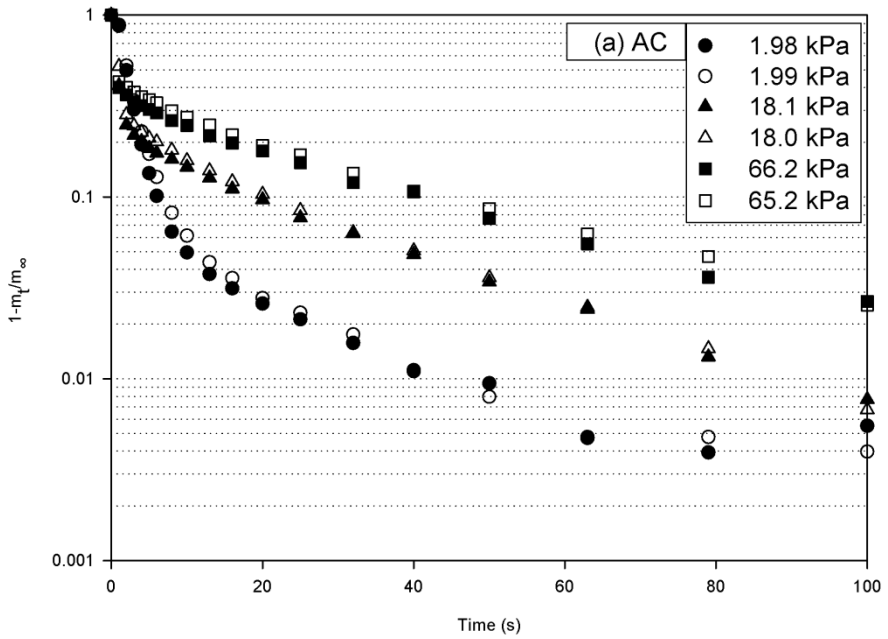

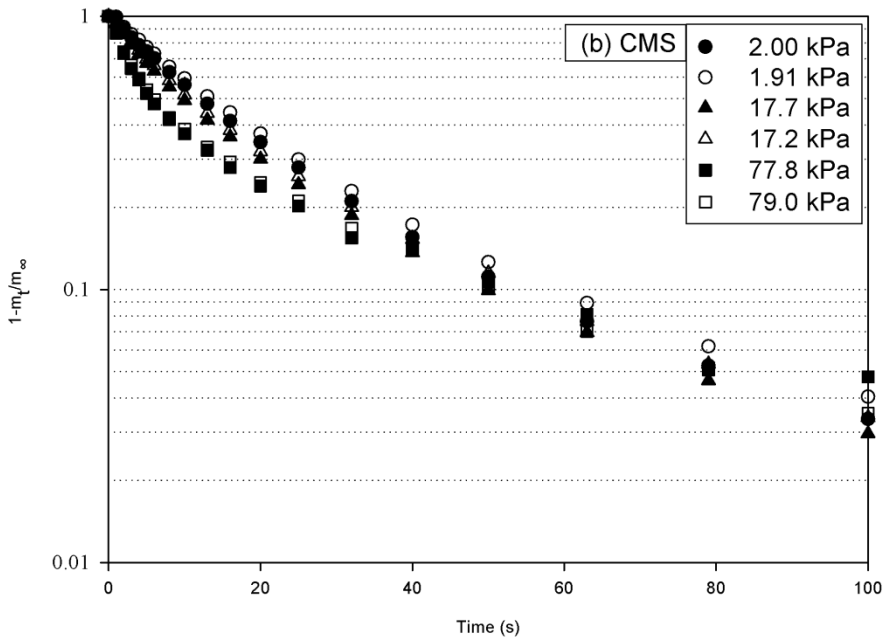

Figure 6. Experimental uptake curves for N_2O on AC (a) and CMS (b) at 308K (closed symbol, particle (200-500 μm); open symbol, pellet).

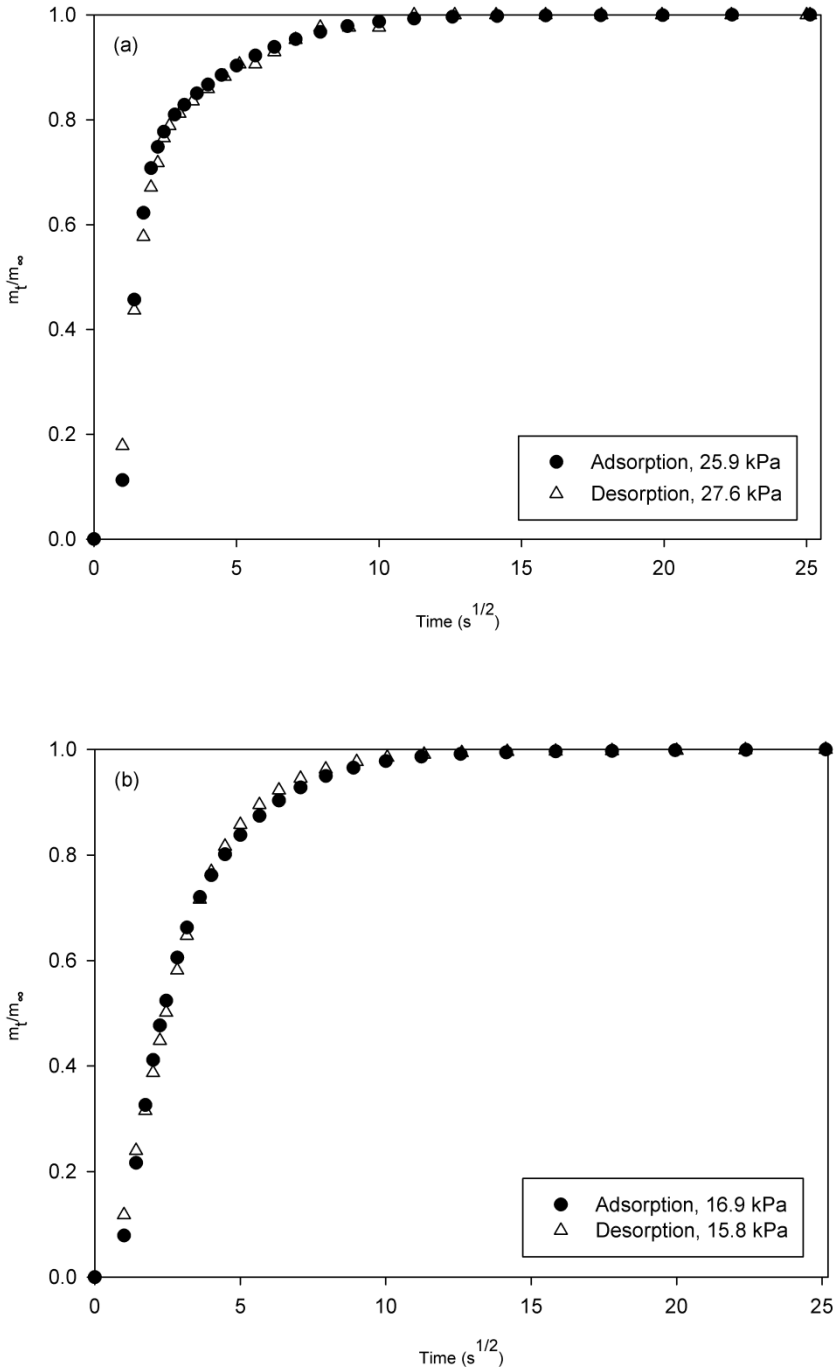

Figure 7. Experimental uptake curves of adsorption and desorption for N_2O on (a) AC and (b) CMS at 308 K: ●, adsorption; △, desorption

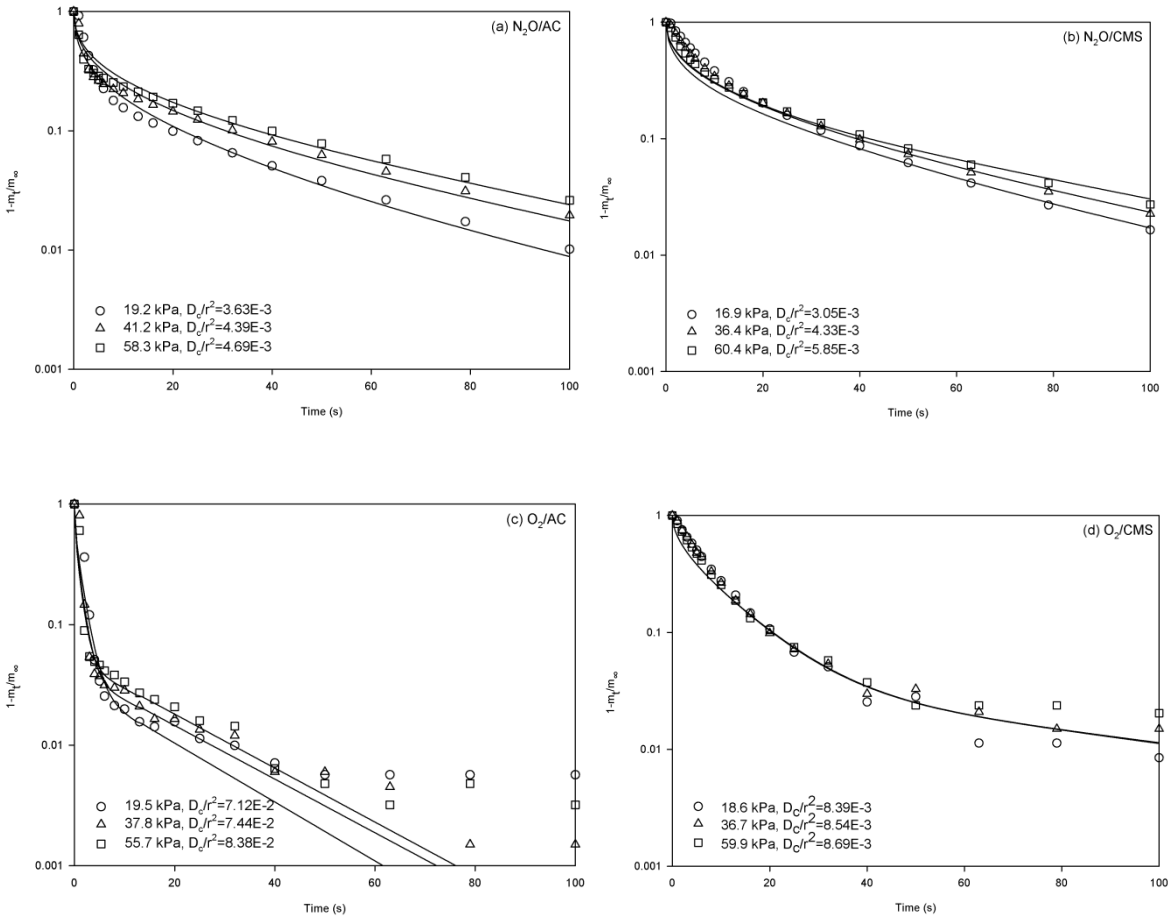

Figure 8. Experimental uptake curves and non-isothermal adsorption model for AC ((a) and (c)) and CMS ((b) and (d)) at 308K: solid line, non-isothermal adsorption model.

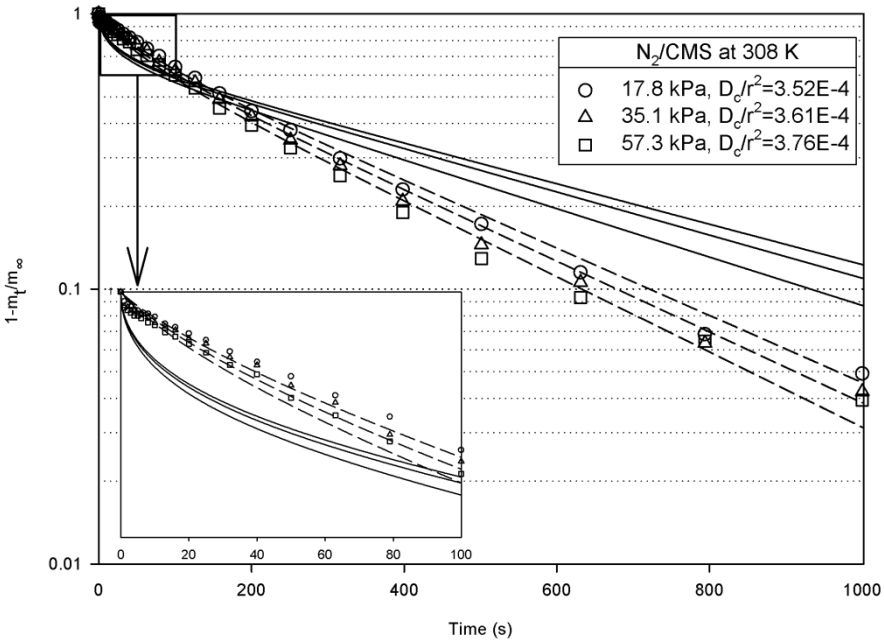

Figure 9. Experimental uptake curves, non-isothermal adsorption model, and isothermal dual resistance model for N_2 on CMS: solid line, non-isothermal adsorption model; dashed line, isothermal dual resistance model.

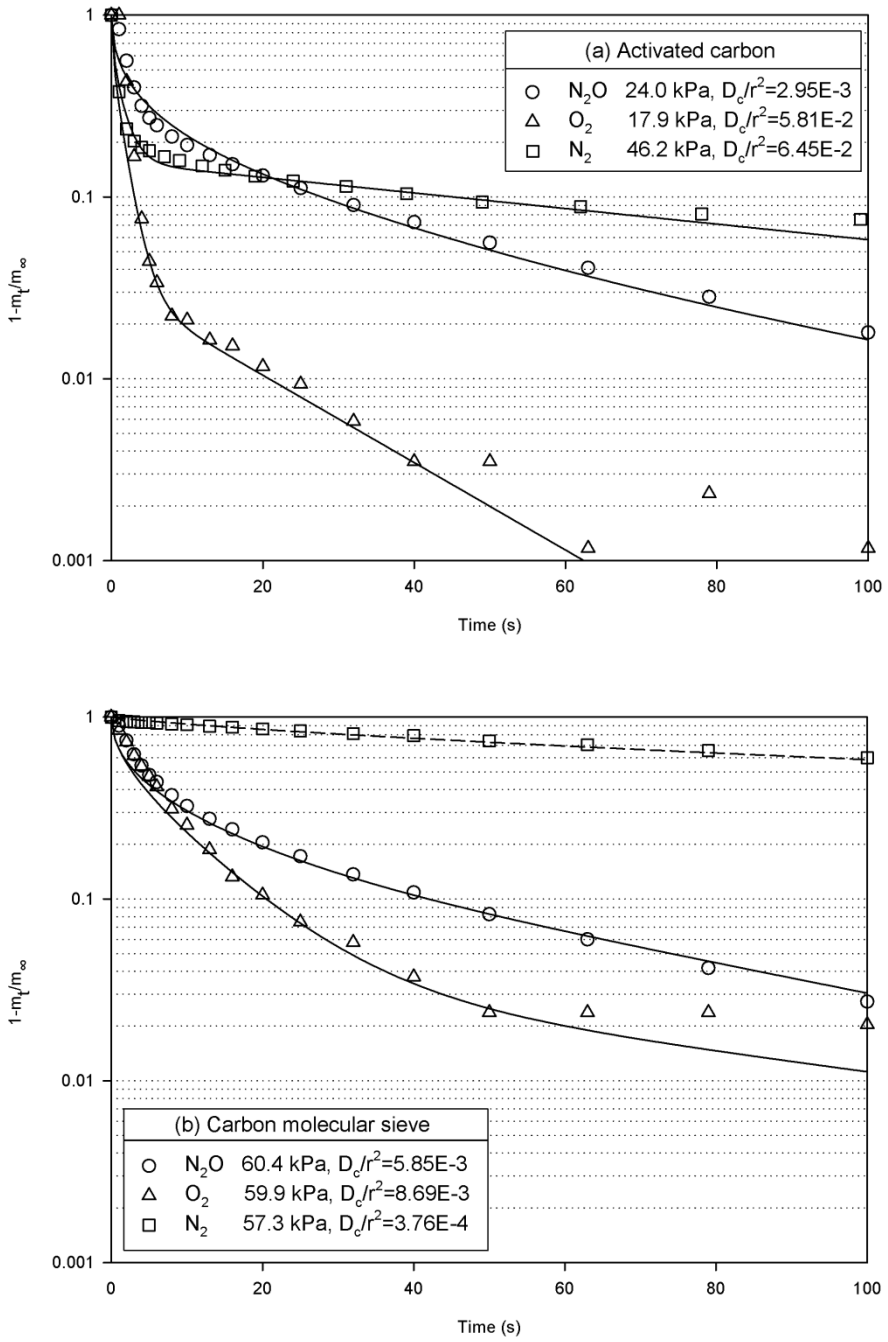

Figure 10. Experimental uptake curves, non-isothermal adsorption model, and isothermal dual resistance model for adsorption of gases on AC (a) at 293 K and on CMS (b) at 308 K: solid line, non-isothermal adsorption model; dashed line, isothermal dual resistance model (data for N_2 adsorption on AC at 293 K are taken from the literature [45]).

Table 1. Physical properties of adsorbents

Property	Activated carbon	CMS
Type	Cylindrical	Cylindrical
Diameter [mm] *	1.7-2.36	1.3-1.5
Specific surface area [m^2/g]	1306.4**	436.8 (BET eqn.)*** 640.9 (DR eqn.)***
Micropore volume [cm^3/g]	0.370****	0.241***
Micropore diameter [nm]	1.67**	0.830***
Macropore volume [cm^3/g] *****	-	0.236
Macropore diameter [nm] *****	-	639
Particle density [g/ cm^3]	0.77	0.96
Heat capacity [J/g K] *	1.05	-

* Information from the manufacturer, KURARAY CHEMICAL Co., Japan.

** Data from [31]

*** Data from [30]

**** Information from the adsorption and desorption isotherms of N_2 at 77 K and CO_2 at 273K

***** Information from the mercury porosimetry

Table 2. Properties of adsorbate gases

Gas	Molar mass [g/mol]	Kinetic diameter [pm]	Van der Waals radius [pm]	Covalent radius [pm]	Electronegativity (Pauling's scale)	Dipole moment [D]
N_2O *	44	330	112.6 for N-N 118.6 for N-O	-	-	0.161
O_2	32	346	152	66±2	3.44	-
N_2	28	364	155	71±1	3.04	-

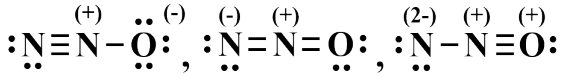

* Three fundamental modes of N_2O

Table 3. Comparison of adsorption equilibrium parameters for N_2O, O_2 and N_2

Adsorbent	Manufacturer	T [K]	P [kPa]	q_m [mol kg^{-1}]	Q_{st} [kJ mol^{-1}]	Model	Ref.
N_2O							
AC	Kureha			15.3	29		
AC (Vruf)	Calgon	195	101	12.7	29.7	Multi-process	[7]
AC (Ovcls)	Calgon			36.9	28.2		
CMS A	Air products	303	9	3.8	31.8	Virial parameters	[8]
AC	Kuraray	293-323	1000	7.40 8.21	31.0 -	DSL Sips	This study
CMS	Kuraray	293-323	1000	3.93 4.14	31.4 -	DSL Sips	This study
O_2							
CMS	Air products	273-313	9	-	22 18.6	Virial parameters Low-P region	[35]
CMS 3A	Takeda	273-323	1300	1.37-2.32 1.74-2.66	18.0	Langmuir Vacancy solution	[36]
CMS 5A	Takeda			1.64-2.78 2.23-2.85	15.5	Langmuir Vacancy solution	
CMS	Bergbau-Forschung	303	1300	1.62 1.74	-	Langmuir Vacancy solution	
CMS 3A	Takeda	293-313	80	1.17-0.98 4.07-3.51 86.2-21.0	-	Langmuir Sips Toth	[37]
CMS	Takeda	293-313	1500	3.48-3.63 4.55-4.83	15.5	Langmuir Langmuir-Freundlich	[38]
AC	Norit	303	3150	5.82	-	Langmuir	[33]
AC	Kuraray	293-323	1000	5.70 5.17	16.1 -	DSL Sips	This study
CMS	Kuraray	293-323	1000	3.27 2.89	18.2 -	DSL Sips	This study
N_2							
CMS	Air products	293	100	0.3	-	Virial parameters	[39]
CMS A	Air products	303-343	100	-	21.5	Virial parameters	[35]
CMS	Changxing Shanli chemical materials	303-343	700	7.25 2.61	17.5 17.6	Multisite Langmuir Toth	[34]
CMS 3K	TAKEDA	308	2000	10.6	15.93	Multisite Langmuir	[40]
CMS 3A	Takeda	273-323	1300	1.68-1.97 1.81-2.12	13.5	Langmuir Vacancy solution	[36]
CMS 5A	Takeda	273-323	1300	1.58-2.14 1.9-2.46	-	Langmuir Vacancy solution	
CMS	Bergbau-Forschung	303	1300	1.48 1.59	-	Langmuir Vacancy solution	
CMS	Takeda	293-313	1500	2.55-3.11 3.40-4.63	25.1	Langmuir Langmuir-Freundlich	[38]
AC	Kuraray	293-323	1000	3.18-3.45 3.71-4.29 4.61-5.60	18.2 - -	Langmuir Sips Toth	[32]
CMS	Kuraray	298-318	1000	1.72-1.99 1.71-2.20	- 16	Langmuir Sips	[30]
AC	Kuraray	293-323	1000	3.93 2.89	16.5 -	DSL Sips	This study
CMS	Kuraray	293-323	1000	2.44 2.21	16.5 -	DSL Sips	This study

Table 4. Parameters for dual-site Langmuir and Sips models

		AC								
		DSL*				Sips**				
Gas	Temp.	$q_{m,d1}$ $q_{m,d2}$	$b_{d1} \times 10^5$ $b_{d2} \times 10^5$	$k_{d1} \times 10^8$ $k_{d3} \times 10^8$	k_{d2} k_{d4}	$q_{m,s}$	$b_s \times 10^4$	$k_{s1} \times 10^7$ k_{s2}	n	k_{s3} k_{s4}
N_2O	293K		565 7262				67.76		1.370	
	308K	5.52 1.882	338 3797	14.9 11.9	3091 3905	8.21	40.16	1.46 3150	1.383	0.5911 40.64
	323K		212 2109				24.99		1.395	
O_2	293K		50.3 289				7.29		1.050	
	308K	4.969 0.7313	36.8 206	82.8 284	1879 2030	5.175	5.26	8.83 1969	1.058	0.8169 39.66
	323K		27.7 152				3.91		1.064	
N_2***	293K		54.0 275				11.13		1.040	
	308K	3.267 1.168	40.2. 194	124 210	1781 2105	3.797	8.04	13.80 1962	1.048	0.8082 44.97
	323K		30.7 141				5.98		1.056	

		CMS								
		DSL*				Sips**				
Gas	Temp.	$q_{m,d1}$ $q_{m,d2}$	$b_{d1} \times 10^5$ $b_{d2} \times 10^5$	$k_{d1} \times 10^8$ $k_{d3} \times 10^8$	k_{d2} k_{d4}	$q_{m,s}$	$b_s \times 10^4$	$k_{s1} \times 10^7$ k_{s2}	n	k_{s3} k_{s4}
N_2O	293K		622 10422				179.3		1.480	
	308K	2.157 1.774	354 5544	5.7 24.4	3400 3801	4.141	100.2	1.15 3506	1.494	0.5472 37.69
	323K		212 3127				59.08		1.506	
O_2	293K		67 408				13.06		1.078	
	308K	2.477 0.7935	48 279	76.3 160	1989 2300	2.895	9.17	9.13 2130	1.081	0.8734 17.76
	323K		36 197				6.65		1.084	
N_2	293K		98 553				19.07		1.089	
	308K	1.776 0.6657	67 382	40.8 270	2283 2235	2.21	12.98	7.07 2316	1.091	0.8775 12.07
	323K		48 273				9.16		1.093	

* DSL model parameters: $q_{m,d1}$ and $q_{m,d2}$ [mol kg^{-1}], b_{d1} and b_{d2}[kPa^{-1}], k_{d1} and k_{d2} [kPa^{-1}], k_{d3} and k_{d4} [K]

** Sips model parameters: $q_{m,s}$ [mol kg^{-1}], n [-], b_s [kPa^{-1}], k_{s1} [kPa^{-1}], k_{s2} [K], k_{s3} [-], k_{s4} [K]

*** Experimental data for N_2 adsorption on AC are taken from the literature [32]

Table 5. Micropore diffusion time constant and parameters for AC from non-isothermal adsorption model

Temperature [K]	Pressure [kPa]	$D_c/r^2 \times 10^4$ [s^{-1}]	α [-]	β [-]
N_2O				
293		17.6*		
	18.3	28.0	6.89	0.213
	24.0	29.5	6.45	0.253
	30.3	29.5	6.41	0.270
	37.2	30.2	6.67	0.291
	44.7	31.0	6.14	0.305
	52.4	32.5	6.41	0.353
	60.6	35.6	5.70	0.398
	72.6	37.8	5.91	0.462
308		26.4*		
	19.2	36.3	6.72	0.219
	25.9	37.8	5.98	0.228
	33.3	39.3	5.83	0.233
	41.2	43.9	5.51	0.313
	49.6	46.1	5.51	0.351
	58.3	46.9	5.14	0.362
	67.2	48.4	4.91	0.381
323		41.5*		
	18.8	49.4	4.72	0.154
	26.9	52.0	4.37	0.197
	35.6	57.3	4.58	0.272
	44.6	65.2	4.31	0.344
	54.2	67.9	3.44	0.350
	67.9	72.3	3.42	0.366
	82.2	74.9	3.15	0.420
O_2				
293		575*		
	17.9	581	0.98	0.035
	35.3	613	0.67	0.040
	52.4	654	0.66	0.062
	69.1	701	0.65	0.072
	85.7	698	0.72	0.088
308		700*		
	19.5	712	0.81	0.033
	37.8	744	0.72	0.043
	55.7	838	0.65	0.055
	73.2	878	0.67	0.065
323		927*		
	19.6	960	0.91	0.031
	38.5	959	0.84	0.038
	56.6	1000	0.68	0.052
	74.4	1020	0.70	0.053

* Corrected diffusivity ($D_{c,0}/r^2$)

Table 6. Micropore diffusion time constant and parameters for CMS from non-isothermal adsorption model

Temperature [K]	Pressure [kPa]	$D_c/r^2 \times 10^4$ [s^{-1}]	α [-]	β [-]
N_2O				
293		15.3*		
	11.6	17.3	9.63	0.240
	18.9	23.7	8.00	0.271
	27.8	28.8	7.27	0.301
	38.1	35.6	6.35	0.306
	49.7	41.7	5.19	0.311
	62.1	49.2	4.37	0.319
	80.1	59.8	3.72	0.350
308		23.2*		
	16.9	30.5	7.57	0.253
	26.0	36.1	6.95	0.279
	36.4	43.3	5.61	0.286
	47.9	50.5	4.59	0.288
	60.4	58.5	3.91	0.292
	78.3	67.3	3.45	0.304
323		30.6*		
	12.5	35.1	7.59	0.247
	21.4	40.3	8.21	0.284
	31.6	46.9	6.79	0.287
	43.0	54.7	5.84	0.298
	55.0	63.8	4.86	0.318
	67.8	76.8	4.06	0.344
O_2				
293		43.9*		
	11.3	45.7	2.27	0.0383
	16.7	46.5	2.26	0.0385
	27.4	48.8	2.16	0.0389
	38.1	50.3	2.17	0.0393
	48.9	52.6	2.11	0.0397
	59.2	51.8	2.19	0.0401
	64.3	49.6	2.31	0.0403
	74.9	53.7	2.17	0.0408
308		73.1*		
	12.6	75.5	2.02	0.0399
	18.6	83.9	2.19	0.0401
	24.5	81.6	2.31	0.0403
	36.7	85.4	2.17	0.0408
	48.3	86.9	2.05	0.0412
	59.9	86.9	1.52	0.0418
	65.6	86.2	1.52	0.0418
	76.5	92.3	1.13	0.0419
323		118*		
	13.0	120	1.22	0.0433
	19.3	129	1.19	0.0434
	25.4	125	1.19	0.0435
	37.6	135	1.16	0.0436
	49.5	135	1.15	0.0437
	61.0	137	1.14	0.0437
	66.7	136	1.13	0.0438
	78.4	138	1.14	0.0438

* Corrected diffusivity ($D_{c,0}/r^2$)

Table 7. Micropore diffusion time constant and parameters for N_2 adsorption by CMS using isothermal dual resistance model

Temperature [K]	Pressure [kPa]	$D_c/r^2 \times 10^4$ [s^{-1}]	L [-]
N_2			
293		1.60*	
	10.9	1.78	8.85
	16.2	1.80	9.63
	27.0	1.82	10.78
	37.7	1.89	11.90
	48.3	1.92	13.17
	58.8	1.95	14.45
	69.0	1.97	14.80
	79.2	2.03	16.95
308		3.20*	
	12.0	3.50	9.93
	17.8	3.52	9.83
	23.7	3.56	10.42
	35.1	3.61	11.11
	46.3	3.65	12.08
	57.3	3.76	12.57
	68.0	3.86	13.74
	78.5	3.87	15.14
323		6.18*	
	12.0	6.54	9.91
	17.7	6.64	10.23
	23.4	6.74	10.75
	34.7	6.85	11.27
	46.0	6.88	12.00
	57.2	7.12	11.85
	67.8	7.26	12.39
	78.5	7.29	13.16

* Corrected diffusivity ($D_{c,0}/r^2$)

Table 8. Comparison of diffusion time constant and barrier mass transfer coefficient for N_2O, O_2 and N_2

Adsorbent	Manufacturer	T [K]	P [kPa]	D/r_c^2 $\times 10^4$ [s^{-1}]	k_b $\times 10^{4*}$ [s^{-1}]	Method**	Kinetic Model	Ref.
N_2O								
CMS A	Air products	303-323	0-9	0.14-0.24(1)	2.25-22.0(1)	G	Combined barrier resistance	[8]
		303-343		-	24.0-111		Linear driving force	
AC	Kuraray	293-323	10-80	28-74.9	-	V	Non-isothermal diffusion	This study
CMS	Kuraray	293-323	10-80	17-76.8	-	V	Non-isothermal diffusion	This study
O_2								
CMS	Air products	293	0-100	-	83.5-114	G	Linear driving force	[39]
CMS	Air products	273-313	0-100	-	18.3-196	G	Linear driving force	[35]
CMS A	-	275-333	400	-	205	G	Fickian and phenomenological	[42]
CMS 3A	Takeda	273-323	0-1300	20-84	-	G	Isothermal diffusion	[36]
CMS 5A				14-117				
CMS	Bergbau-Forschung	303		52	-			
CMS	Bergbau-Forschung	303	0-73	20	-	G	Dual-resistance	[43]
			-	37	-	C		
CMS	Bergbau-Forschung	300	1144	35	-	DAB	Isothermal diffusion	[18]
CMS	Takeda	293-313	0-1635	38.3-72.2(2)	-	V	Piezometric Method	[44]
CMS	Bergbau-Forschung	253-302	Low coverage (3)	18.5-68.4	457-2400	V	Dual-resistance	[48]
CMS 3A Ⅰ	Takeda	253-267		28.0-47.8	445-810			
CMS 3A Ⅱ	Takeda	253-302		16.0-121.9	277-1248			
AC	Kuraray	293-323	10-80	548-1179	-	V	Non-isothermal diffusion	This study
CMS	Kuraray	293-323	10-80	45.7-137.5	-	V	Non-isothermal diffusion	This study
N_2								
CMS	Air products	293	0-100	-	2.14-3.23	G	Linear driving force	[39]
CMS	Air products	303-343	0-9	-	3.07-23.65	G	Linear driving force	[35]
CMS A	Air products	303-343	0-100	-	2.85-23.45	G	Linear driving force	[8]
CMS A	-	275-333	400	-	5	G	Fickian and phenomenological	[42]
CMS 3A	Takeda	273-323	0-1300	1-8.3	-	G	Isothermal diffusion	[36]
CMS 5A				4.2-29	-			
CMS	Bergbau-Forschung	303		2	-			
CMS	Bergbau-Forschung	303	0-88	1.0	-	G	Dual-resistance	[43]
			-	1.2	-	C		
CMS	Bergbau-Forschung	300	1144	0.095	-	DAB	Isothermal diffusion	[18]
CMS	Takeda	293-313	0-1665	1.0-35.1(2)	-	V	Piezometric Method	[44]

CMS	Shanli chemical materials	303-323	0-100	1.44-5.44	29-65	G	Dual-resistance	[34]
CMS 3K	TAKEDA	298-323	low P	2.77-8.31	60-72	G	Dual-resistance	[40]
AC	Kuraray	293-323	20-90	442-804(2)	-	V	Non-isothermal diffusion	[45]
CMS	Kuraray	298-318	0-600	1.97-6.06	-	G	Isothermal diffusion	[30]
CMS	Bergbau-Forschung	275-302	Low coverage (3)	1.3-4.3	44-106			
CMS 3A Ⅰ	Takeda	273-302		1.3-5.8	26-88	V	Dual-resistance	[48]
CMS 3A Ⅱ	Takeda	273-302		0.67-2.8	14-53			
CMS	Kuraray	293-323	10-80	1.78-7.29	-	V	Isothermal dual resistance	This study

* Barrier mass transfer coefficient

** Experimental methods: Gravimetric (G), Volumetric (V), Chromatographic (C), Differential adsorption bed (DAB)

(1) Using a particle radius of 0.2 cm

(2) Apparent diffusion time constant

(3) Surface coverage (θ) values varied in the range of 0.01-0.03

Table A. 1. Experimental adsorption isotherm data for N_2O on AC and CMS

Activated carbon											
293K				308K				323K			
P [kPa]	q [mol/kg]	P [kPa]	q [mol/kg]	P [kPa]	q [mol/kg]	P [kPa]	q [mol/kg]	P [kPa]	q [mol/kg]	P [kPa]	q [mol/kg]
0.1	0.012	105.0	3.704	0.1	0.009	246.8	4.218	0.2	0.011	390.8	4.201
2.2	0.346	142.9	4.177	3.4	0.318	297.1	4.502	5.3	0.292	447.4	4.400
5.1	0.661	185.5	4.577	7.9	0.604	350.0	4.749	11.6	0.549	505.3	4.578
8.8	0.964	231.8	4.916	13.1	0.872	405.1	4.963	18.8	0.788	564.5	4.741
13.2	1.252	281.5	5.204	19.2	1.126	462.3	5.150	26.9	1.012	624.6	4.883
18.3	1.528	334.4	5.448	25.9	1.364	520.6	5.314	35.6	1.221	685.9	5.009
24.0	1.789	389.4	5.655	33.3	1.590	580.2	5.462	44.6	1.412	747.9	5.126
30.3	2.038	446.6	5.833	41.2	1.804	641.1	5.592	54.2	1.593	810.5	5.232
37.2	2.274	505.1	5.987	49.6	2.002	702.8	5.707	67.9	1.823	874.0	5.324
44.7	2.500	564.9	6.121	58.3	2.188	765.1	5.814	82.3	2.034	937.6	5.412
52.4	2.707	625.8	6.238	67.2	2.360	828.4	5.905	91.3	2.159	1002.0	5.491
60.6	2.902	687.8	6.339	82.2	2.609	892.2	5.989	100.4	2.275		
72.6	3.157	750.1	6.431	90.7	2.745	956.2	6.067	141.0	2.711		
80.4	3.302	813.4	6.509	99.4	2.869	1013.4	6.131	185.4	3.091		
88.6	3.446	876.9	6.580	114.8	3.070			233.2	3.424		
97.0	3.581	940.7	6.646	155.1	3.510			283.4	3.716		
105.0	3.704	1004.9	6.702	199.3	3.890			336.1	3.974		

Carbon molecular sieve											
293K				308K				323K			
P [kPa]	q [mol/kg]	P [kPa]	q [mol/kg]	P [kPa]	q [mol/kg]	P [kPa]	q [mol/kg]	P [kPa]	q [mol/kg]	P [kPa]	q [mol/kg]
0.1	0.018	215.2	2.945	0.1	0.014	273.2	2.734	0.1	0.005	334.3	2.534
2.3	0.406	275.9	3.080	3.8	0.373	335.2	2.852	5.2	0.318	397.7	2.641
6.2	0.763	338.5	3.182	9.4	0.684	398.7	2.950	12.5	0.590	462.1	2.734
11.6	1.078	402.0	3.264	16.9	0.962	462.8	3.031	21.4	0.822	527.0	2.810
18.9	1.359	466.5	3.331	26.0	1.199	527.7	3.102	31.6	1.023	592.9	2.874
27.8	1.602	531.8	3.385	36.4	1.403	593.0	3.164	43.0	1.198	659.1	2.927
38.1	1.813	597.3	3.431	47.9	1.580	658.4	3.221	55.0	1.348	725.5	2.978
49.8	1.995	663.0	3.471	60.4	1.734	724.2	3.275	67.8	1.482	792.4	3.023
62.1	2.147	729.1	3.512	78.3	1.910	790.3	3.325	89.7	1.651	859.4	3.063
80.1	2.321	795.1	3.549	89.9	2.009	856.8	3.370	102.0	1.740	926.9	3.099
91.7	2.415	861.1	3.584	102.2	2.095	923.0	3.420	155.2	2.026	994.0	3.138
103.7	2.500	926.8	3.619	155.3	2.376	988.6	3.475	212.5	2.239		
157.3	2.762	992.6	3.657	212.9	2.579	1025.0	3.520	272.5	2.403		

Table A. 2. Experimental adsorption isotherm data for O_2 on AC and CMS

Activated carbon											
293K				308K				323K			
P [kPa]	q [mol/kg]	P [kPa]	q [mol/kg]	P [kPa]	q [mol/kg]	P [kPa]	q [mol/kg]	P [kPa]	q [mol/kg]	P [kPa]	q [mol/kg]
0.5	0.002	400.5	1.220	0.9	0.003	413.4	0.995	0.6	0.001	423.9	0.807
17.9	0.081	462.3	1.352	19.5	0.064	476.4	1.106	19.6	0.048	488.3	0.901
35.3	0.155	524.4	1.474	37.8	0.121	539.8	1.211	38.5	0.092	553.0	0.993
52.4	0.224	587.0	1.591	55.7	0.175	603.7	1.313	56.6	0.134	618.0	1.079
69.2	0.288	649.9	1.700	73.2	0.226	667.6	1.408	74.4	0.174	683.1	1.163
85.7	0.350	713.2	1.802	88.7	0.271	732.0	1.498	90.6	0.207	748.5	1.241
100.1	0.403	776.4	1.902	104.0	0.313	796.6	1.584	106.4	0.243	814.0	1.315
158.6	0.595	840.1	1.992	164.8	0.470	861.1	1.663	169.1	0.369	879.6	1.386
218.0	0.770	904.0	2.080	226.3	0.615	925.8	1.744	232.4	0.488	945.1	1.454
278.2	0.931	968.0	2.167	288.2	0.748	990.5	1.822	295.9	0.601	1010.8	1.519
339.2	1.079	1017.3	2.228	350.6	0.876	1026.2	1.860	359.8	0.708		

Carbon molecular sieve											
293K				308K				323K			
P [kPa]	q [mol/kg]	P [kPa]	q [mol/kg]	P [kPa]	q [mol/kg]	P [kPa]	q [mol/kg]	P [kPa]	q [mol/kg]	P [kPa]	q [mol/kg]
0.7	0.003	411.6	1.032	0.5	0.002	420.2	0.838	0.8	0.002	430.1	0.687
18.3	0.085	475.1	1.121	19.2	0.063	484.7	0.921	20.2	0.048	495.6	0.761
35.7	0.159	539.1	1.205	37.6	0.119	549.6	0.998	39.2	0.091	561.1	0.829
52.8	0.225	603.5	1.282	55.4	0.170	614.7	1.070	57.5	0.130	626.8	0.894
69.7	0.285	668.0	1.357	72.9	0.218	680.3	1.128	75.6	0.167	692.8	0.955
86.4	0.341	732.9	1.424	88.9	0.254	745.6	1.188	92.1	0.200	758.9	1.012
101.6	0.391	797.6	1.490	104.2	0.295	811.3	1.244	107.9	0.228	824.8	1.072
162.0	0.555	862.5	1.554	166.0	0.431	876.9	1.304	171.3	0.340	890.9	1.128
223.4	0.698	927.3	1.620	228.6	0.548	942.7	1.359	235.3	0.439	956.4	1.187
285.5	0.822	972.9	1.666	292.1	0.654	978.9	1.392	300.1	0.530		
348.2	0.935			355.8	0.753			364.9	0.612		

Table A. 3. Experimental adsorption isotherm data for N_2 on CMS

Carbon molecular sieve											
293K				308K				323K			
P [kPa]	q [mol/kg]	P [kPa]	q [mol/kg]	P [kPa]	q [mol/kg]	P [kPa]	q [mol/kg]	P [kPa]	q [mol/kg]	P [kPa]	q [mol/kg]
0.6	0.005	158.9	0.546	0.6	0.002	161.9	0.429	0.5	0.001	164.6	0.336
5.8	0.031	217.7	0.673	6.3	0.023	222.3	0.536	6.2	0.016	226.6	0.425
10.9	0.063	278.1	0.784	12.0	0.044	283.6	0.631	12.0	0.031	289.9	0.507
16.2	0.088	338.9	0.879	17.8	0.064	345.9	0.714	17.7	0.046	353.2	0.583
27.0	0.137	400.8	0.964	23.7	0.084	409.3	0.790	23.4	0.060	417.4	0.651
37.7	0.181	463.6	1.039	35.1	0.120	472.8	0.859	34.7	0.087	482.3	0.713
48.3	0.221	527.1	1.106	46.3	0.154	537.0	0.921	46.0	0.113	547.1	0.770
58.8	0.259	590.9	1.167	57.3	0.186	601.7	0.976	57.2	0.138	612.4	0.821
69.0	0.294	655.3	1.221	68.0	0.216	666.4	1.029	67.8	0.161	678.5	0.866
79.2	0.328	719.8	1.271	78.5	0.243	731.4	1.077	78.5	0.183	744.3	0.910
84.1	0.343	784.4	1.316	83.6	0.256	796.8	1.125	84.0	0.193	810.2	0.957
89.0	0.358	849.7	1.357	88.6	0.268	862.6	1.166	89.4	0.204	876.6	0.994
93.8	0.373	915.0	1.395	93.8	0.280	928.5	1.203	94.3	0.213	943.1	1.029
98.2	0.386	979.9	1.430	98.4	0.292	994.5	1.241	99.3	0.221	1009.7	1.065
102.0	0.397	1023.1	1.452	102.7	0.303			103.8	0.230		